Thomas Gamse (editor)

Book of Abstracts

ERASMUS+ BIP ESS-HPT 2023

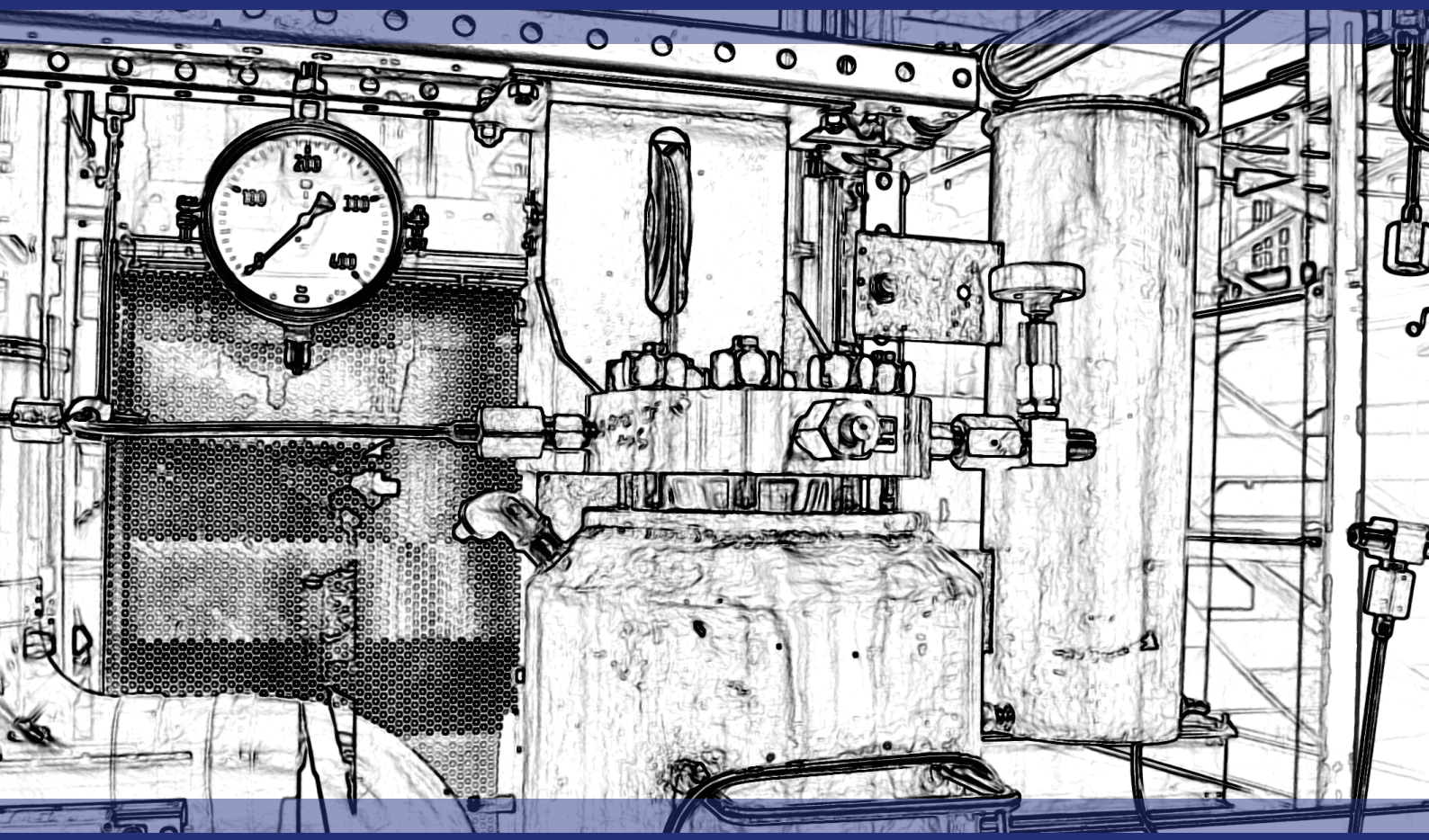

The European Summer School in High Pressure Technology

9.7. – 22.7.2023

TU Graz
Graz University of Technology

Erasmus+

EFCE
European Federation of Chemical Engineering
Europäische Föderation für Chemie-Ingenieur-Wesen
Fédération Européenne de Génie Chimique

Imprint

Organisation: Thomas Gamse
Institute of Chemical Engineering and Environmental Technology
Graz University of Technology,
Inffeldgasse 25/C, 8010 Graz, Austria
Tel. +43 (0)316 873-7477
E-Mail: thomas.gamse@tugraz.at

Editor: Thomas Gamse
Layout: Thomas Gamse
Cover: Verlag der Technischen Universität Graz,
Thomas Gamse

2023 Verlag der Technischen Universität Graz
www.tugraz-verlag.at

Book of Abstracts, ERASMUS+ BIP ESS-HPT 2023
"The European Summer School in High Pressure Technology"
9.7.-22.7.2023, Graz University of Technology

ISBN (e-book) 978-3-85125-963-6

DOI 10.3217/978-3-85125-963-6

Preface

The European Summer School in High Pressure Technology (ESS-HPT) is the continuation of many years of high pressure intensive courses. The history of this very successful series of courses started in 1995, when the first intensive course took place in Monselice, Italy. Most of these Intensive Courses were supported by SOCRATES and later Life Long Learning, as shown in following overview:

SOCRATES IP "Current Trends in High Pressure Technology and Chemical Engineering"
- 1995 Monselice / Italy
- 1996 Nancy / France
- 1997 Erlangen / Germany

SOCRATES IP "High Pressure Technology in Process and Chemical Engineering"
- 1999 Abano Terme / Italy
- 2000 Valladolid / Spain
- 2001 Maribor / Slovenia and Graz / Austria

SOCRATES IP "High Pressure Chemical Engineering Processes: Basics and Applications"
- 2002 Graz / Austria and Maribor / Slovenia
- 2003 Budapest / Hungary
- 2004 Barcelona / Spain

SOCRATES IP "Basics, Developments, Research and Industrial Applications in High Pressure Chemical Engineering Processes"
- 2005 Prague / Czech Republic
- 2006 Lisbon / Portugal
- 2007 Albi / France

Life Long Learning IP "SCF- GSCE: Supercritical Fluids – Green Solvents in Chemical Engineering"
- 2008 Thessaloniki / Greece
- 2009 Istanbul / Turkey
- 2010 Budapest / Hungary

EFCE Intensive Course "High Pressure Technology - From Basics to Industrial Applications"
- 2011 Belgrade / Serbia

Life Long Learning IP "PIHPT: Process Intensification by High Pressure Technologies – Actual Strategies for Energy and Resources Conservation"
- 2012 Maribor / Slovenia and Graz / Austria
- 2013 Darmstadt / Germany
- 2014 Glasgow / Great Britain

Unfortunately the financial support for these Intensive Programmes was cancelled within ERASMUS+. The EFCE Working Party "High Pressure Technology" decided in September 2014 to go on with this course in the form of a Summer School.

ESS-HPT "The European Summer School in High Pressure Technology"

ESS-HPT 2015	Maribor / Slovenia and Graz / Austria
ESS-HPT 2016	Maribor / Slovenia and Graz / Austria
ESS-HPT 2017	Maribor / Slovenia and Graz / Austria
ESS-HPT 2018	Maribor / Slovenia and Graz / Austria
ESS-HPT 2019	Maribor / Slovenia and Graz / Austria
ESS-HPT 2021	Online Course, Graz / Austria
GEHPT and ESS-HPT 2022	Maribor / Slovenia and Graz / Austria

The ESS-HPT takes place every year within the first 2 weeks of July at University of Maribor, Slovenia and Graz University of Technology, Austria.

This year ESS-HPT 2023 is organised as an ERASMUS+ Blended Intensive Programme (BIP). As it was not possible to organise it in two countries the whole intensive programme will take place at Graz University of Technology in the period 9.7.2023 till 22.7.2023.

All participants have to give an oral presentation and the abstracts of these presentations, which are peer-reviewed by the EFCE WP Members, are published in this book of abstracts.

The editor

Thomas Gamse
Organiser of ESS-HPT 2023

Many thanks to our sponsors,

Erasmus+

COST action CA18224 “GREENERING”,

Greenering

cost
EUROPEAN COOPERATION IN SCIENCE & TECHNOLOGY

NATEX Prozesstechnologie GesmbH,

natex
PROZESSTECHNOLOGIE

INNOWELD-Metallverarbeitung GmbH

INNO WELD

and Tourismusverband Stadt Graz.

TOURISMUS GRAZ

Time Schedule and Abstracts

Oral Presentations Participants

	Wednesday, 12 July 2023		
1	17:15 - 17:30	**Laura Göhlich** Development of a Jet Cutting Process with Liquefied Carbon Dioxide as Cutting Medium under Atmospheric Conditions	1
2	17:30 - 17:45	**Gal Slaček**, Azra Osmić, Maša Knez Marevci, Željko Knez Optimization of Extraction Procedure for Recovery of Bioactive Content from Curcuma and its Formulation into Organogel	5
3	17:45 - 18:00	**Svenja Albus**, Markus Busch Transitiometry - Investigation of Individual Peroxide Decomposition Kinetics in Cocktails under High-Pressure	10
4	18:00 - 18:15	**de-Souza Ribeiro, M.M.**[1,2], Alonso, E.[1,2], Mato Chain R.[1,2], Loya-Pérez, H.[1,2], Casas-Gonzalez A.P.[1,2], Rodríguez-Rojo, S.[1,2] Cascade Fractionation of Crustacean Shell Residues Preventing the Degradation of Chitin and its Subsequent Industrial Application	14
5	18:15 - 18:30	**Dóra Arany**, Márton Kőrösi, Edit Székely Development of an Automatic Method for Measuring Melting Point under Carbon Dioxide Pressure	18
6	18:30 - 18:45	**Martina Miloloža**, Kristina Bule Možar, Viktorija Martinjak, Matija Cvetnić, Marinko Markić, Šime Ukić, Tomislav Bolanča, Dajana Kučić Grgić Bioremediation of Water Polluted with Microplastics by Bacteria Isolated from the Environment Enriched with Microplastics	24
7	18:45 - 19:00	**Julian Kirsch**, Nicola Schreiner, Markus Busch Modeling of Grafted LDPE Copolymers with a Reactor Combination and Comparison to Analytical Results from Thermal Fractionation	30

	Friday, 14 July 2023		
8	17:15 - 17:30	**Goicoechea Torres A,** Dos Santos LC, Quintana L., Ciordia V, Almarza M, Martín Á, Bermejo MD Construction of a Pilot Plant for the Reduction of CO_2 Captured by Amines	33
9	17:30 - 17:45	**Sandra Pietrasch**, Markus Busch, Kristina Zentel Influence of Reaction Parameters on the Solution Polymerisation of Vinyl Acetate	39

10	17:45 - 18:00	**Mateusz Jackowski**, Reshma Babu, Anna Trusek High Pressure Processes for the Brewing Industry – Extraction of Valuable Compounds from Brewing Byproducts	43
11	18:00 - 18:15	**Gunay Ismiyeva** Ethybenzene/Styrene Multicomponent Distillation Column	48
12	18:15 - 18:30	**Ivana Nikolić** Supercritical Extraction of Milk Thistle and Cannabis	53
13	18:30 - 18:45	**Adéla Šlachtová**, Michal Zym, Ivana Troppová, Lenka Matějová Design of TiO2-CeO2 Based Catalysts for Dichloromethane Oxidation; from Powders Catalysts to Catalytic Foams by Using Subcritical Water Processing	59
14	18:45 - 19:00	**Laura Ständecke,** Markus Busch Investigating Mixing Characteristics of Polymerization Reactors	62

	Monday, 17 July 2023		
15	17:15 - 17:30	**Franjo Frešer**, Urban Bren, Gregor Hostnik Influence of Tannins Structure on the Formation of Coordination Compounds with Fe(II) Ions	65
16	17:30 - 17:45	**María Constanza Maciel**, María José Cocero Alonso, Rafael Bartolomé Mato Chaín Characterization of Cutin Monomers from Tomato Peel by Microwave-Assisted Basic Hydrolysis	70
17	17:45 - 18:00	**Stephan Heuser**, Lucas Hoof, Eduardo García Alanís, Michael Prokein, Andreas Kilzer, Ulf-Peter Apfel, Marcus Petermann Continuous Electroreduction of Compressed CO2 to CO	73
18	18:00 - 18:15	**Joshua Stahl,** Nicola Schreiner, Markus Busch Modelling the High-Pressure Process of Ethylene-Methyl Acrylate Copolymerization	81
19	18:15 - 18:30	Małgorzata Djas, Marek Henczka, **Przemysław Rakowski** Supercritical Carbon Dioxide as a Solvent in Graphene Production via Ultrasound Assisted Exfoliation with Intercalating Compounds	84
20	18:30 - 18:45	**Roland Gall** Dosing of Powder by Vibration Stimulation	88

INNOWELD Metallverarbeitung GmbH

ADRESSE ADDRESS	8682 Hönigsberg, Hönigsberggasse	GEGRÜNDET ESTABLISHED	1987
TELEFON TELEPHONE	+43 3852 5412-0	MITARBEITER EMPLOYEES	140
FAX	+43 3852 5412-25	AUSLANDSANTEIL EXPORT VOLUME	80%
E-MAIL	office@innoweld.at	EXPORTMÄRKTE EXPORT MARKETS	weltweit
INTERNET	www.innoweld.at		

Unternehmensprofil Company Profile

Seit 35 Jahren beliefert der Hönigsberger Anlagen- und Apparate-hersteller unterschiedlichste Industriezweige mit seinen hochwertigen und funktionalen Produkten.

Angefangen bei der chemischen Industrie, wo Höchstdruck-apparate mit einem Gewicht von bis zu 150.000 kg, teilweise in walz- oder schweißplattierter Ausführung und unter Verwendung automatisierter Schweißverfahren erforderl ich sind, über die Marine, die auf amagnetische Werkstoffe für den Einsatz in allen Weltmeeren angewiesen sind, die Gasturbinenindustrie, wo spezielle Komponenten aus hochwarmfesten Materialien mit einem hohen Umformgrad und sehr engen Toleranzen benötigt werden, bis hin zur Luftfahrt – INNOWELD Metallverarbeitung liefert Apparate und höchstbelastbare Einheiten für jeden Einsatzbereich.
Renommierte Engineering-Unternehmen wie Air Liquide, Uhde, BHDT, Linde, Primetals u.v.m. zählen zu den zufriedenen Kunden der steirischen Innovationsschmiede.

Produkte & Dienstleistungen Products & Services

Unsere Dienstleistungen beinhalten Komplettdesign, Detail-Engineering, mechanische Konstruktion, Herstellung, Montage, Testläufe (einschl. Testberichte)

Unser Herstellungsprogrm umfasst:

HOCHDRUCK - TECHNIK:

- Hochdruckapparate (Reaktoren, Kolonnen usw.)
- Hochdruckrohrleitungen und Isometrien
- Hochdruckverschlüsse
- Wärmetauscher (Rohrbundel, U-Rohr, Doppelroh usw.)










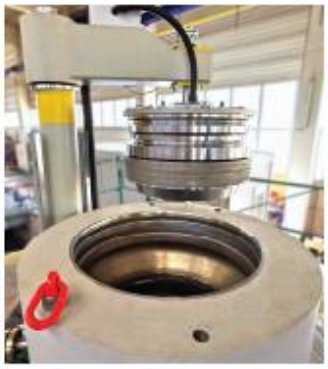
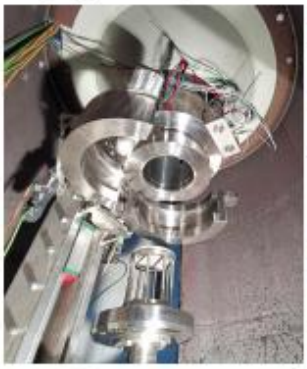

Development of a Jet Cutting Process with Liquefied Carbon Dioxide as Cutting Medium under Atmospheric Conditions

Laura Göhlich

Chair for Particle Technology, Ruhr-University Bochum, Germany, goehlich@fvt.rub.de

Introduction

Water jet cutting is a well-established industrial manufacturing technique for cutting various materials. For the jet cutting process, the cutting medium is pressurised to some thousand bar before being depressurised through a nozzle to atmospheric conditions to form a jet. [1] Instead of water other fluids can be used as cutting medium. The use of liquid carbon dioxide (CO_2) as a cutting medium instead of water enables residue-free and dry processing of water-sensitive materials because CO_2 completely evaporates after impinging the workpiece. [2]

In the special case of CO_2 jet cutting, the medium cannot exist in a liquid state under atmospheric conditions in thermodynamic equilibrium because of its triple point pressure of 5.18 bar. Nevertheless, under certain pre-expansion conditions liquid CO_2 jets can be observed. With sufficient cooling, it is possible to generate liquid jets which decompose into a gas and a solid phase after a few centimetres of liquid jet length. For this, it is necessary to cool the CO_2 down to near the solidus line before it is depressurised through the nozzle. With the resulting coherent liquid jet, it is possible to process soft materials such as polymers, metal foils or natural material. [3] In the last years CO_2 jet cutting has been subject to intensive research, which has shown that cutting properties such as stability or jet length are significantly influenced by the factors pre-expansion temperature and pressure and the density of the atmosphere into which the jet is expanded. So far, it has been possible to generate liquid CO_2 jets suitable for cutting soft materials by adjusting these parameters. To generate the jets, mostly conventional waterjet technology with some modifications has been used. Due to the necessity of elaborate cooling, a stationary nozzle was used. So far, it was not possible to move the cutting head and thus the jet. In order to cut materials, they must be moved under the nozzle. This limits the flexibility and the field of application of CO_2 jet cutting. In course of the research a completely redesigned jet cutting system for the use of carbon dioxide was developed, which is characterized by a compact and modular structure. An efficient cooling concept allows the use of a cutting head movable in two directions and thereby the cutting of complex 2D-geometries.

Experimental

In a first step a system with a flexible spiral pipeline was developed that allows the cutting head to be moved. Since both high pressure and low temperature are required, a high-pressure pipeline was used, which was insulated accordingly. Extensive investigations of the CO_2 jet cutting system were made. A scheme of the system and the measured temperature values can be seen in Fig. 1. It was found that due to the heat input from the environment, the CO_2 does not reach the nozzle sufficiently cold to form a liquid CO_2 jet. After the CO_2 has been precooled by heat exchanger I to a temperature of about -6 °C, its temperature is raised to about ambient temperature by the compression in the pump. Afterwards, the CO_2 is cooled down to -30 °C by heat exchanger II and led through a spiral pipe to the cutting head. On its way to the nozzle, the CO_2 absorbs a lot of heat despite the insulation, so that it arrives at a temperature of about 14 °C at the nozzle. This temperature is too high to generate a liquid jet for cutting.

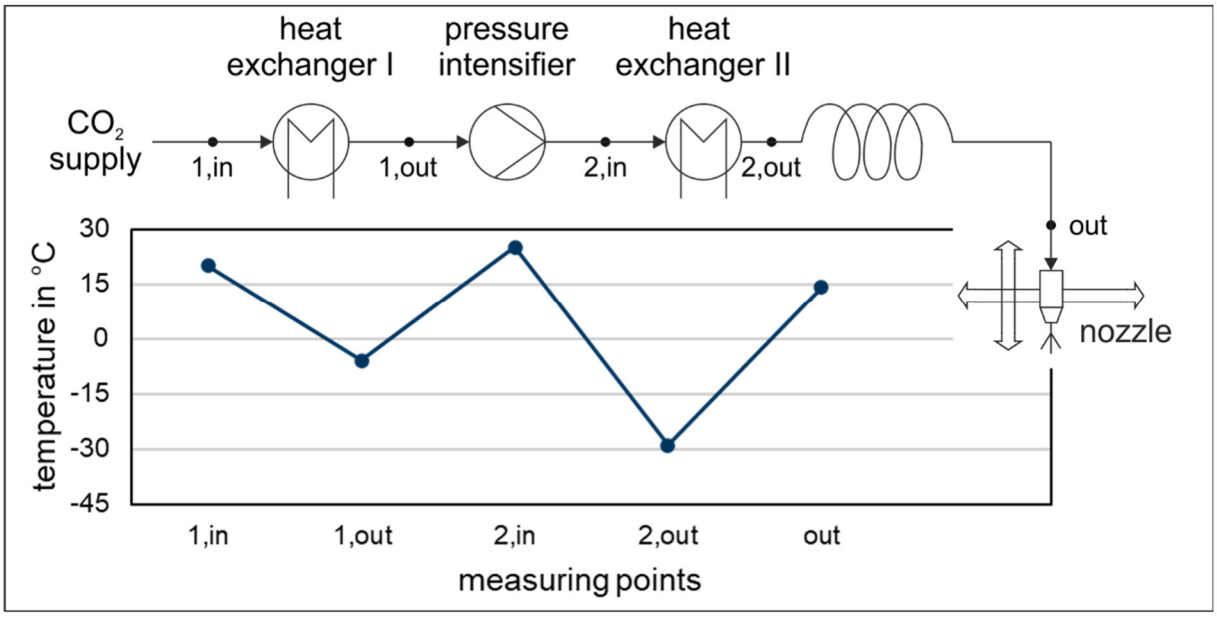

Fig. 1.: System setup 1 - temperature profile of CO_2 at 800 bar pre-pressure.

The measurement of the thermodynamic parameters revealed the necessity for some modifications. To improve cooling, the system was modified again. A compact, movable heat exchanger for temperatures down to -40 °C and pressures up to 4000 bar was designed and mounted directly above the nozzle. In order to compare the previous and new cooling concept the new jet cutting system was tested again and it was found that lower pre-expansion temperatures can be reached. A scheme of the new system with the measuring points and the measured temperatures can be seen in Fig. 2. The temperature profile is similar to the one in the first setup up to the point where the CO_2 is fed into the

heat exchanger III. The heat exchanger near the nozzle makes it possible for the CO_2 to reach temperatures down to -27 °C before the nozzle. This is lower than in all previous experiments and allows working with a liquid, moving CO_2 jet for cutting materials. This contributes significantly to the jet stability and will improve the cutting result as well as increase the area of application due to the movable cutting head.

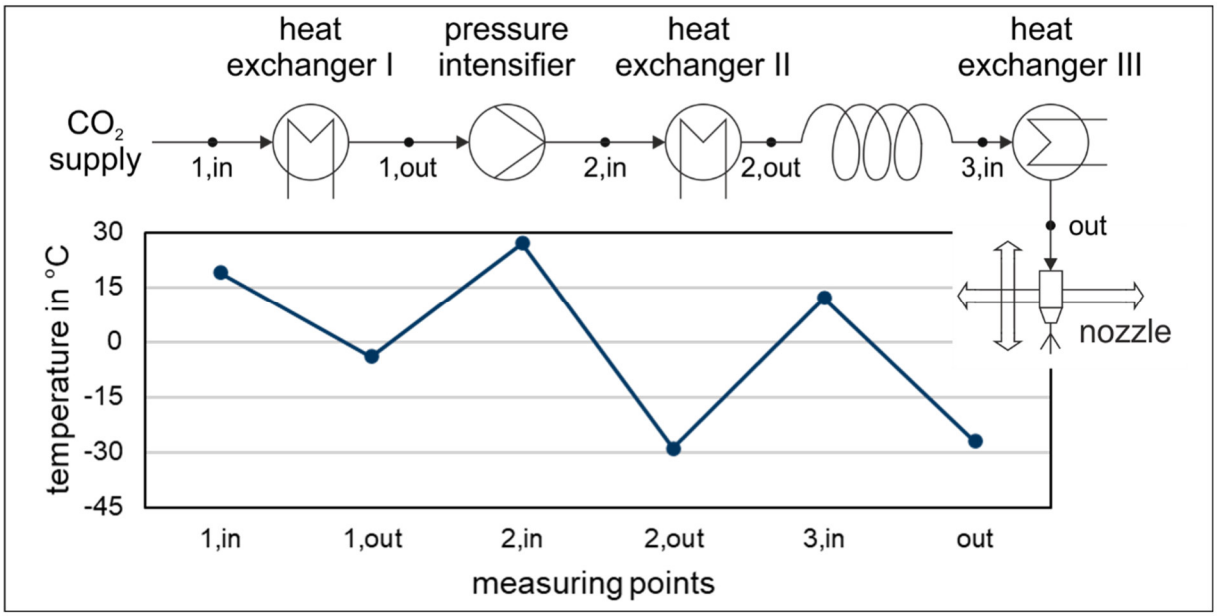

Fig. 2.: System setup 2 - temperature profile of CO_2 at 800 bar pre-pressure.

The cutting head, which can be moved in two directions, makes it possible to process complex geometries. Fig. 3 shows a piece of leather that was machined with the new system. The cutting force is so far not high enough to cut through the material completely, but a very precise and accurate work is possible, so that the fine cut edges are clearly visible.

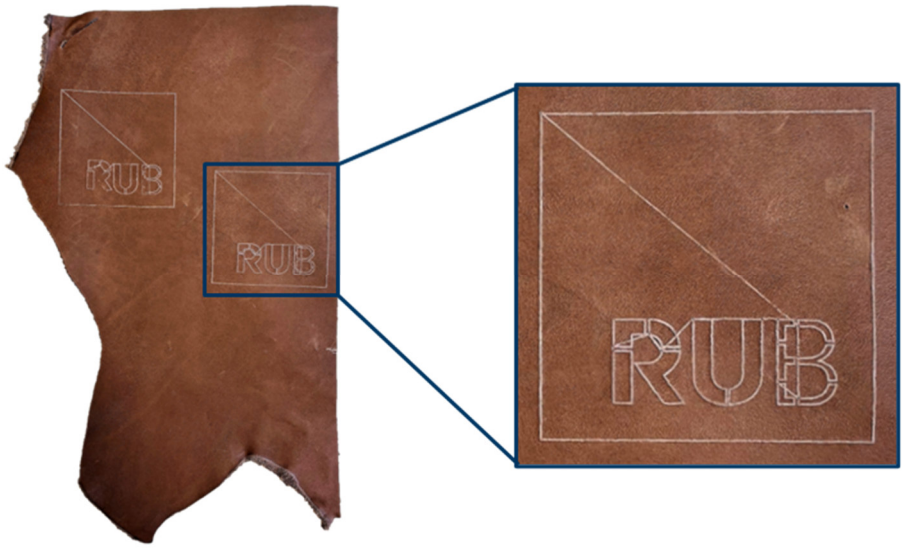

Fig. 3.: Leather processed with liquid CO_2 jets.

Summary

A modular system for generating liquid CO_2-jets at atmospheric pressure has been designed. In comparison to previous used setups, which are based on conventional water jet cutting technology, the system has been built for the use of liquid carbon dioxide. To maintain a temperature of -27 °C in the nozzle, it was necessary to design a very compact heat exchanger that can be moved along with the nozzle. Thereby it is now possible to program and cut complex geometries in two dimensions.

References

[1] Schulze, Günter (2010): Wasserstrahlschneiden. In: A. Herbert Fritz und Günter Schulze (Hg.): Fertigungstechnik. Berlin, Heidelberg: Springer Berlin Heidelberg, S. 386–392.

[2] Dunsky, C.; Hashish, M. (1994): Cutting with high-pressure CO_2 jets. In: Papers presented at the 12th International Conference on Jet Cutting Technology.

[3] Engelmeier, Lena (2016): Flüssige, kohärente Kohlendioxidstrahlen zum Schneiden von Materialien in atmosphärischer Umgebung. Dissertation. Ruhr-Universität Bochum, Bochum. Fakultät für Maschinenbau.

Optimization of Extraction Procedure for Recovery of Bioactive Content from Curcuma and its Formulation into Organogel

Gal Slaček, Azra Osmić, Maša Knez Marevci, Željko Knez

Faculty of Chemistry and Chemical Engineering, University of Maribor, Smetanova ulica 17, 2000 Maribor

Laboratory for separation processes and production design

gal.slacek@um.si

Introduction

Turmeric (*Curcuma longa*) is a perennial herb belonging to the ginger family (*Zingiberaceae*) and is renowned as the "golden spice" due to its vibrant yellow colour. It is primarily cultivated in warm regions such as Africa, the West Indies, the Caribbean, and Latin America [1]. The extract of turmeric, which is soluble in both water and fat, exhibits potent antioxidant effects comparable to vitamins C and E. These effects can be attributed to its active constituents known as curcuminoids, including curcumin, demethoxycurcumin, and bisdemethoxycurcumin [2,3]. In addition to curcuminoids, turmeric's rhizomes contain fatty acids, saccharides, flavonoids, and alkaloids. The essential oil derived from the rhizome comprises ar-turmerone, *α*-turmerone, and *β*-turmerone, giving it a yellow to light brown colour [4]. Turmeric has a rich history of use as a spice and in traditional medicine, particularly in India. Its antioxidant and anti-inflammatory properties make it valuable in combating oxidative damage and reducing the production of pro-inflammatory cytokines. Turmeric has shown potential benefits such as antioxidant, anticarcinogenic, anti-inflammatory, antimicrobial, and antitumor effects, which have sparked significant interest for its medicinal applications. It is widely utilized in the treatment of various conditions including colds, coughs, skin ailments, rheumatism, arthritis, asthma, and psoriasis [5–7].

The aim of the research work was, in the first part, to determine the optimal conditions for extraction of turmeric and to achieve high levels of bioactive compounds by the most suitable extraction method. Based on the values of bioactive compounds, the extract with the highest content was formulated into an organogel. In addition to the organogels, other formulations will be made on which release studies will be carried out. The aim is to bind as high a concentration of turmeric as possible in the blood and transport it to the target point.

Experimental

In this present research, extracts from turmeric were prepared by conventional methods such as Soxhlet extraction (SOX), Ultrasonic extraction (US), and cold maceration (CM) using ethanol as the solvent. Supercritical extraction (SCE) was also performed using carbon dioxide (CO_2) as the solvent and ethanol as the co-solvent. The content of antioxidants, total phenols, and proanthocyanidins in the extracts was determined using UV/VIS (Cary 50 Scan, Varian, Surrey, England) spectrophotometry [8]. The Folin-Ciocalteu method [9] was employed to measure the total phenolic content, while proanthocyanidins were analyzed through acid hydrolysis and color formation [10]. The antioxidant activity was determined by measuring the scavenging ability of the extracts against DPPH· and ABTS· radicals. Additionally, the curcumin content in the turmeric extract was determined using Agilent 1200 HPLC and Agilent 6460 JetStream triple quadrupole mass spectrometer (Agilent Technologies, Santa Clara, CA, USA). Two types of organogels, aqueous and anhydrous, were prepared from the extract obtained by ultrasonic extraction. Based on the literature review, other formulations have been prepared and used for release studies in human fluids (simulated gastric fluid, intestinal fluid).

Summary

- **Yield of extraction**: comparisons of four different extractions (SOX, CM, US, SCE) with solvents ethanol and CO_2.

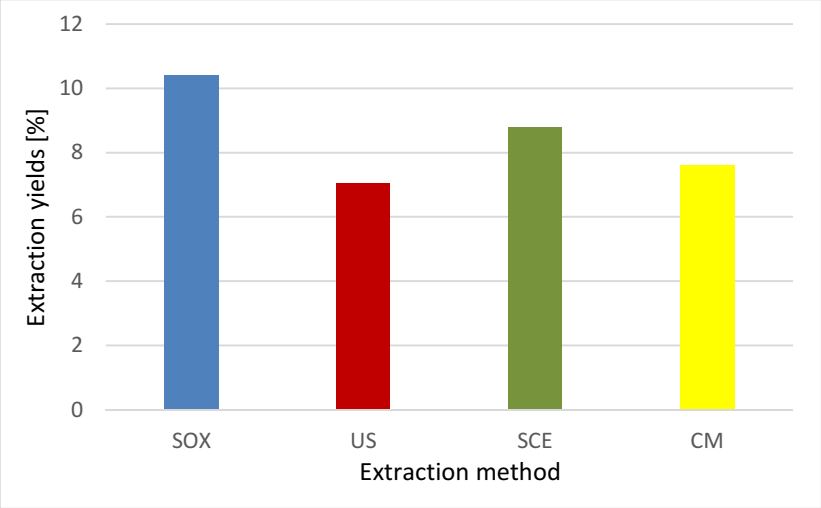

Figure 1: Yield of extraction.

- **Antioxidant activity, total phenols and proanthocyanidins:** antioxidant activity determined by DPPH· and ABTS· are shown on Fig. 2 and Fig. 3. The total phenolic content is calculated as the equivalent of gallic acid in mg per 100 gram of the

selected material (Fig. 4). The content of the proanthocyanidins in mg per 100 gram of material selected (mPAC/100 g material) are shown in Fig. 5.

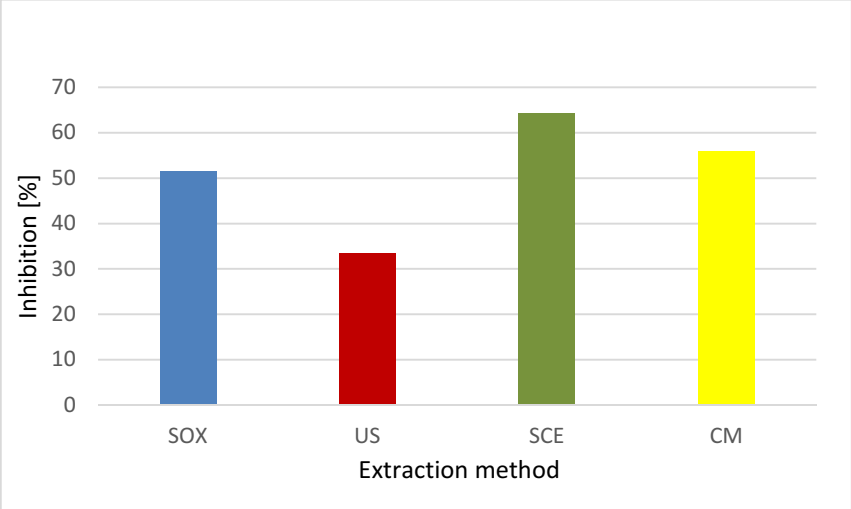

Figure 2: Antioxidant activity in turmeric (DPPH·).

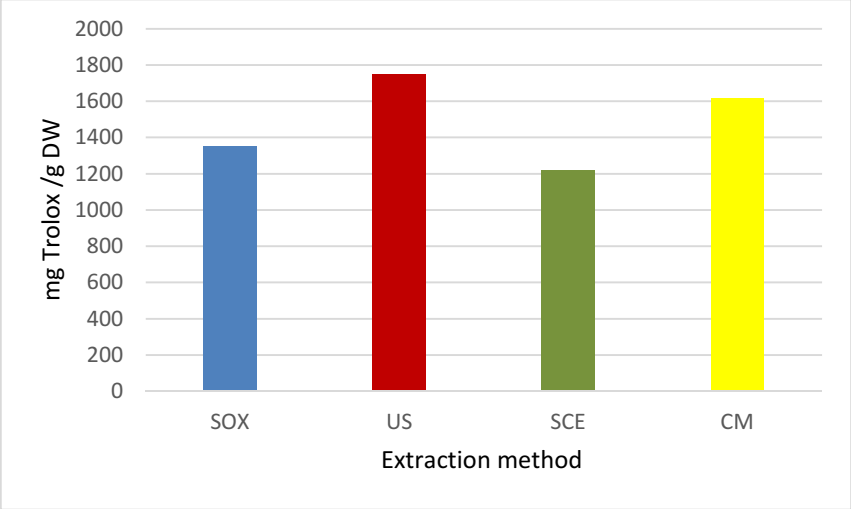

Figure 3: Antioxidant activity in turmeric (ABTS·).

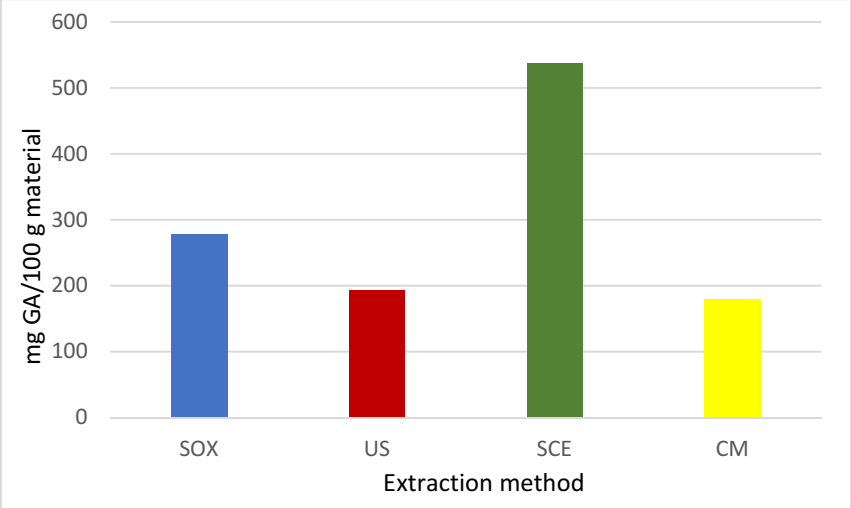

Figure 4: Total phenolic content of turmeric.

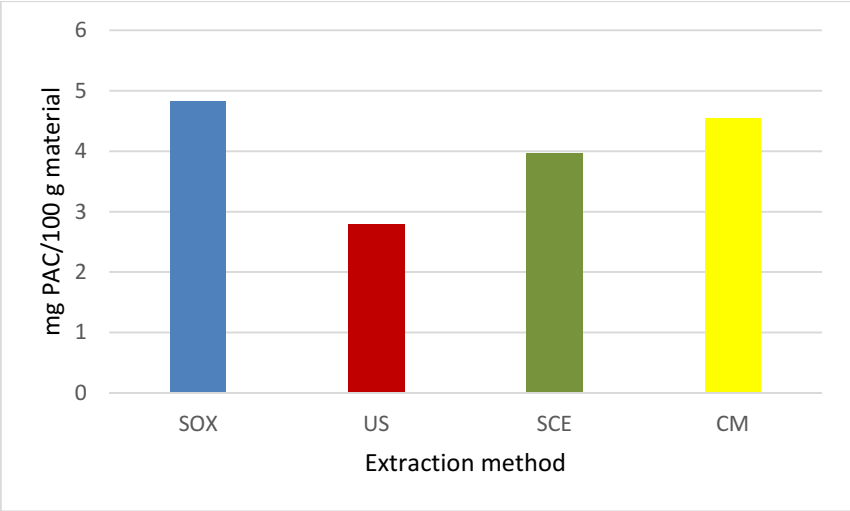

Figure 5: Proanthocyanidin content in turmeric.

- **Curcumin content:**

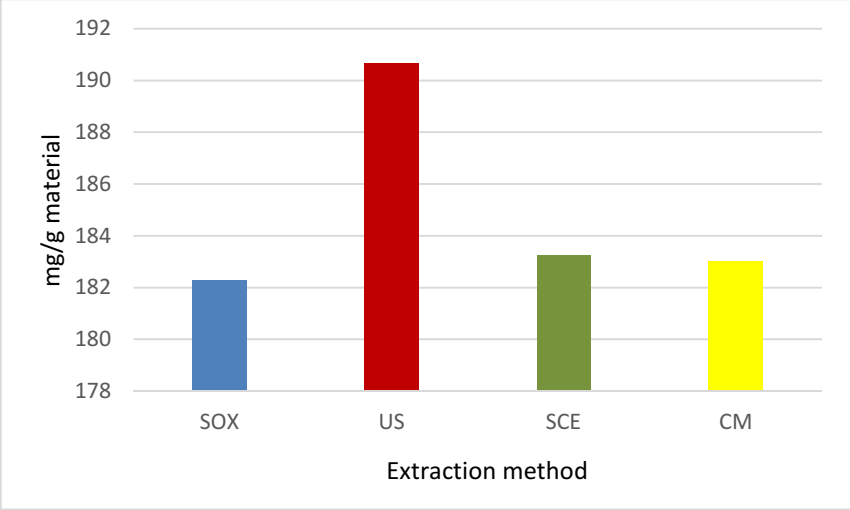

Figure 6: Curcumin content in turmeric extract.

Extract obtained by supercritical extraction method contained the highest proportion of antioxidant (64% inhibition) and total phenols (545 mg GA/100 g material). HPLC-MS resulted in the highest curcumin content (190,8 mg/g material) in the extracts obtained by US extraction. Both the US and SCE methods resulted in high antioxidant, total phenolics, and curcumin content. The choice of extraction method should be tailored to the desired result and the specific application to ensure optimal results. Two (aqueous and anhydrous) organogels have been prepared and will be used for further release studies. The present study has confirmed that turmeric is an excellent and potent antioxidant, containing a high proportion of total phenols and curcuminoids. Study showed that most of the curcumin is released and dissolved in the simulated gastric fluid of the anhydrous organogel after 240 min, while the proportion of curcumin released and dissolved from the aqueous organogel is much lower at only about one tenth (16 %) at the same time.

References

[1] S. Prasad, B.B. Aggarwal, Turmeric, the Golden Spice: From Traditional Medicine to Modern Medicine, in: I.F.F. Benzie, S. Wachtel-Galor (Eds.), Herbal Medicine: Biomolecular and Clinical Aspects, 2nd ed., CRC Press/Taylor & Francis, Boca Raton (FL), 2011. http://www.ncbi.nlm.nih.gov/books/NBK92752/ (accessed May 9, 2022).

[2] T. Ahmed, A.-H. Gilani, Therapeutic Potential of Turmeric in Alzheimer's Disease: Curcumin or Curcuminoids, Phytotherapy Research. 28 (2014) 517–525. https://doi.org/10.1002/ptr.5030.

[3] P. Anand, S.G. Thomas, A.B. Kunnumakkara, C. Sundaram, K.B. Harikumar, B. Sung, S.T. Tharakan, K. Misra, I.K. Priyadarsini, K.N. Rajasekharan, B.B. Aggarwal, Biological activities of curcumin and its analogues (Congeners) made by man and Mother Nature, Biochemical Pharmacology. 76 (2008) 1590–1611. https://doi.org/10.1016/j.bcp.2008.08.008.

[4] I.A. Oyemitan, C.A. Elusiyan, A.O. Onifade, M.A. Akanmu, A.O. Oyedeji, A.G. McDonald, Neuropharmacological profile and chemical analysis of fresh rhizome essential oil of Curcuma longa (turmeric) cultivated in Southwest Nigeria, Toxicology Reports. 4 (2017) 391–398. https://doi.org/10.1016/j.toxrep.2017.07.001.

[5] P.N. Ravindran, K.N. Babu, K. Sivaraman, eds., Turmeric: The genus Curcuma, CRC Press, Boca Raton, 2007. https://doi.org/10.1201/9781420006322.

[6] S. Naz, S. Ilyas, Z. Parveen, S. Javed, Chemical analysis of essential oils from turmeric (Curcuma longa) rhizome through GC-MS., Asian Journal of Chemistry. 22 (2010) 3153–3158.

[7] C. Araújo, L. Leon, Biological activities of Curcuma longa L., Mem. Inst. Oswaldo Cruz. 96 (2001) 723–728. https://doi.org/10.1590/S0074-02762001000500026.

[8] M. Škerget, P. Kotnik, M. Hadolin Kolar, A. Rižner Hraš, M. Simonič, Ž. Knez, Phenols, proanthocyanidins, flavones and flavonols in some plant materials and their antioxidant activities, in: Food Chemistry, 2005. https://doi.org/10.1016/j.foodchem.2004.02.025.

[9] T. Vatai, M. Škerget, Ž. Knez, Extraction of phenolic compounds from elder berry and different grape marc varieties using organic solvents and/or supercritical carbon dioxide, Journal of Food Engineering. 90 (2009) 246–254. https://doi.org/10.1016/j.jfoodeng.2008.06.028.

[10] L. Majhenič, M. Škerget, Ž. Knez, Antioxidant and antimicrobial activity of guarana seed extracts, in: Food Chemistry, 2007. https://doi.org/10.1016/j.foodchem.2007.01.074.

Transitiometry - Investigation of Individual Peroxide Decomposition Kinetics in Cocktails under High-Pressure

Svenja Albus, Markus Busch*

TU Darmstadt, Darmstadt/Germany, *markus.busch@pre.tu-darmstadt.de

Introduction

The global demand for plastics is still increasing nowadays, thereby polyethylene is one of the most produced polymers with an annual production of hundreds of mega tons per year. Low-density polyethylene (LDPE) is radically polymerized with pressures up to 3000 bar and temperatures up to 300 °C. On an industrial scale peroxide cocktails are utilized as initiating agents for radical polymerization processes resulting in smoother reaction starts and broader radical generation spectra. Multiple injections of peroxide mixtures can influence and regulate the polymer product properties, as well as the reactor productivity and conversion. However, not much is known or reported in the literature about the decomposition kinetics of peroxide cocktails under relevant process conditions. In order to be able to guarantee a defined product spectrum or to improve product properties, it is beneficial to understand the entire polymerization process, including the sub steps such as the decomposition of initiators. The high-pressure calorimetric method transitiometry provides a suitable method for investigating decomposition kinetics under process-relevant conditions.

Experimental

Transitiometry is a special calorimetric measurement technique that allows the investigation of thermophysical properties and thermodynamic behaviour under high-pressure and -temperature conditions. The three most important thermodynamic parameters temperature, pressure, and volume can be controlled during the whole measurement. All experiments were performed in the Standard Unit Transitiometer from BGR TECH. To study the decomposition of peroxide cocktails, mixtures of several peroxides are prepared in different solvents and placed in the sample cell of the transitiometer on a mercury column. The peroxides are measured by performing an isobaric temperature scan until all the peroxides have decomposed. The pressure is built up using a step motor which presses the almost incompressible mercury towards the

sample and the closure of the measuring cell. The heating rate for each measurement is 2 mK s^{-1}. The kinetic evaluation is performed by the Borchardt & Daniels method[1].

Preliminary results have shown that transitiometry provides a convenient method for investigating the decomposition kinetics of peroxides.[2] Comparative measurements of the decomposition of pure peroxides with the data of Buback[3] available in the literature have shown that similar values for kinetics and activation volumes were calculated. Therefore, it was continued to investigate different peroxide cocktails to compare the results with them of pure peroxides.

Figure 1 compares the decomposition signals and the calculated kinetics of three peroxides in a cocktail with those of the pure peroxides. The measurements were performed at 2000 bar with a heating rate of 2 mK s^{-1}. As repeat measurements coincide very well regarding peak shape and occurrence, it was assumed that the kinetic and chemical influence of the peroxides among each other can be represented with high reproducibility using transitiometry. To determine the kinetics of the peroxides in the cocktail separately, a method must first be developed to separate the overlapping decomposition signals from the others. For this purpose, the signals were first separated from each other using a deconvolution app in the analysis program Origin Pro®.

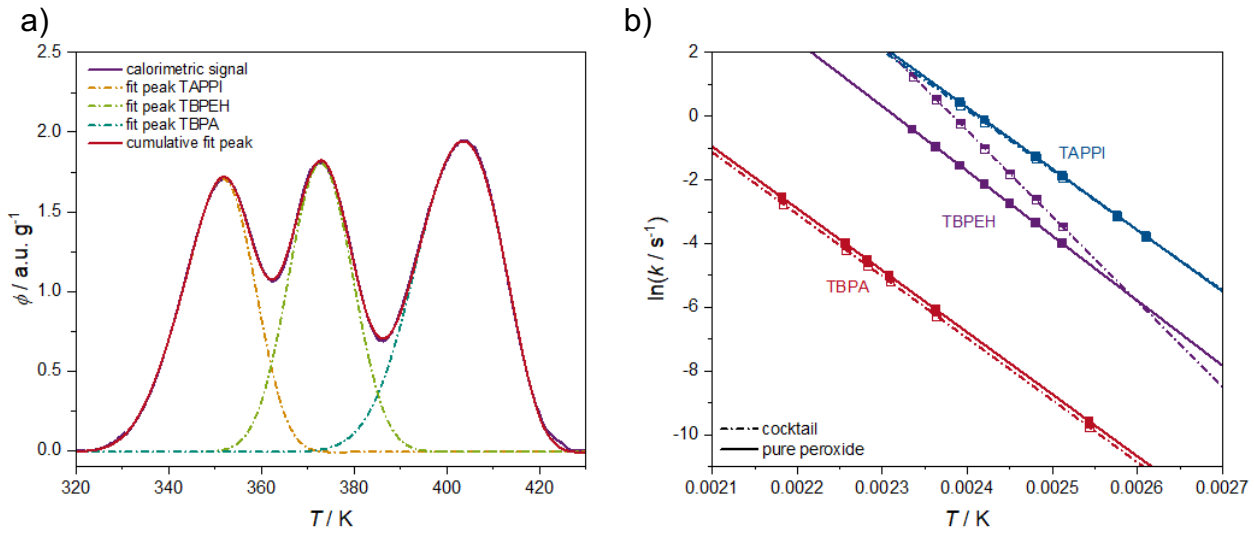

Fig. 1.: Cocktail containing tert-amyl-peroxypivalate (TAPPI), tert-butyl-2-ethyl-peroxy-hexanoate (TBPEH) and tert-butyl-peroxyacetate (TBPA) in squalane. **a)** Baseline corrected and mass normalized decomposition signals of the cocktail with marked separated signals of individual peroxides. **b)** Arrhenius plots for the decomposition of the peroxides in the respective cocktail compared to that of pure peroxides measured under same conditions.

The Arrhenius curves of the cocktail in Figure 1b displays a slight slowdown of the decomposition rate of TAPPI and TBPA in the cocktail compared to the single measurement and almost none for TAPPI. TBPEH behaves differently, the reaction in the cocktail appears faster and the change in decomposition rate is much more pronounced.

Following it was now possible to separate the overlapped signals of peroxides in cocktails and calculate their decomposition kinetics separately, further influences on the decomposition kinetics in cocktails were able to be investigated. One influence in this context relates to the weight fraction of the peroxide in the cocktail solution (Figure 2). Cocktails were examined by keeping the concentration of one peroxide constant and varying the concentration of the other one.

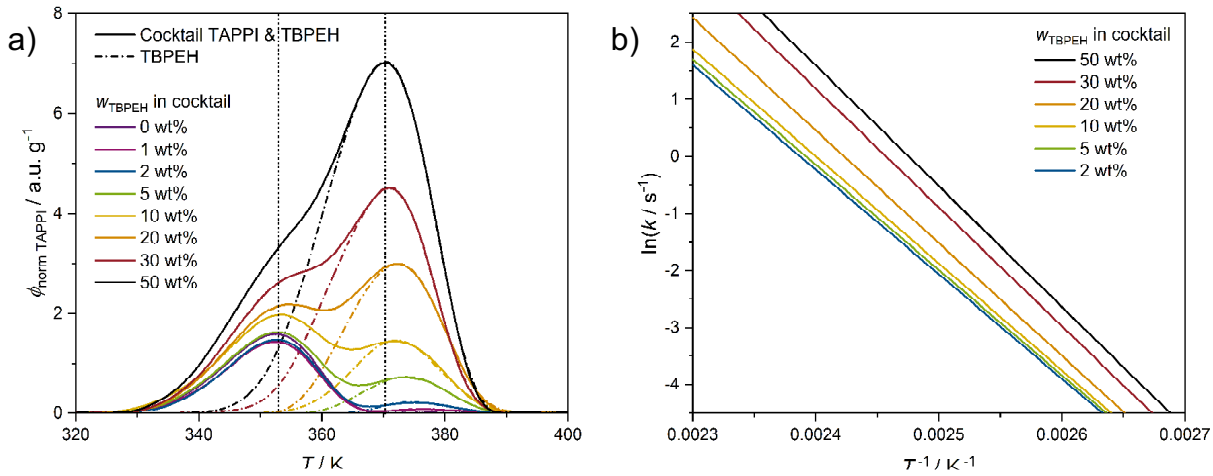

Fig. 2.: Cocktail with TAPPI and TBPEH in squalane. The measurements were performed at 2000 bar with a heating rate of 2 mK s^{-1}. **a)** Baseline corrected decomposition signals of the cocktail containing different weight fractions of TBPEH normalized to the mass of TAPPI. **b)** Arrhenius plots for the decomposition of TAPPI in the cocktail with different weight fractions of TBPEH.

Figure 2 illustrates the significant effect of the additional peroxide TBPEH on the decomposition of TAPPI in the cocktail. Thereby, only the weight fraction of TBPEH, the peroxide which decomposes at higher temperatures, was varied. The weight fraction of the low temperature decomposer TAPPI remained constant with 10 wt%. The higher the weight fractions of TBPEH the more the maxima of decomposition of both peroxides shifted towards each other and the faster the decomposition of TAPPI. TBPEH therefore possesses an accelerating effect on the decomposition of TAPPI.

Summary

In each of the cocktails studied so far, the maximum decomposition temperatures of the peroxides in the cocktails differ from those of the pure peroxides. The peroxide that decomposes at higher temperatures was consistently the most affected. In addition, the rate of decomposition was increased or decreased depending on the peroxides in the cocktail. The influence of weight fraction on the decomposition kinetics was also demonstrated by measuring peroxide cocktails with different peroxide amounts. Summarized it was observed that external influences such as chemical environment have an effect on the decomposition. The results also show that it is meaningful to consider each cocktail individually.

We acknowledge the generous support of United Initiators.

References

[1] H.J. Borchardt, F. Daniels, J. Am. Chem. Soc., **1957**, 79(1), 41-46.

[2] S. Albus et al., Journal of Solution Chemistry, **2023**, 1-17.

[3] M. Buback et al., Zeitschrift für Physikalische Chemie, **1999**, 210(2), 199–221.

Cascade Fractionation of Crustacean Shell Residues Preventing the Degradation of Chitin and its Subsequent Industrial Application

de-Souza Ribeiro, M.M.[1,2], Alonso, E.[1,2], Mato Chain R.[1,2], Loya-Pérez, H.[1,2], Casas-Gonzalez A.P.[1,2], Rodríguez-Rojo, S.[1,2]

[1] BioEcoUVa, Research Institute on Bioeconomy, PressTech Group, University of Valladolid, Pº Prado de la Magdalena 3-5, 47011, Valladolid, Spain

[2] Dpt. of Chemical Engineering and Environmental Technology, Escuela de Ingenierías Industriales (sede Mergelina), Universidad de Valladolid, Pº Prado de la Magdalena 3-5, 47011, Valladolid, Spain

mauriciomasaru.souza@uva.es

Introduction

According to the Food and Agriculture Organization (FAO) of the United Nations, by the year 2022, crustacean production represented 10% of all global production from fisheries and aquaculture [1]. The consumption and production of shrimps generates as residue the cephalothorax and its exoskeleton (shell) [2]. This shrimp shell represents approximately 47% (w/w) of the animal [2], and it is a potential source of waste in the production process, since in the molting process occurs the exchange of the shell, releasing the old shell. These molt shells are not commonly valorized, compared to the shell of the adult animal [3], that is currently used to obtain chitin and chitosan by harsh acid and alkaline treatments [4,5]. Moreover, the shell also contains other compounds of commercial interest, such as proteins (30-40%), minerals (mostly calcium carbonate, 20-30%) and lipid compounds in smaller proportion [6]. Besides that, the current process of obtaining chitin is not considered sustainable due to the use of high quantities of inorganic solvents and the impossibility of using the co-extracted compounds [2,7]. Within this context this work aims to develop a biorefining process to maximize the valorization of the shrimp (*Litopenaeus vannamei*) molt shell fractions using sustainable technologies such as high pressure and microwave assisted technologies for the reduction of environmental impact, with the subsequent use of the mineral-chitin composite as catalytic support.

Experimental

This project is divided into 5 stages, which were: the chemical and structural characterization of the shrimp shell, pre-treatment and extraction of the lipid fraction, extraction of proteins, study of the behavior of the mineral-chitin composite in sub and supercritical water, and application of the mineral-chitin composite as a catalyst support.

In the pretreatment and extraction of the lipid fraction, the conventional pretreatment process (by steam cooking) and drying in the oven, will be compared with the process employing microwave technology, using supercritical carbon dioxide extraction afterwards. In this step it will be aimed a faster drying process with the breaking of the bonds of the lipid fraction with the shell structure, for a better extraction.

In the protein extraction step, two extraction processes will be studied: microwave-assisted batch aqueous extraction, and continuous extraction with sub and supercritical water. As a parallel step to this, in the continuous process the stability of the mineral-chitin compound under sub and supercritical conditions will also be studied, evaluating its possible dissociation and subsequent, depolymerization and deacetylation of the chitin. After obtaining the mineral-chitin as a composite or separate materials, its application as a catalytic support for ruthenium will be studied.

Summary

This work has currently finished the chemical characterization of the biomass, and the physical-chemical structure is being analyzed by microscopic techniques, X-ray diffraction and Fourier transform infrared spectroscopy (FTIR). In parallel, the step of pretreatment and protein extraction with microwave-assisted technology is being carried out.

Based on the results obtained by chemical characterization (Tab. 1), it was possible to verify that the molt shell has a higher mineral content, compared to the chitin and protein content. This chemical distribution can be observed by FTIR (Fig. 1 - a) in which the shell spectrum more closely resembles the calcium carbonate spectrum, and in relation to XRD (Fig. 1 - b) in which the shell crystallinity more closely resembled the calcium carbonate crystallinity.

Tab. 1 - Chemical composition of the shrimp molt shell.

Component	Content (g/100 g of dried shell)
Ash	53.7 ± 0.5
Protein	10.6 ± 0.4
Free amino acid	1.37 ± 0.12
Fatty acid	3.8 ± 0.9
Chitin	17.8 ± 0.7

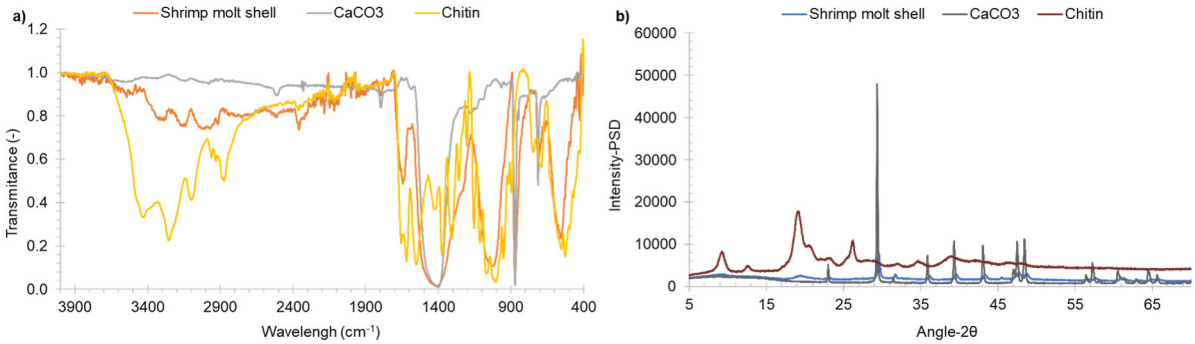

Fig. 1 - Comparison of shrimp molt shell structure with commercial calcium carbonate and chitin a) FTIR and b) XRD.

In the pretreatment and extraction part of the lipid fraction, the kinetic comparison between the drying process in a conventional oven at two temperatures (105 and 60 °C) and in a microwave oven at three powers (250, 440 and 600 W) is being carried out. For the extraction of proteins using microwaves, an experimental design is being carried out considering the variables temperature, isothermal time, and solvent-solid ratio (S/F).

Acknowledgment

This work/project (project PID2020-119481RA-I00) was supported by the Regional Government of Castilla y León and the EU-FEDER program (CLU-2019-04). M.M. de-Souza-Ribeiro thanks the Department of Education of the Regional Government of Castilla y León and the European Social Fund Plus (ESF+) for his doctoral grant.

References

[1] FAO, World Food and Agriculture – Statistical Yearbook 2022, FAO, Rome, 2022. https://doi.org/10.4060/cc2211en.

[2] N. Mezzomo, J. Martínez, M. Maraschin, S.R.S. Ferreira, Pink shrimp (P. brasiliensis and P. paulensis) residue: Supercritical fluid extraction of carotenoid

fraction, Journal of Supercritical Fluids. 74 (2013) 22–33. https://doi.org/10.1016/j.supflu.2012.11.020.

[3] P.T.D. Phuong, T.S. Trung, W.F. Stevens, N.C. Minh, H.N.D. Bao, N. Van Hoa, Valorization of Heavy Waste of Modern Intensive Shrimp Farming as a Potential Source for Chitin and Chitosan Production, Waste Biomass Valorization. 13 (2022) 823–830. https://doi.org/10.1007/s12649-021-01557-0.

[4] X. Hu, Z. Tian, X. Li, S. Wang, H. Pei, H. Sun, Z. Zhang, Green, Simple, and Effective Process for the Comprehensive Utilization of Shrimp Shell Waste, ACS Omega. 5 (2020) 19227–19235. https://doi.org/10.1021/acsomega.0c02705.

[5] M. Rinaudo, Chitin and chitosan: Properties and applications, Progress in Polymer Science (Oxford). 31 (2006) 603–632. https://doi.org/10.1016/j.progpolymsci.2006.06.001.

[6] W. Arbia, L. Arbia, L. Adour, A. Amrane, Chitin extraction from crustacean shells using biological methods -A review, Food Technol Biotechnol. 51 (2013) 12–25.

[7] H. El Knidri, R. Belaabed, A. Addaou, A. Laajeb, A. Lahsini, Extraction, chemical modification and characterization of chitin and chitosan, Int J Biol Macromol. 120 (2018) 1181–1189. https://doi.org/10.1016/j.ijbiomac.2018.08.139.

Development of an Automatic Method for Measuring Melting Point under Carbon Dioxide Pressure

Dóra Arany, Márton Kőrösi, Edit Székely

Department of Chemical and Environmental Process Engineering, Faculty of Chemical Technology and Biotechnology, Budapest University of Technology and Economics, Műegyetem rkp. 3., H-1111 Budapest, Hungary

arany.dora@edu.bme.hu

Introduction

High pressure processes play a crucial role in various technological applications for example extraction and polymer processes. One of the advantages of supercritical fluids is the possibility of adjusting thermodynamic properties by varying the operating pressure and temperature. [1] Therefore measuring and modelling solubility, vapor-liquid, and solid-liquid-gas (S-L-G) phase equilibrium in high-pressure media are needed for supercritical fluid process design.

During the investigation of S-L-G phase equilibrium, a decrease in melting point can often be observed. [2] The change in melting temperature caused by high-pressure carbon dioxide is used in preliminary parameter-estimation of high-pressure processes, for example in case of PGSS (food industry [3] , pharmaceutical research [4], etc…) and polymer processing [5]. Determining melting temperature in a pressurized medium is always challenging because it is usually only possible with equipment that is difficult to access and requires a lot of expertise. The most common measurement methods are based on visual observation [6]–[10], but the most information is carried by high-pressure differential calorimetry (DSC) [11], [12] and transitiometry [13].

An alternative method was developed in which melting temperature measurements were taken in a fixed volume view cell. During the measurement pressure was recorded as a function of temperature. The first freezing point method was used, and a sharp pressure increase during freezing was observed. [14]

Our aim was to develop a new, automated method for determining melting temperature in a pressurized atmosphere. Measurement results should be as independent from the operator as possible, and installation should be cheaper than the currently used equipments. To increase sensitivity, the new method is based on detecting pressure difference between a reference cell and a sample-holder during melting and freezing under high-pressure carbon dioxide.

Experimental

We are working on the development of a new and automated measuring device and method, which is suitable to study S-L-G phase-equilibria in a pressurized medium in a time-efficient and objective way. The operation of the new device is based on the pressure change that occurs during melting, which is the consequence of the dissolution of the medium into the melt of the solid sample. [14] During the measurement, the pressure difference between a reference and a sample-holder cell (containing solid material) is recorded. With a gradual heating, pressure difference changes, but when the sample starts to melt, the pressure in the sample-holder decreases due to the dissolution of the medium into the melt of the solid sample. This change in the pressure difference can be detected as a function of the temperature by a differential pressure-transmitter. The schematic picture of the device is shown in Fig. 1.

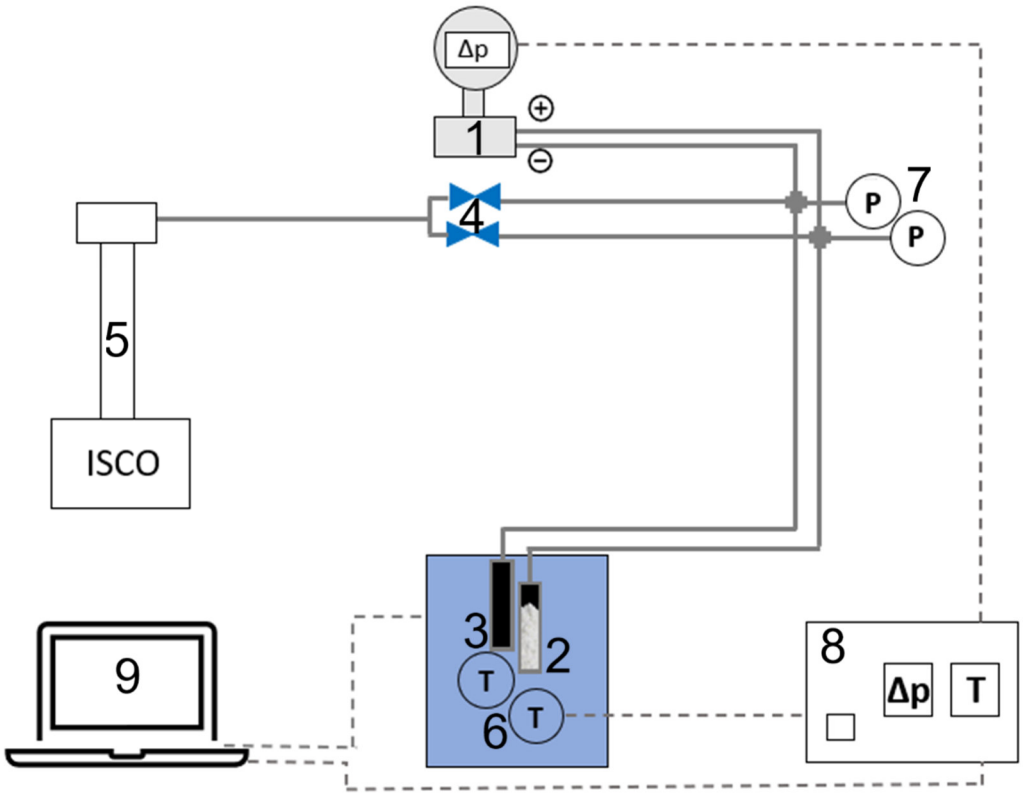

Fig 1.: The schematic depiction of the device: 1. Differential pressure-transmitter, 2. Reference cell, 3. Sample holder cell, 4. Filling valve, 5. ISCO 260D syringe pump, 6. Thermometers, 7. Pressure gauges 8. Data logger, 9. Computer

An algorithm was developed for processing the registered time – temperature – pressure difference data, which enables the automated determination of the initial (onset) and final (offset) temperature of melting. The detailed evaluation showed that the results of the measurements from the literature and the high-pressure view cell can be precisely reproduced by the new device. In Fig. 2 one typical result of the evaluation is shown. We

use the first melting point method in our measurements, so in this case the melting temperature is the onset value.

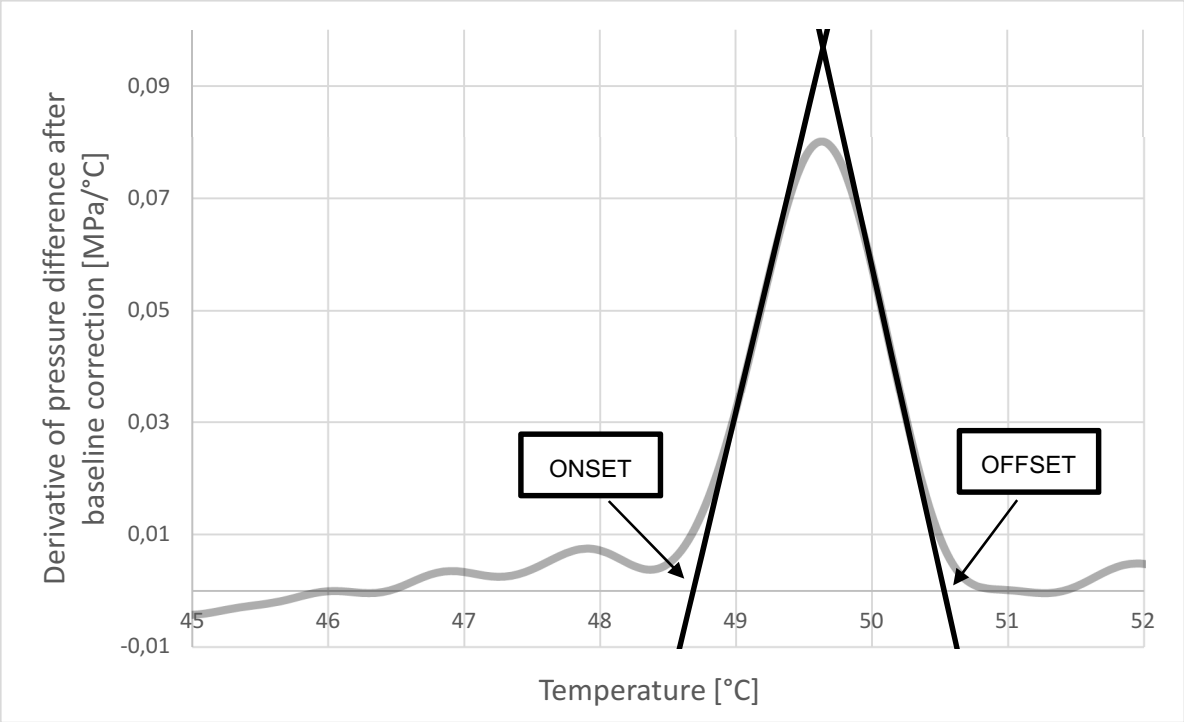

Fig 2.: A typical result of the evaluation

The device has already been validated with ibuprofen and benzoic acid. Before the validating measurements, the chosen samples were investigated also in a variable volume high-pressure view cell in our laboratory. Various compounds were investigated previously in our research group with this device, and we found that it is suitable for accurate melting temperature measurements. [8], [15] Beside measurements in a high-pressure view cell, melting temperature data of the chosen compounds under carbon dioxide pressure are also available in the literature. [16]–[19]

Summary

The newly developed method provides an easily automated and precise possibility to investigate S-L-G phase equilibria under high-pressure carbon dioxide. The new device has been shown to be suitable for measuring the melting temperature of simple crystalline compounds in high pressure media, but more complex systems have not been investigated yet. In addition to further development of the device, we would like to investigate the melting behaviour of for example chiral compounds and polymer-drug systems in the future.

Acknowledgment

This work was supported by the New National Excellence Program of the Ministry of Culture and Innovation, financed by the National Research, Development and Innovation Fund. (Personal reference number ÚNKP-22-2-III-BME-91).

Project no. 2019-1.3.1-KK-2019-00004 has been implemented with the support provided by the National Research, Development and Innovation Fund of Hungary, financed under the 2019-1.3.1-KK funding scheme.

Dóra Arany thanks the ERASMUS+ BIP funding (Project number: 2022-1-AT01-KA131-HED-000052815) for the opportunity of participating in "The European Summer School in High Presssure Technology".

References

[1] Knez, E. Markočič, M. Leitgeb, M. Primožič, M. Knez Hrnčič, and M. Škerget, “Industrial applications of supercritical fluids: A review,” *Energy*, vol. 77, pp. 235–243, Dec. 2014, doi: 10.1016/j.energy.2014.07.044.

[2] K. Fukné-Kokot, A. König, Ž. Knez, and M. Škerget, “Comparison of different methods for determination of the S-L-G equilibrium curve of a solid component in the presence of a compressed gas,” *Fluid Phase Equilib*, vol. 173, no. 2, pp. 297–310, May 2000, doi: 10.1016/S0378-3812(00)00437-4.

[3] E. Weidner, “High pressure micronization for food applications,” *Journal of Supercritical Fluids*, vol. 47, no. 3, pp. 556–565, Jan. 2009, doi: 10.1016/J.SUPFLU.2008.11.009.

[4] M. Fraile *et al.*, “Production of new hybrid systems for drug delivery by PGSS (Particles from Gas Saturated Solutions) process,” *Journal of Supercritical Fluids*, vol. 81, pp. 226–235, 2013, doi: 10.1016/J.SUPFLU.2013.06.010.

[5] Ž. Knez, M. K. Hrnčič, and M. Škerget, “Particle Formation and Product Formulation Using Supercritical Fluids,” *Annu Rev Chem Biomol Eng*, vol. 6, pp. 379–407, Jul. 2015, doi: 10.1146/annurev-chembioeng-061114-123317.

[6] O. N. Ciftci and F. Temelli, “Melting point depression of solid lipids in pressurized carbon dioxide,” *Journal of Supercritical Fluids*, vol. 92, pp. 208–214, 2014, doi: 10.1016/j.supflu.2014.05.009.

[7] D. Hua *et al.*, “A high-pressure polar light microscopy to study the melt crystallization of myristic acid and ibuprofen in CO2,” *Journal of Supercritical Fluids*, vol. 87, pp. 22–27, Mar. 2014, doi: 10.1016/j.supflu.2013.12.023.

[8] M. Kőrösi, J. Béri, D. Arany, C. Varga, and E. Székely, “Experimental investigation of chiral melting phase diagrams in high-pressure CO2 containing organic modifiers,” *Journal of Supercritical Fluids*, vol. 178, Dec. 2021, doi: 10.1016/J.SUPFLU.2021.105352.

[9] Z. Lian, S. A. Epstein, C. W. Blenk, and A. D. Shine, “Carbon dioxide-induced melting point depression of biodegradable semicrystalline polymers,” *J. of Supercritical Fluids*, vol. 39, pp. 107–117, 2006, doi: 10.1016/j.supflu.2006.02.001.

[10] A. M. Scurto *et al.*, “Melting point depression of ionic liquids with CO2: Phase equilibria,” *Ind Eng Chem Res*, vol. 47, no. 3, pp. 493–501, 2008, doi: 10.1021/ie070312b.

[11] S. Spilimbergo, G. Luca, N. Elvassore, and A. Bertucco, “Effect of high-pressure gases on phase behaviour of solid lipids,” *Journal of Supercritical Fluids*, vol. 38, no. 3, pp. 289–294, Oct. 2006, doi: 10.1016/J.SUPFLU.2005.11.016.

[12] V. Kutcherov and A. Chernoutsan, “Crystallization and glass transition in crude oils and their Fractions at high pressure,” *Int J Thermophys*, vol. 27, no. 2, pp. 474–485, Mar. 2006, doi: 10.1007/S10765-005-0005-2.

[13] S. L. Randzio, “Scanning Transitiometry,” 1996. doi: 10/3/2022 8:39:14 AM.

[14] S. González-Arias, F. J. Verónico-Sánchez, O. Elizalde-Solis, A. Zúñiga-Moreno, and L. E. Camacho-Camacho, “An enhanced ‘first freezing point’ method for solid-liquid-gas equilibrium measurements in binary systems,” *Journal of Supercritical Fluids*, vol. 104, pp. 301–306, Aug. 2015, doi: 10.1016/J.SUPFLU.2015.07.009.

[15] M. Korösi, J. Béri, A. Hanu, S. Kareth, and E. Székely, “High-pressure melting equilibrium of chiral compounds: A practical study on chlorinated mandelic acids under carbon dioxide atmosphere,” *Journal of CO2 Utilization*, vol. 37, pp. 173–179, Apr. 2020, doi: 10.1016/j.jcou.2019.11.026.

[16] H. Uchida, M. Yoshida, Y. Kojima, Y. Yamazoe, and M. Matsuoka, “Measurement and Correlation of the Solid-Liquid-Gas Equilibria for the Carbon Dioxide + S-(+)-Ibuprofen and Carbon Dioxide + RS-Ibuprofen Systems,” 2005, doi: 10.1021/je034228o.

[17] J. Hong, D. Hua, X. Wang, H. Wang, and J. Li, “Solid-liquid-gas equilibrium of the ternaries ibuprofen + myristic acid + CO2 and ibuprofen + tripalmitin + CO2,” *J Chem Eng Data*, vol. 55, no. 1, pp. 297–302, Jan. 2010, doi: 10.1021/JE900342A/ASSET/IMAGES/LARGE/JE-2009-00342A_0003.JPEG.

[18] E. Bertakis *et al.*, “Measurement and thermodynamic modeling of solid-liquid-gas equilibrium of some organic compounds in the presence of CO2,” *Journal of Supercritical Fluids*, vol. 41, no. 2, pp. 238–245, Jun. 2007, doi: 10.1016/J.SUPFLU.2006.10.003.

[19] K. Fischer, M. Wilken, and J. Gmehling, “The effect of gas pressure on the melting behavior of compounds,” *Fluid Phase Equilib*, vol. 210, no. 2, pp. 199–214, 2003, doi: 10.1016/S0378-3812(03)00180-8.

Bioremediation of Water Polluted with Microplastics by Bacteria Isolated from the Environment Enriched with Microplastics

Martina Miloloža, Kristina Bule Možar, Viktorija Martinjak, Matija Cvetnić, Marinko Markić, Šime Ukić, Tomislav Bolanča, Dajana Kučić Grgić

University of Zagreb Faculty of Chemical Engineering and Technology, Department of Industrial Ecology, miloloza@fkit.hr

Introduction

Microplastics are considered a priority pollutant because they are increasingly found in aquatic media such as oceans[1], seas[2], surface waters[3], as well as in sediments[4], soils[5], and even on Arctic ice[6], and in drinking and tap water[7]. Microplastics are polymer particles smaller than 5 mm and are divided into primary and secondary microplastics. Primary microplastics are formed during industrial production, and when released into the environment, they degrade through physical, chemical, and biological processes into smaller particles that form secondary microplastics. There are numerous sources of microplastics in the environment, including industry (plastic residues after industrial production of polymers, the automotive, textile, and cosmetics industries), households, municipal wastewater, wastewater treatment plants, treated wastewater, the abrasion of tires during transportation, and the decomposition of macroplastics[2,6,8]. Microplastics enter the oceans through surface waters. The main sources of microplastics in the ocean are coastal and marine human activities, tourism, and fisheries[9]. In addition, hydrogeological influences (water movement, winds, soil runoff) promote the boundaryless spread of microplastics[3]. Microplastic concentration is expressed as the number of microplastic particles per volume for aquatic media and as the number of microplastic particles per kg dry or wet mass for soils and sediments[6]. Concentrations of microplastics in the environment depend on the type of polymer and environment, climatic conditions, level of development, and standard of living. Microplastics occur in the environment in various forms, such as beads, fragments, fibers, films, foams, and spherical particles[10]. The most commonly produced and used polymer types are polyethylene (PE), polypropylene (PP), polyvinyl chloride (PVC), polyethylene terephthalate (PET) and polystyrene (PS).

Microplastics pose a problem because they remain in the environment for a long time, are insoluble in water, are difficult to degrade, the polymers have a complex composition,

hydrophobic pollutants adsorbed on microplastics can be transferred, have effects on aquatic organisms with the possibility of bioaccumulation, enter the food chain, and can affect human health[11,12]. Biodegradation is an economical, efficient and environmentally friendly process for removing pollutants from the environment. This process of degradation of pollutants is based on the use of microorganisms in terms of their enzymatic composition. It leads to the degradation of the substrate into the final products CO_2, H_2O and other inorganic molecules with the release of energy and the growth of microorganisms[13]. Microorganisms can be isolated from different media such as soil, sediment, compost, activated sludge, wastewater, surface water, seawater, and landfills[13,14]. The diversity and abundance of microorganisms in different media varies, and it is necessary to study their characteristics for the application of bioremediation in these fields. From the available literature, the most studied microorganisms for microplastic degradation are bacteria and molds, while yeasts are less represented. Bacteria of the genera *Bacillus*[15,16], *Brevibacillus*[15], *Comamonas*[17], *Clostridium*[17], *Micrococcus*[17], *Pseudomonas*[15,16], *Rhodococcus*[18], *Streptomyces*[17], *Microbacterium*[19] and molds of the genera *Aspergillus*[9,15], *Curvularia*[20], *Fusarium*[21], *Paecilomyces*[20], *Penicillium*[20], *Polyporus*[20], *Rhizopus*[20], *Trichoderma*[9] were tested with respect to the biodegradation of microplastics. Generally, biodegradation is influenced by numerous conditions - abiotic, biotic, and polymer properties[21].

Experimental

Microplastics

Microplastics were obtained by grinding plastic disposable accessories like spoons for PS and plastic box for PVC. These materials were, firstly, cut into smaller pieces with scissors and then ground in cryo-mill (Retsch, Haan, Germany) accompanied with liquid nitrogen and dried on the air during 24/48 h at room temperature. Obtained particles were sieved on stainless steel screens (W. S. Tyler RX-86-1 Sieve shaker, USA) to isolate those particles in size ranges: 500-700 μm, 300-500 μm and 100-300 μm. After sieving, the particles were stored in glass bottles. Before the experiments, microplastic particles were sterilized in 100-mL flasks containing 70% ethanol during 10 min on rotary shaker (Heidolph unimax 1010, Heidolph incubator 1000, Germany) at 160 rpm. Particles were separated from the ethanol by vacuum membrane filtration (through cellulose nitrate 0.45 μm sterile filter (Ahlstrom ReliaDiscTM) and additionally washed with sterile deionised water.

Bacteria

Bacteria *Bacillus cereus* and *Delftia acidovorans* were isolated from the activated sludge and river sediment, respectively. Bacteria were cultivated on nutrient agar at 37 ºC during 24 hours.

Biodegradation experiments

The experiments were conducted in Erlenmeyer flasks volume of 250 mL, with working volume of 100 mL, during 30 days at the thermostatic rotary shakers (Heidolph unimax 1010, Heidolph incubator 1000, Germany). Temperature (25±0.2 ºC) and agitation speeds were set on the rotary shakers. The flasks contained mineral medium, bacterial suspension and PS and PVC particles. These experiments were performed by full factorial design and three factors were investigated at three levels. Microplastics concentration (50-1000 mg/L), particle size (100-700 μm) and agitation speed of the rotary shaker (100-200 rpm)/optical density (OD) of bacterial suspension (0.1-0.5) were three test factors in the biodegradation experiment of PS and PVC by *Bacillus cereus*, respectively. In the experiments with *Delftia acidovorans* the three test factors were pH (6-8), agitation speed (100-200 rpm) and OD (0.1-0.5) for both PS and PVC. During the experiments, the number of living cells of bacteria was determined. Microplastic particles were characterized by FTIR spectroscopy. Control flasks without microplastics were, also, set in the purpose of monitoring bacterial growth.

Summary

Increased standard of living and comfortable lifestyle require extensive use and production of plastic products. Microplastics are a pollutant that is of concern to the scientific community because of its ubiquitous presence in the environment. Sources of microplastics are numerous, and exposure to aquatic organisms is increasing, so a risk assessment is needed. Although plastics are considered as non-biodegradable, microplastics can be removed from the environment by bioremediation. Biodegradation of microplastics can be achieved by different groups of microorganisms, such as bacteria, mold and yeast, or by a mixed consortium. Enhancement of the biodegradation process is possible by various pre-treatments of microplastics, such as biostimulation of microorganisms, or a combination of degradation processes. Economical, efficient and environmentally friendly bioremediation provides many possibilities and solutions for microplastic removal. In this work, bioremediation of water contaminated with microplastics using bacteria, which were isolated from environmental samples enriched

with microplastics, were conducted. The research was conducted according to the full factorial design. The main purpose of these experiments was determination of optimal conditions for biodegradation of PS and PVC by bacteria. Optimal conditions for biodegradation of PS by *Bacillus cereus* were 66.20 mg/L, 413.29 μm, and 100.45 rpm, while for PVC were 658.40 mg/L, 400.00 μm, and OD = 0.40. In the case with *Delftia acidovorans*, optimal conditions were achieved at: pH = 7.99, 104.93 rpm, and OD = 0.46 for PS, and pH = 8.00, 200.00 rpm, and OD = 0.50 for PVC. According to the performed experiments, these environmental bacteria are suitable for application for the purpose of bioremediation of microplastics.

Key words: microplastics, bacteria, *Bacillus cereus*, *Delftia acidovorans*, Full Factorial design

Acknowledgment

The authors would like to acknowledge the financial support of the Croatian Science Foundation through project entitled Advanced Water Treatment Technologies for Microplastics Removal (**AdWaTMiR**) (IP-2019-04-9661).

References

1. Shan J, Zhao J, Liu L, Zhang Y, Wang X, Wu F. A novel way to rapidly monitor microplastics in soil by hyperspectral imaging technology and chemometrics. Environ Pollut 2018;238:121-129.
2. Auta HS, Emenike CU, Fauziah SH. Distribution and importance of microplastics in the marine environment: A review of the sources, fate, effects, and potential solutions. Environ Int 2017;102:165-176.
3. Li J, Liu H, Chen JP. Microplastic in freshwater systems: A review on occurrence, environmental effects, and methods for microplastics detection. Water Res 2018;137:362-374.
4. Bergmann M, Wirzberger V, Krumpen T, Lorenz C, Primpke S, Tekman MB, Gerdts G. High quantities of microplastic in arctic deep-sea sediments from the hausgarten observatory. Environ Sci Technol 2017;51:11000-11010.
5. He D, Luo Y, Lu S, Liu M, Song Y, Lei L. Microplastics in soils: Analytical methods, pollution characteristics and ecological risks. TrAC 2018;109:163-172.

6. Bond T, Ferrandiz-Mas V, Felipe-Sotelo M, van Sebille E. The occurrence and degradation of aquatic plastic litter based on polymer physicochemical properties: A review. Crit Rev Environ Sci Technol 2018;48:685-722.
7. Gong J, Kong T, Li Y, Li Q, Li Z, Zhang J. Biodegradation of microplastic derived from poly(ethylene terephthalate) with bacterial whole-cell biocatalysts. Polymers 2018;10:1-13.
8. Rodrigues MO, Gonçalves AMM, Gonçalves FJM, Nogueira H, Marques JC, Abrantes N. Effectivness of a methodology of microplastics isolation for environmental monitoring in freshwater systems. Ecol Indic 2018;89:488-495.
9. Urbanek AK, Rymowicz W, Mironczuk AM. Degradation of plastic and plastic-degrading bacteria in cold marine habitats. Appl Microbiol Biotechnol 2018;102:7669-7678.
10. Silva AB, Bastos AS, Justino CIL, da Costa JP, Duarte AC, Rocha-Santos TAP. Microplastics in the environment: Challenges in analytical chemistry – A review. Anal Chim Acta 2018;1017:1-19.
11. Ng E-L, Huerta Lwanga E, Eldridge SM, Johnston P, Hu H-W. Geissen V et al. An overview of microplastic and nanoplastic pollution in agroecosystems. Sci Total Environ 2018;627:1377-1388.
12. Zhang S, Wang J, Liu X, Qu F, Wang X, Wang X, Li Y, Sun Y. Microplastics in the environment: A review of analytical methods, distribution and biological effects. TrAC 2019.
13. Tokiwa Y, Calabia BP, Ugwu CU, Aiba S. Biodegradability of plastics. Int J Mol Sci. 2009;10:3722-3742.
14. Roohi Bano K, Kuddus M, Zaheer MR, Zia Q, Khan MF, Ashraf GM, Gupta A, Aliev G. Microbial enzymatic degradation of biodegradable plastics. Curr Pharm Biotech 2017;18:1-13.
15. Muhonja CN, Makonde H, Magoma G, Imbuga M. Biodegradability of polyethylene by bacteria and fungi from Dandora dumpsite Nairobi-Kenya, PLOS One 2017;13:e0198446.
16. Mohan AJ, Sekhar VC, Bhaskar T, Madhavan Nampoothiri K. Microbial assisted high impact polystyrene (HIPS) degradation. Biosour Techn 2016;1-19.
17. Pathak VM, Navneet. Review on the current status of polymer degradation: a microbial approach. Bioresour Bioprocess 2017;4:1-31.
18. Mor R, Sivan A. Biofilm formation and partial biodegradation of polystyrene by the actinomycete *Rhodococcus ruber*. Biodeg 2008;19:851-858.

19. Atiq N, Ahmed S, Ali MI, Andleeb S, Ahmad B, Robson G. Isolation and identification of polystyrene biodegrading bacteria from soil. African J Microbiol Res 2010;4:1537-1541.
20. Kim DY, Rhee YH. Biodegradation of microbial and synthetic polyesters by fungi. Appl Microbiol Biotechnol 2003;61:300-308.
21. Hasan F, Shah AA, Hameed A, Ahmed S. Synergistic effect of photo- and chemical treatment on the rate of biodegradation of low density polyethylene by *Fusarium* sp. AF4. J App Polymer Sci 2007;105:1466-1470.

Modeling of Grafted LDPE Copolymers with a Reactor Combination and Comparison to Analytical Results from Thermal Fractionation

Julian Kirsch, Nicola Schreiner, Markus Busch*

TU Darmstadt, Darmstadt/Germany, *markus.busch@pre.tu-darmstadt.de

Introduction

Low-density polyethylene (LDPE) is one of the most frequently produced polymers. It is produced under high temperatures and pressures up to 300 °C and 3500 bar via free radical polymerization in bulk [1]. Characterized by its long-chain branching density, it possesses low temperature impact toughness and impact resistance since the long chain branches can entangle under stress [2]. In addition, backbiting reactions occur during polymerization leading mainly to butyl side chains within the polymer structure [3]. The number of short-chain branches thus determines the degree of crystallinity of the polymer and has a direct influence on the density and melting behavior of the polymer [4]. By the introduction of comonomer additional short side chains are incorporated in the polymer which have an effect on the crystallinity of the polymer.

Experimental

To investigate the influence of additionally fed comonomers to the crystallinity and the microstructure of the resulting LDPE-copolymer a combination of an autoclave reactor and a tubular-tail reactor in mini-plant scale is used. In this setup it is possible to feed the comonomer butyl acrylate into the autoclave as well as into the tubular tail separately or combined. With this comonomer-rich side chains can be grafted on a polyethylene backbone to obtain gradients in the comonomer content distribution. Samples may then be analyzed by size-exclusion chromatography (SEC) to determine their molecular weight distribution (MWD) and their comonomer content distribution (CCD). To get information on the degree of crystallinity of the polyethylene-co-butyl acrylate differential scanning calorimetry (DSC) can be used. If thermal fractionation is subsequently carried out, it is also possible to obtain information about chain heterogeneities and the distribution of short-chain branches. A thermal fractionation protocol can be performed using a standard differential scanning calorimeter called SSA (successive self-nucleation and annealing). In this method, polymer chains of different crystallinity are never physically separated,

which is why this technique is sensitive to linear and uninterrupted chain sequences, or methylene sequence lengths (MSL) [5].

Modeling

The analytical results are compared with a hybrid stochastic modeling approach. This approach includes both deterministic and stochastic modeling. The deterministic simulation is performed in the commercially available program Predici®. It solves the differential equation system resulting from the reaction network of the polymerization numerically. The resulting reaction frequencies are required as starting point for the stochastic simulation applying a Monte Carlo algorithm based on a single molecule approach. In addition to the molecular weight distribution of the ensemble of molecules, the algorithm obtains the exact topology for each individual polymer.

Since methylene sequence length distributions (MSLDs) can be obtained by SSA, it is possible to compare these MSLDs to the length of segments generated by the Monte Carlo algorithm. This approach allows polymers with identical comonomer content but different CCDs within their microstructure to be distinguished both analytically and in modeling. Last an algorithm based on the random-walk-theory can be applied to the topologies preserved. The combined approach allows the specific structure of each polymer of the entire ensemble to be visualized and polymer specific parameters such as the radius of gyration to be derived.

Summary

In this work, the heterogeneity of special grafted LDPE polymers is investigated. For that a reactor combination in mini-plant scale is used to synthesize samples first. These are analyzed regarding CCD and crystallinity with SEC and a thermal fractionation technique. The results are also used to validate a hybrid stochastic modeling approach which is able to predict the exact microstructure of the polymers.

References

[1] K. S. Whiteley, Polyethylene. Ullmann’s encyclopedia of industrial chemistry, Wiley-VCH Verlag GmbH & Co. KGaA, Weinheim, 2012.

[2] M. A. Rodrguez-Prez, A. Duijsens, J. A. de Saja, J. Appl. Polym. Sci. 1998, 68, 1237.

[3] E. F. McCord, W. H. Shaw, R. A. Hutchinson, Macromolecules 1997, 30, 246.

[4] A. H. Willbourn, J. Polym. Sci. 1959, 34, 569.

[5] A. J. Müller, M. L. Arnal, Progress in Polymer Science 2005, 30, 559.

Construction of a Pilot Plant for the Reduction of CO_2 Captured by Amines

Goicoechea Torres A, Dos Santos LC, Quintana L., Ciordia V, Almarza M, Martín Á, Bermejo MD,

BioEcoUva Research Institute on Bioeconomy, High Pressure Process Group, Department of Chemical Engineering and Environmental technology, Universidad de Valladolid, Valladolid, 47011, Spain

Corresponding author email: alberto.goicoechea@uva.es

Abstract

There is growing concern about the increasing levels of CO_2 in the atmosphere, prompting efforts to reduce CO_2 emissions and develop methods for its capture. The PressTech research group at Universidad Valladolid has made significant advancements in converting CO_2 collected in aqueous solutions [1]. Recently, they have demonstrated a novel approach where gaseous hydrogen can be used as a reductant to immediately convert CO_2 captured by amines into formic acid without the need for intermediate separation or purification steps. By utilizing amines such as 2-amino-2-methyl-1-propanol and 3-amino-1-propanol, this reaction can be successfully carried out within residence times of 60 to 120 minutes and at temperatures ranging from 70 to 125°C. Optimizing the reaction duration, temperature, and hydrogen pressure yields formic acid in the range of 30 to 67%.

Considering the reliability of the CO_2 capture by amines technique and the increasing availability of green hydrogen, this method holds immense promise. The PressTech group is actively focused on scaling up the process and is currently developing a pilot plant that integrates the various stages of the procedure, including absorption, reaction, separation of the formed formic acid, and recovery and recirculation of the amine.

Introduction

In light of the escalating concerns surrounding the accumulation of CO_2 in the atmosphere, the development of effective strategies for CO_2 capture and conversion has become an urgent priority. Addressing this critical issue, the PressTech research group at Universidad Valladolid has made remarkable progress in devising a highly promising solution for the conversion of CO_2 into formic acid. Their innovative approach involves the use of amines

and gaseous hydrogen as a reductant, eliminating the need for intermediate separation or purification steps. Notably, this method has achieved impressive formic acid yields ranging from 30% to 67%.

Driven by the potential of this breakthrough, the PressTech group has now shifted their focus towards scaling up the process and designing a pilot plant that seamlessly integrates the multiple stages of absorption, reaction, separation, and the recovery/recirculation of the amine. This concerted effort aims to pave the way for large-scale implementation of this novel approach. The reliability of CO_2 capture by amines, coupled with the anticipated future availability of green hydrogen, underpins the immense promise of this method in combating the rising CO_2 levels and mitigating their environmental impact.

Experimental

Materials

This study investigated CO_2 capture using two different amines, namely 2-amino-2-methyl-1-propanol (≥95%) and 3-amino-1-propanol (99%), both purchased from Sigma Aldrich (Spain). The catalyst used in all experiments was Pd/C with a 5% Pd content, also obtained from Sigma Aldrich (Spain). Formic acid standards for calibration were prepared using formic acid (~98%) from Sigma Aldrich. The gases CO_2, N_2, and H_2 with a purity of 5.0 were purchased from Linde. No additional treatment or purification was performed on the reagents before use.

Experimental Methods

CO_2 Capture

In this study, CO_2 was captured using two different aqueous amine solutions. For the 2-amino-2-methyl-1-propanol solution, a 5%wt amine concentration in MilliQ H_2O was prepared. For the 3-amine-1-propanol solution, the amine concentration in MilliQ H_2O was 3.7%wt. The CO_2 was then bubbled through 100 g of each amine solution for a duration of 30 to 35 minutes at a flow rate of approximately 1.7 L/min, maintaining room pressure and temperature. This loading time resulted in a CO_2 concentration of 0.5±0.05 M in both amine solutions.

CO_2 Conversion

The hydrogenation of the captured CO_2 in both the 2-amino-2-methyl-1-propanol and 3-amine-1-propanol solutions was performed in a 25 mL Parr reactor placed on a magnetic plate. Initially, a magnetic stirrer and 0.05 g of Pd/C catalyst were added to the reactor. Then, 10 mL of the amine solution was introduced, and the reactor was sealed. Prior to filling the reactor with H_2, it was purged three times with 5 bar of N_2 each time. After releasing the N_2, the reactor was purged twice with 5 bar of H_2. Subsequently, the reactor was pressurized with H_2 to the desired reaction pressure. The heating and stirring at 700 rpm were initiated, marking the start of the reaction time. The desired reaction temperature was achieved within 3 to 5 minutes, depending on the selected temperature. After the reaction, the reactor was cooled in an ice bath to halt the reaction. Then, the reactor was depressurized, and a liquid sample was collected.To ensure reproducibility, the experiments were repeated.

Sample Analysis

The concentration of CO_2 in the amine solution was determined by analyzing the inorganic carbon content using a Total Organic Carbon Analyzer (TOC-V CHS) from Shimadzu. The software used for analysis was TOC-Control V Version 2.30, also from Shimadzu. A 100 ppm standard of total inorganic carbon was prepared by mixing $NaHCO_3$ and Na_2CO_3.

Liquid samples obtained after the reaction were analyzed using an HPLC system composed of a binary HPLC pump (Waters 1525), an autosampler (Waters 717 plus), and a refractive index (RI) detector (Waters 2414 Refractive Index Detector) from Waters. The column employed was a Rezex-ROA-Organic Acid column (8% pore size, 300x7.8 mm) from Phenomenex. Before analysis, all samples were filtered through a 0.22 µm filter. The mobile phase consisted of a 5 mM H_2SO_4 solution, flowing at a rate of 0.5 mL/min. The column temperature was maintained at 40 ºC, while the detector temperature was set at 30 ºC. The HPLC method had a total runtime of 60 minutes.

Results

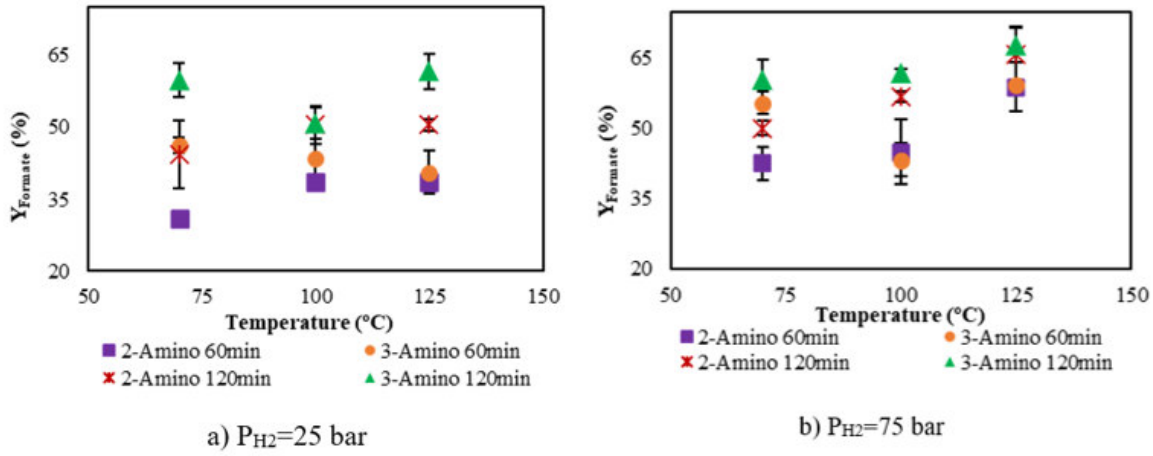

Figure 1. Yield to formate at different reaction temperatures. CO_2 captured with 2-amino-2-methyl-1-propanol and 3-amino-1-propanol aqueous solutions. Reaction conditions: reactor filling: 40%, mass of Pd/C catalyst: 0.05 g. a) H_2 pressure: 25 bar; b) H_2 pressure: 75 bar. Error bar with a standard deviation < 1.5 are not appreciated in the figure.

The results shown in Figure 3a, and 3b indicate that higher pressures and longer reaction times lead to higher yields of formate formation. At 120 minutes of reaction time, the yields were higher compared to 60 minutes. The highest observed yield was 68% with 3-amino after 120 minutes of reaction at a H_2 pressure of 75 bar, while under the same conditions, 2-amino yielded 66% of formate. At 60 minutes, the yields were 59% in both cases (Figure 3c).

In Figure 3a, when using 25 bar of H_2, the yields to formate for 2-amino at 60 and 120 minutes followed a similar trend. The yield increased from 31% to 36% at the shorter time and from 44% to 50% at 120 minutes when the temperature increased from 70 to 100 ºC. However, at 125 ºC, the yield remained constant. On the other hand, for 3-amino, the behavior was different. At 60 minutes, the yield decreased from 46% at 70 ºC to 41% at 125 ºC. Nevertheless, considering the standard deviation of the measurements, it can be concluded that the yield to formate remained relatively constant within the studied temperature range. At 120 minutes and 100 ºC with 25 bar of H_2, 3-amino showed a decrease in yield, while it remained approximately 60% at 70 and 125 ºC (Figure 3a).

Scale Up

The pressing need for large-scale implementation of the CO_2 conversion process has prompted the ongoing efforts to scale up the previous facility into a pilot plant. The primary objective is to achieve a flow rate of 5 kg/h, enabling the conversion of 100-400g of CO_2

per hour. The scale-up process entails several key steps. Initially, CO_2 is absorbed into amines within an absorber, followed by its reduction in a tubular reactor utilizing a supported catalyst and gaseous hydrogen. To facilitate this process, a powerful electrolyzer capable of producing pressurized hydrogen through water electrolysis has been procured. The outlet from the reactor will then be directed to a flash separator, and subsequently, a separation process will isolate both amines and formic acid. For a better understanding of the process design, the accompanying Piping and Instrumentation Diagram (P&ID) and diagrams of the reactor and electrolyzer are presented below, providing further insights into the planned pilot plant configuration.

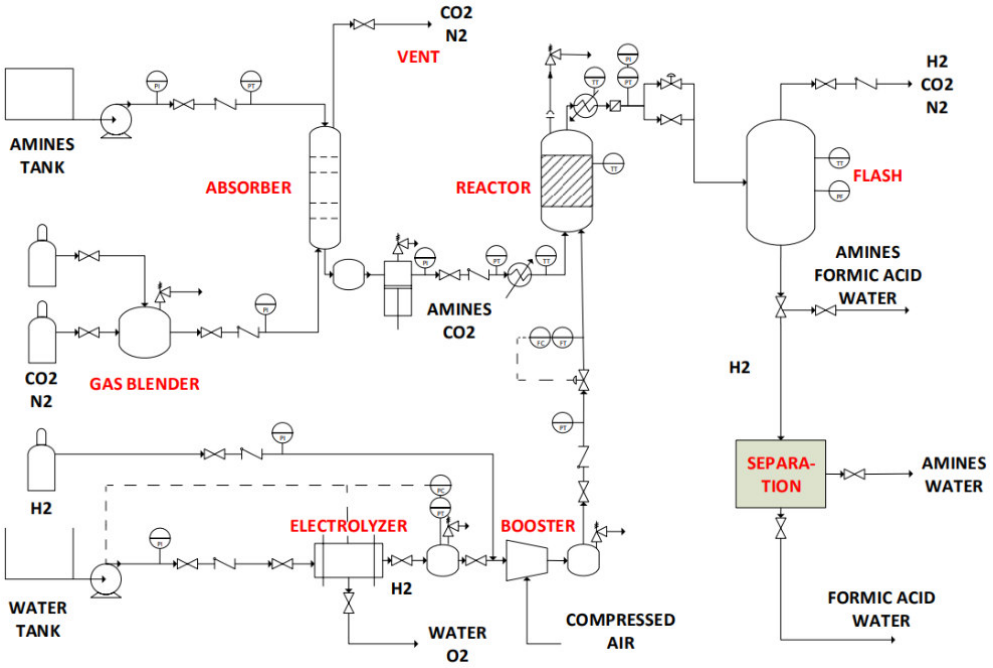

(a)

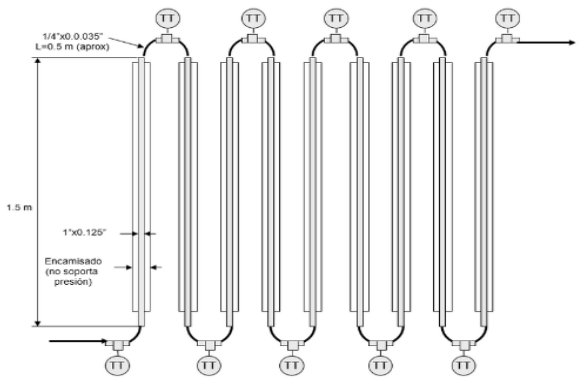

(b)

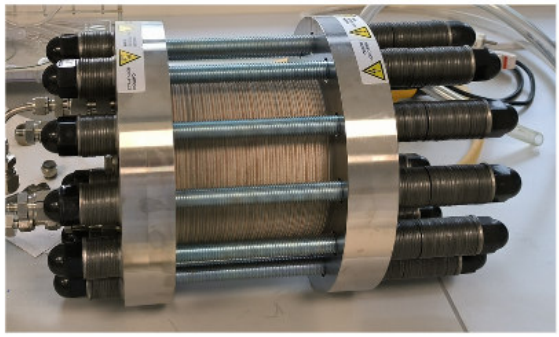

(c)

Figure 2. Pilot plant planned configuration. a) Piping and Instrumentation Diagram (P&ID) , b) Reactor Schematic, c) Photograph of the electrolyzer.

Acknowledgment

This project has been funded by the Ministry of Science and Universities through project RTI2018-097456-B-I00 and by the Junta de Castilla y León through project by FEDER FUNDS under the BioEcoUVa Strategic Program (CLU-2019-04).

References

[1] Quintana-Gómez L, Martínez-Álvarez P, Segovia JJ, Martín A, Bermejo MD (2023) Hydrothermal reduction of CO_2 captured as $NaHCO_3$ into formate with metal reductants and catalysts, J. CO_2 Utilization 68: 102369

Influence of Reaction Parameters on the Solution Polymerisation of Vinyl Acetate

Sandra Pietrasch, Markus Busch, Kristina Zentel*

TU Darmstadt, Darmstadt/Germany, *kristina.zentel@pre.tu-darmstadt.de

Introduction

Vinyl acetate is a monomer widely used in everyday life due to its flexible polymerisation possibilities and extensive range of product properties. Due to the large production volume, an accurate product design or swift changes of the product properties would be especially desirable to minimise waste, production costs and time. It is known that computer simulations can assist towards reaching that goal, but only a few modern publications exist concerning the simulation of the PVAc polymerisation.[1] Therefore, this work addresses this topic for the free radical solution polymerisation. On the experimental side, the data situation is improved by systematically varying three of the most important reaction parameters in a broad range. Additionally, a deterministic model is created, which is validated and adjusted by comparing its simulated results to the experimental ones and literature data. The overall goal is to create a model capable of predicting product properties to achieve a simulation-based product design.

Experimentals & Modeling

Vinyl acetate is polymerised in solution under atmospheric pressure, while monomer content (20 wt%, 40 wt%, 50 wt% and 60 wt%), solvent (methanol, ethyl acetate and toluene) and temperature (50 °C, 70 °C and 90 °C) are systematically varied. The development of the conversion is monitored via gravimetry, while the molecular weight distribution is determined by gel permeation chromatography (GPC). In parallel, a deterministic model based upon models from Nowottny[1] and Feuerpfeil[2] is built up in Predici© to simulate the conducted experiments, after which the conversions and molecular weight distributions are compared.

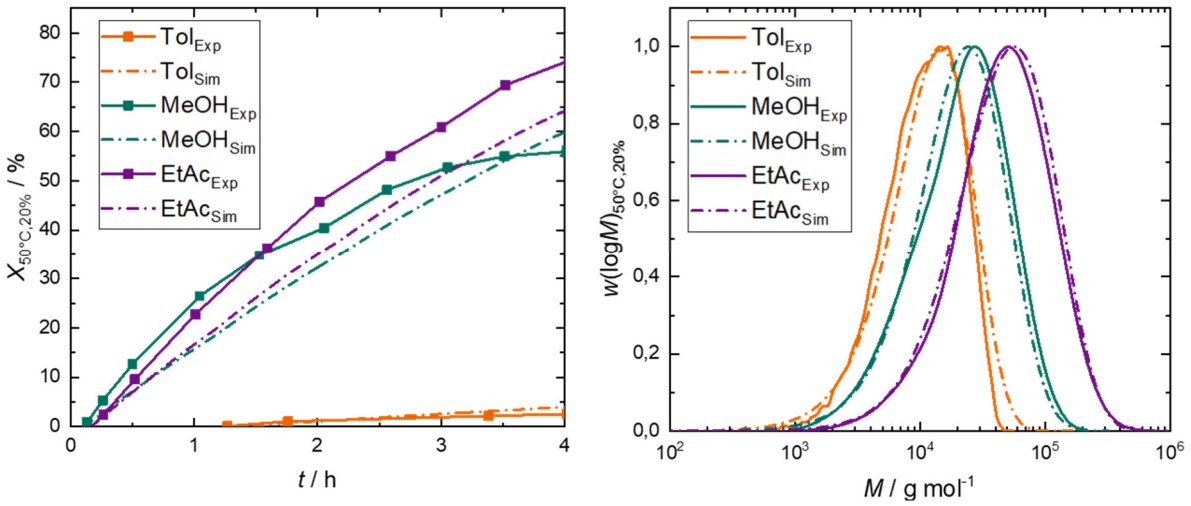

Fig. 1.: Influence of various solvents on the solution polymerisation of vinyl acetate: (left) conversion profile, (right) molar mass distributions at the end of the reaction.

In Figure 1, the experimental results (solid lines) and the simulated ones (dotted lines) of the solvent variation are compared. The left graph shows the conversion profile, while the right graph displays the molar mass distributions. It is apparent that the model is able to describe the experimental trends in the conversions and molecular weight distributions well. The degree of accuracy is varying but in general, a good accordance can be found between simulation and experiment. An exception are the polymerisations in toluene, which is why the model is adjusted to accommodate its retarding properties. A sensitivity analysis for the preexponential factor and the activation energy is conducted on this objective. The new simulated curves match the experimental ones better, but a discrepancy is still visible.

To further validate the model and expand the range of screened reaction conditions regarding e.g. the temperature, initiator concentration and batch/semi-batch mode, literature experiments from Feuerpfeil,[2] McKenna[3] and Lyoo[4] are simulated as well and their molecular weight distributions and conversions are compared.

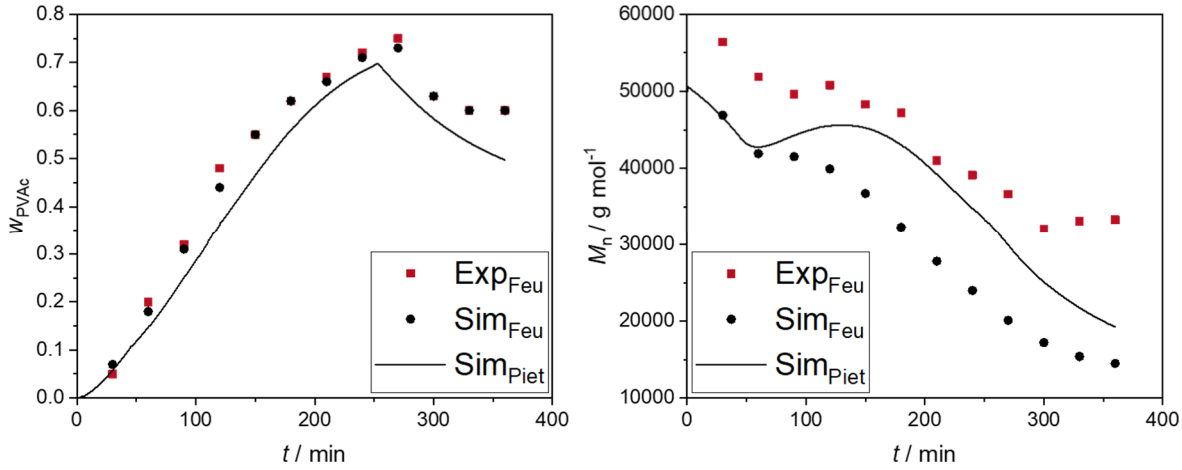

Fig. 2.: Comparison between data from Feuerpfeil (experiment #a)[2] and the created model: (left) solid content profile, (right) development of M_n.

This is shown exemplary in Figure 2 for the development of the solid content profile and the average molecular weight during the reaction of Feuerpfeil's experiment #a[2]. There, his experimental and model data is compared to the simulation results of this work. Especially the experiments conducted in methanol show a good to very good agreement between experiment and simulation over a wide range of reaction conditions. When looking at toluene as a solvent, the conversions are systematically overestimated by the model.

Summary & Outlook

To better understand the influence of temperature, solvent and monomer content on the free radical solution polymerisation of vinyl acetate, these three reaction parameters are varied systematically and their influence on the conversion and the molecular weight distribution is quantified. The experimental results are used furthermore to validate and optimise a created deterministic model, which is based upon models of Nowottny[1] and Feuerpfeil[2]. Additional model validation and extension of the parameter range is conducted by simulating literature experiments. Overall, a good to very good accordance between model and experiment can be achieved, especially with methanol as a solvent. The model was adjusted to consider the retarding properties of toluene but there is still room for further improvement. In the next step, a simulation based product design is aimed for by planning experiments with the validated model to realise a desired process and product.

References

[1] E. Nowottny, *unpublished dissertation*, Technische Universität Darmstadt, **2022**.

[2] A. Feuerpfeil, M. Drache, L.-A. Jantke, T. Melchin, J. Rodríguez-Fernández, S. Beuermann, *Ind. Eng. Chem. Res.* **2021**, *60*, 18256.

[3] T. F. Mckenna, A. Villanueva, *J. Polym. Sci. A Polym. Chem.* **1999**, *37*, 589.

[4] W. S. Lyoo, H. Du Song, W. C. Lee, S. S. Han, S. K. Noh, *J. Appl. Polym. Sci.* **2006**, *102*, 4831.

High Pressure Processes for the Brewing Industry – Extraction of Valuable Compounds from Brewing Byproducts

Mateusz Jackowski[1], Reshma Babu[2], Anna Trusek[1]

1) Wrocław University of science and Technology, Department of Micro, Nano and Bioprocess Engineering, Faculty of Chemistry,

email: mateusz.jackowski@pwr.edu.pl

2) Department of Chemistry and Industrial Chemistry, University of Genoa

Introduction

Beer is a drink known for millennia and nowadays widely consumed around the world. It is estimated that beer is the third most popular drink across the world after potable water and tea [1]. The brewing industry is a constantly developing branch of the industry. The market is mainly divided among large corporations, but there is also room for medium and small breweries, as well as numerous microbreweries and brewpubs. In recent years, changes in consumer preferences can be observed as they increasingly reach for beverages with lower alcohol content. As a result, many people are shifting their preferences from strong alcoholic beverages such as whisky or vodka towards milder alcoholic beverages like beer [2]. Europe produces over a quarter of the world's beer production. Currently, Europe is experiencing a "Beer Revolution," resulting in an increase in the number of regional and craft breweries. Additionally, consumers increasingly expect producers to offer products with new flavour profiles and of top quality. Consequently, further growth in the brewing industry can be expected worldwide, including in Europe.

Beer production is a complex process (Figure 1.). At the beginning, malt grains and unmalted materials (if used) are ground. Then the raw material is mixed with water and heated up to the temperatures optimal for enzymes activity. This phase is called mashing, and its purpose is to extract sugars from grains. The most important enzymes active during this stage are alpha and beta amylases present in malt. Beta amylase cleaves every second α-1,4 bond in starch chains starting from its non-reducing end. The optimal working temperature for this enzyme is 62-67 ^{o}C. Alpha amylase cleaves mentioned bonds in random order. This enzyme represents the highest activity at 71-75 ^{o}C. Mashing ends with heating the mixture to 78 ^{o}C in order to denature the remaining enzymes and stop their activity. The next step is lautering, during which wort is being separated from

spent grains. After that, the filtrate is boiled. The purpose of that step is to sterilise the wort and provide beer aroma and bitterness. To achieve that, hop is added to the boiling wort in two doses. The first step takes place 60 minutes before the end of boiling in order to raise the bitterness of the wort and to make sure that bitter substances from hops are extracted into wort due to the thermal isomerisation of α-acids and β-acids into iso-α-acids and iso-β-acids. The second dose is added 15 or fewer minutes before the end of boiling - in this step, the second portion of hops will be boiled long enough to extract aroma compounds, and short enough to not remove them completely through evaporation. Finally, wort needs to be cooled down, and yeast is added. Depending on the strain and fermentation conditions, beer will represent different alcohol levels and organoleptic properties. The last step of the process of beer production is maturation, after which it is ready to be packed and sent to consumers [3]–[5].

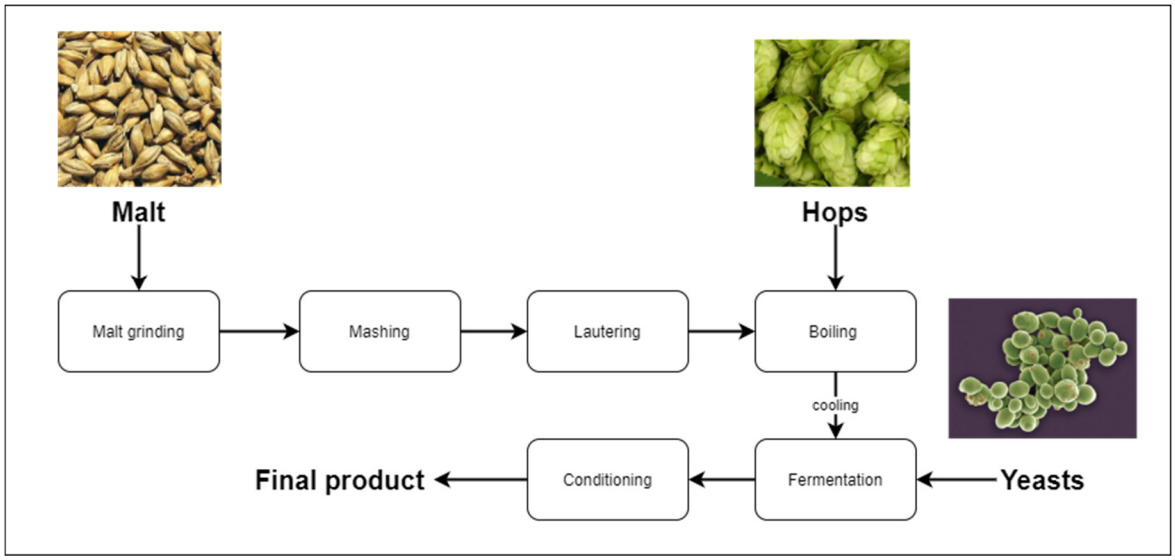

Fig. 1.: Beer production scheme

In modern large-scale breweries, there are strong attempts to improve the quality and shelf life of a product. Moreover, there is a strong focus on cost reduction in order to gain an advantage on the market.

Experimental

During beer production various byproducts are being created. Among them are brewing spent grains, hot trubs (mixture of spent hops and precipitated proteins created during wort boiling) and spent yeasts. Hot trubs may be a source of valuable bioflavonoids and spent yeasts are rich in proteins and vitamins (mainly group B). Whereas brewers

spent grains may be a source of polyphenols, proteins and sacharides. Bewers spent grains are baing produced in the large quantities among brewing byproducts.

Duing preliminary tests various techniques of pretreatment and extraction were tested in order to extract polyphenols from brewers spent grains. Among tested methods of hydrolysis were chemical treatment with 0.5 M H_2SO_4, 0.5 M HCl, 0.5 M NaOH and water. Moreover samples were stirred, heated up to 70 ºC, ultrasonicated and exposed to microwaves. Such samples were compared with supercritical CO_2 extraction with ethanol as a co solvent.

Brewers spent grains were collected from Wrocław University of Science and Technology's pilot scale brewery. Prior the experiment byproduct was dried in 50 ºC for 48 hours. In the next step hydrolyses were performed in order to extract polyphenols from brewers spent grains (Fig. 2).

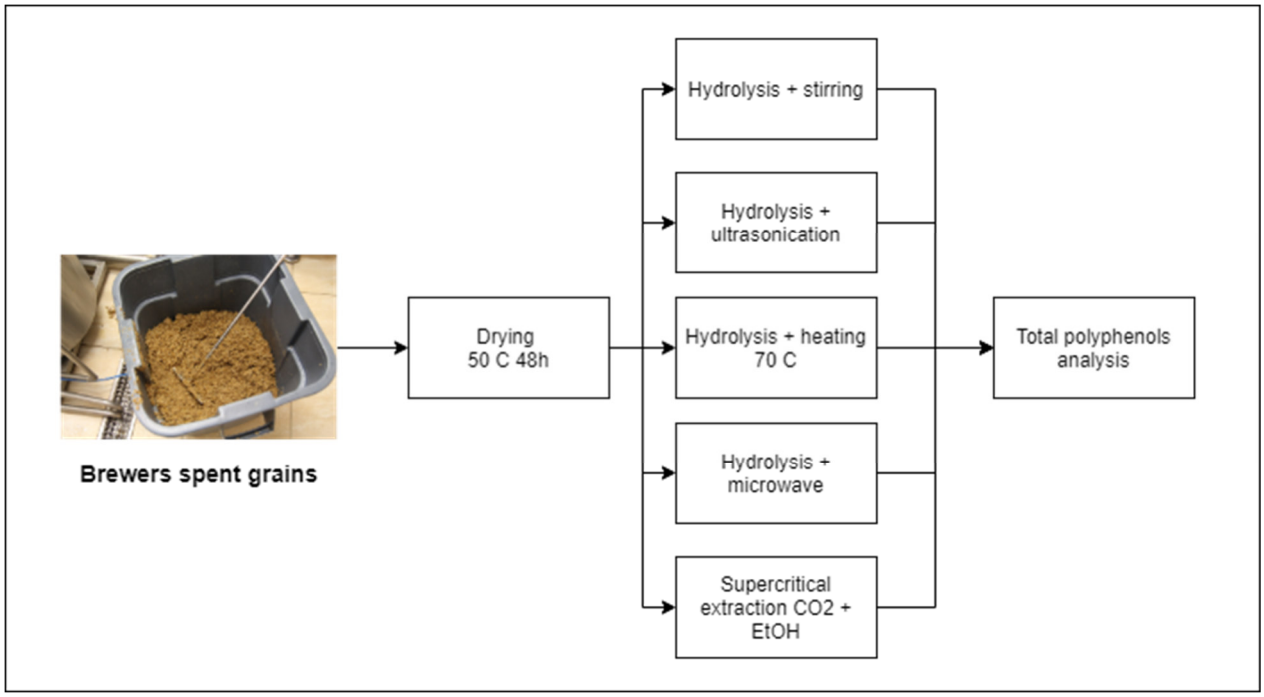

Fig. 2.: Scheme of the experiment

Total polyphenols were estimated using Folin-Ciocialteu method, concentration of polyphenols is calculated as a gallic acid equivalent [6]. In a test tube, 20 µL of sample was added followed by 100 µL Folin reagent. The reactants were mixed and left to stay at room temperature for 3 min. Then, 300 µL of sodium carbonate solution (20%) and 1580 µL of distilled water was added to the test tube and mixed. Control sample was prepared with distilled water instead of sample. The solution mixture was incubated in a dark place at room temperature for 2 h. The absorbance values were measured at 765 nm using UV-1800 Spectrophotometer .

Results of the hydrolusis are depicted in table (Tab. 1.)

Tab. 1.: Total polyphenols in experimental samples

Method of extraction	Total polyphenols [mg/g]
0.5 M H_2SO_4 stirring (1h, 100 rpm)	0.0073
0.5 M HCl stirring (1h, 100 rpm)	0.0088
0.5 M NaOH stirring (1h, 100 rpm)	0.0406
Water stirring (1h, 100 rpm)	0.0088
0.5 M H_2SO_4 ultrasonication (1 h)	0.0074
0.5 M HCl ultrasonication (1 h)	0.0084
0.5 M NaOH ultrasonication (1 h)	0.0474
Water ultrasonication (1 h)	0.0084
0.5 M H_2SO_4 heating (1h, 70ºC, 100 rpm)	0.0135
0.5 M HCl heating (1h, 70ºC, 100 rpm)	0.0169
0.5 M NaOH heating (1h, 70ºC, 100 rpm)	0.0657
Water heating (1h, 70ºC, 100 rpm)	0.0082
0.5 M H_2SO_4 microwave 4 min	0.0086
0.5 M HCl microwave 4 min	0.0077
0.5 M NaOH microwave 4 min	0.0454
Water microwave 4 min	0.0059
Supercritical extraction (CO_2 + ethanol, 90 min)	0.0395

Results show that NaOH extraction in 70 ºC was the most efficient method for polyphenols extraction. Nevertheless supercritical extraction is an efficient method for polyphenol extraction from brewers spent grains giving similar amounts of polyphenols as NaOH and by an order of magnitude more than other tested methods. On the other hand samples after NaOH treatment were hard to separate and a lot of extract was lost due to the separation problems. To summarize supercritical extraction seems to be a reasonable method for polyphenol extraction from brewers spent grains.

Summary

Beer industry is constantly growing branch of food industry. Due to the competition between major companies present on the market it is highly possible that big brewing companies will be forced to improve quality of the products and to lower the costs of production. One of the possible ways to obtain mentioned results is focusing on new technologies including supercritical processes especially for the valorisation of brewing byproducts.

References

[1] M. Nelson, *The Barbarian's Beverage: A History of Beer in Ancient Europe*. New York: Routledge, 2005.

[2] V. Pozynak and D. Rekve, Eds., "Global status report on alcohol and health 2018," World Health Organization, Geneva, 2018.

[3] W. Dylkowski and T. Gołębiewski, *Technologia browarnictwa*. Warszawa: Wydawnictwo przemysłu lekkiego i spożywczego, 1963.

[4] C. McGregor and N. McGregor, *The Beer Brewing Guide EBC Qualiy Handbook for Small Breweries*, 1st ed. Tielt: Lannoo, 2021.

[5] D. E. Briggs, P. A. Brookes, R. Stevens, and C. A. Boulton, *Brewing: Science and Practice*. CRC Press, 2004.

[6] H. P. S. Makkar, "Measurement of Total Phenolics and Tannins Using Folin-Ciocalteu Method BT - Quantification of Tannins in Tree and Shrub Foliage: A Laboratory Manual," H. P. S. Makkar, Ed. Dordrecht: Springer Netherlands, 2003, pp. 49–51.

Ethylbenzene/Styrene Multicomponent Distillation Column

Gunay Ismiyeva

Chemical Engineering Department, Heriot-Watt University

gunay.ismiyeva@studenti.unipd.it

Introduction

This report is devoted design of ethylbenzene/styrene multicomponent distillation column by indicating each step of mechanical and thermodynamically design procedure. As main product of styrene plant is obtained from this column the first requirement of the design process is to keep purity of styrene monomer above 99%. The shortcut hand calculations are conducted, and results are compared to Aspen HYSYS shortcut calculations. In addition, rigorous design is also done in the same software program due to selection of optimum condition for this column. Based on chosen condition vapor and liquid composition profiles are explained in detail. Valve tray is selected from tray design and its efficiency is determined by representing relationship with overall column efficiency. Besides the mechanical design, thermodynamics is also shown by plotting vapor-liquid equilibrium (VLE) diagram. Control of the system is done based on bottom product under inventory control because as mentioned it is major product. Furthermore, costs analysis of equipment including vessel, condenser and reboiler is done for 2006 and then converted to 2018. HAZOP and Fault tree analysis of this column are also considered. Combustion power plant cycle is chosen as secondary topic and design in each detail. The required power output for electricity is obtained during the design process. This report helps to students to improve their chemical engineering knowledge by learning basic of engineering in each detail.

Experimental

In order to produce polystyrene and other styrenic resins including, acrylonitrile butadiene styrene (ABS), styrene acrylonitrile (SAN), styrene-butadiene copolymer, styrene-butadiene rubber (SBR) and many others styrene monomer (SM) is used as a vital petrochemical. Large scale production of styrene is needed and for this purpose ethylbenzene styrene multicomponent distillation column is operated as one of the major units of styrene plant due to acquirement of nearly pure styrene as basic product. This column mainly consists of four components: benzene, toluene, ethylbenzene and styrene.

The key components of this column are ethylbenzene and styrene and their splitting are quite difficult because of similarity in boiling points which are 136.168 °C and 145.15 °C at atmospheric pressure, respectively.

Styrene (C_6H_5–CH=CH_2), also called vinylbenzene, styrol, cinamene or phenylethylene is the most significant and straightforward member of unsaturated aromatic monomer. The first removal of styrene was achieved in the nineteenth century by the purification of storax, a natural balsam. During the 1930s the modern technology and commercial processes of styrene were succeeded while dehydrogenation of ethylbenzene was developed. As there was a demand for styrene production due to manufacture of synthetic rubber during World War II many styrene plants were constructed in Germany. Styrene is a colourless liquid with specific, sweetish aromatic odour under normal conditions and because of its phase usage of styrene is very simple and not dangerous. The existence of vinyl group streamlines copolymerization and polymerization and consumption of almost all the commercial styrene is observed in these two proceedings. Unbounded solubility of styrene makes it miscible with several organic solvents such as, ether, acetone, benzene, ethanol [1].

Ethylbenzene (C_6H_5-CH_2-CH_3) is essentially manufactured by alkylation reaction of benzene with ethylene and utilized entirely (>99%) for styrene monomer production by dehydrogenation reaction. Approximately, 50% of the benzene over the world is depleted for this aim. The remaining manufactured ethylbenzene (less than 1%) is applied for other chemicals production or as a paint solvent. Ethylbenzene is also a colourless, clear liquid with distinctive aromatic odour and high flammability. Moreover, this organic compound is an irritant to the human body and eyes [1].

In order to visualize better view, distillation column is constructed in 3D design software: Autodesk AutoCAD 2017 and shown in the Figure.

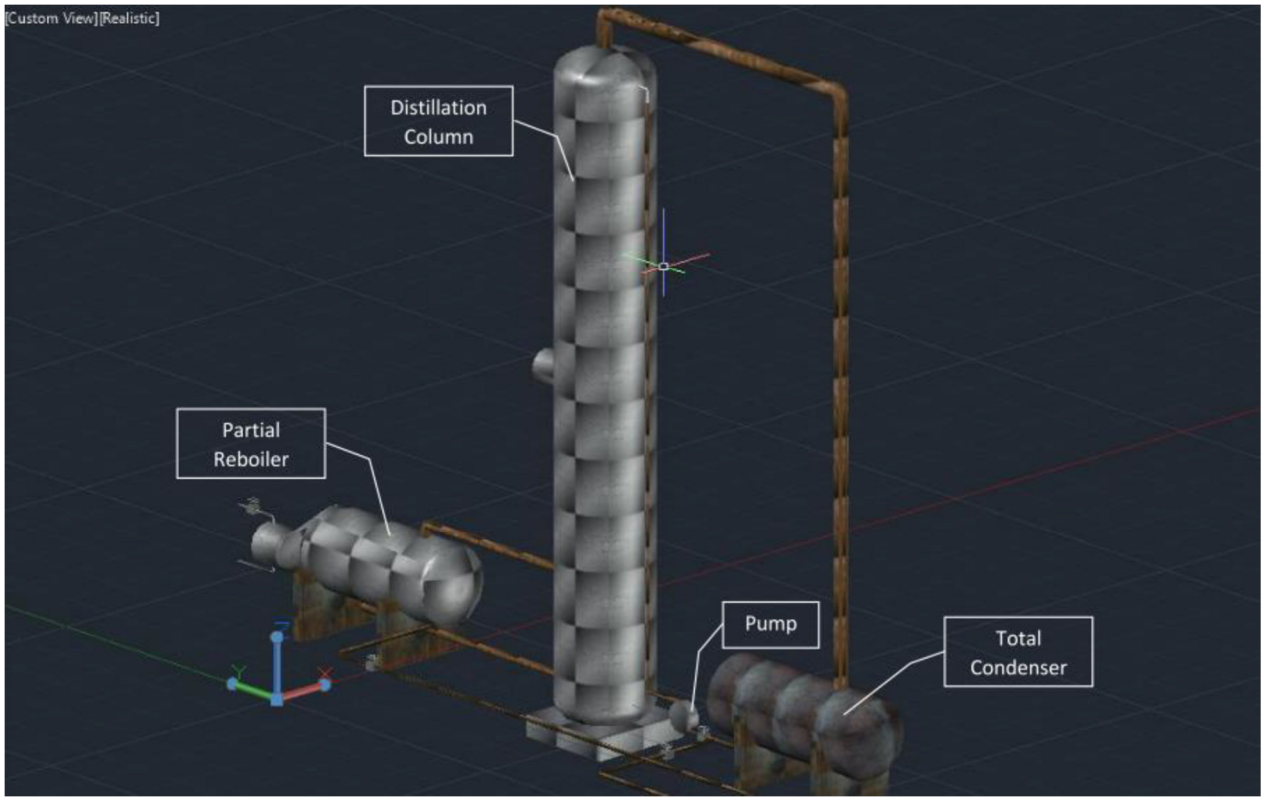

As mentioned, the main product of styrene plant with high purity is received from ethylbenzene/styrene multicomponent distillation column in which feed components (benzene, toluene, ethylbenzene, styrene) are bottom products of toluene/benzene distillation column. Bottom product of this column is almost pure styrene (99.5%) while the distillate products are recycled to the reactor. According to a slight dissimilarity between boiling points of ethylbenzene and styrene their separation factor which is relative volatility is below approximately 1.35 and it causes difficulty in separation of these components. Based on impurity of ethylbenzene in the bottom stream this column requires about 70-100 stages. Taking into account, undesirability of polymers in the monomer distillation column polymerization ability of styrene at high temperature is minimized by operating this column under vacuum condition. Thus, overall pressure drop of the column will be low because of vacuum condition. Apart from temperature minimization of residence time which has direct proportionality with polymerization rate is also required. In order to keep vacuum at the top of the column steam ejector systems are commonly applied. Furthermore, inhibitors usually a phenol are added to the column and lead to prevention of polymerization, improvement of heat recovery and increase of capacity [2].

Summary

In order to get low a pressure drop across the column sieve and valve trays design are conducted. Design of both trays are satisfactory in terms of flooding and entrainment. When results are met, it is concluded that for this column valve trays are more appropriate in terms of low pressure drop.

Parameters	Valve trays	Sieve trays
Top diameter (m)	2.80	2.89
Bottom diameter (m)	4.00	4.10
Pressure drop in top (kPa)	0.59	0.94
Pressure drop in bottom (kPa)	0.52	0.94
Plate efficiency	60.48 %	59.75%

Key components have close boiling points and it creates some troubles during separation. Moreover, reflux ratio gets large value and number of trays also increases. Different values are given to the reflux ratio and results are checked by using rigorous design in Aspen HYSYS. However, one requirement should be always considered which is purity of styrene. Thus, for 99.56% purity actual reflux ratio is 7.19 while actual number of stages are 57. When it is tried to reduce these numbers purity of styrene is also reduced. Hence, optimum condition is selected by giving 15% recovery to styrene and 99% to ethylbenzene in distillate. In this case, reflux ratio equals and actual number of theoretical stages to 5.32 and 46, respectively. The purity is also satisfactory (99.51%). In addition, the best vapor and liquid composition profiles are obtained for this case.

Non-light keys (benzene and toluene) disappear rapidly below the feed because of high volatilities. Variations in fractions are nearly constant above the feed because they are being passed to the condenser. The compositions of heavy key enhance down the column but above the reboiler its fraction reduces. The compositions of light key increase up the column since it begins to separate from the non-light keys below the condenser its fraction drops. Furthermore, the optimum feed stage also is observed for this case based key ratio plots.

As the main product of this column is bottom product control system is constructed based on bottom product under inventory control. LC-1 should drive one of other flows into or from reflux drum. These flows are the reflux and vapor flows. Controlling of reflux is chosen on the grounds which is more direct. This case it would take long time for variations in the vapor flow for reaching to the distillate. Remaining degrees of freedom for cut and separation control is provided due to top product and bottom steam valves.

References

1. Kirk-Othmer., Encyclopedia of Chemical Technology, 4th Edition, Vol. 22, chapter "Styrene". In Silicon Compounds to Succinc Acid and Succinic Anhydride (p. 476). New York: Wiley-Interscience, 1992.

2. Karl Kolmetz, Andrew W. Sloley, Timothy M. Zygula, Peter W. Faessler, Dr. Wai Kiong Ng, K. Senthil, Tau Yee Lim. Designing Distillation Columns for Vacuum Service. Grand Hyatt,Mumbai, India: The 11th India Oil and Gas Symposium and International Exhibition, (6-7 September 2004).

3. Unit Operation A – Advanced Distillation (B40EA), produced by Heriot-Watt University, Edinburgh EH 14 4AS, United Kingdom, 2016.

4. Woods, D.R. Rules of Thumb in Engineering Practice. Wilecy-VCH Verlag GmbH & and Co., KGaA, Weinheim, 2007

5. Coulson and Richardson's, CHEMICAL ENGINEERING, VOLUME 6, FOURTH EDITION, Chemical Engineering Design, R.K. SINNOT, Chapter 11: Separations columns (Distillation, Absorption, Extraction), page 493.

6. J. R. Backhurst and J. H. Harker, HEINEMANN CHEMICAL ENGINEERING SERIES Process Plant Design, Chapter 6: Sieve and Valve Tray Design, page 163, 1973.

7. Carl L. Yaws Thermophysical Properties of Chemicals and Hydrocarbons, Second Edition, 2014

8. Yaws, Carl L. Transport properties of chemicals and hydrocarbons: viscosity, thermal conductivity, and diffusivity of Cl to Cl 00 organics and Ac to Zr inorganic.

9. Henry Z. Kister, Engineering Advisor Brown & and Root Braun, Alhambra, California Chapter 7: Tray efficiency, page 365.

10. Gavin Towler, Ray Sinnot. Chemical Engineering Design. Principles, Practice and Economics of plant and Process design, Chapter 6: Costing and process evaluation, page 297.

11. Page S. Buckley, William L. Luyben, Joseph P. Shunta, Design of Distillation column control systems, Chapter 9: Application of Protective Controls to Distillation Columns, page 193.

12. Qusai Zuhair Mohammed Al-Hamdan, Design criteria and performance of gas turbines in a combined power and power plants for electrical power generation, 2002

13. Energy generation and utilization (B40DC), produced by Heriot-Watt University, Edinburgh EH 14 4AS, United Kingdom, 2016

Supercritical Extraction of Milk Thistle and Cannabis

Ivana Nikolić

Faculty of Technology and Metallurgy, University of Belgrade, inikolic30@gmail.com

Introduction

Supercritical fluids are fluids that are at a higher temperature than the critical temperature and at a higher pressure than the critical pressure for that fluid. The most used supercritical fluid is carbon(IV)-oxide due to low values of critical parameters (Tc=31.1°C, pc=74 bar), acceptable price, as well as non-toxicity, non-flammability and chemical inertness. [1]

A scheme of a typical supercritical extraction apparatus can be seen in Figure 1. The parts of the apparatus are a bottle with carbon(IV)-oxide, a cryostat, a high-pressure pump, an extractor with an electric heater, and a separator. [1]

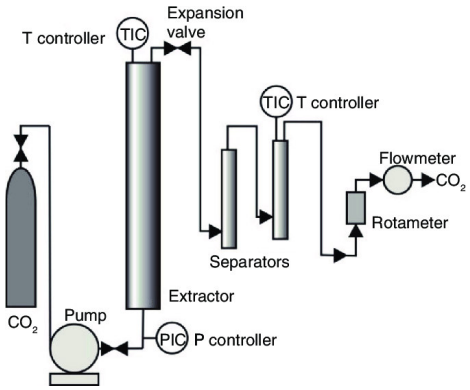

Figure 1. A scheme of a typical supercritical extraction apparatus

Experimental

In our laboratory, we performed supercritical extraction of milk thistle and cannabis. We are planning experiments of supercritical extraction of dogwood.

Milk thistle (*Silybum marianum*) is used in traditional European and Asian medicine, mainly to treat liver disorders. It can also affect the cardiovascular system, lowering the level of cholesterol in the blood and thus reducing the risk factors for the development of atherosclerosis of blood vessels. [2]

The fruit contains about 0.2% essential oil, and pharmacologically active ingredients (flavonoids, tannins, proteins, carbohydrates, fats and resins). Silymarin is an active

substance from milk thistle seeds. It is believed that silymarin restores damaged liver cell membranes. Milk thistle also contains compounds with anti-cancer activity. [3]

In figure 2 you can see the appearance of the milk thistle.

Figure 2. Milk thistle

In the process of supercritical extraction we used the seeds of the milk thistle. We performed five supercritical extraction experiments. 10 g of milk thistle was used for each experiment. Table 1 shows the achieved yields and extract mass for the combination of pressures and temperatures, as well as CO_2 density under experimental conditions.

T[°C]	P[MPa]	Y[%]	m_e[g]	ρ_{CO_2}[kg/m³]
40	30	11.93	0.735	909.9
	20	9.72	0.620	839.8
	10	1.4	0.034	628.6
60	30	14.41	0.977	829.7
80	30	12.12	0.814	745.6

Table 1. Yields, a mass of extract for a combination of pressures and temperatures and CO_2 density at experimental conditions

Figure 3 shows the dependence curves of the yield of the extract on the consumption of supercritical carbon(IV)-oxide per mass of the plant for experiments performed at a temperature of 40°C and at pressures of 10, 20 and 30 MPa. It can be concluded that with an increase in pressure, the yield of the extract also increases, which is expected considering that with an increase in pressure, the density of CO_2 also increases.

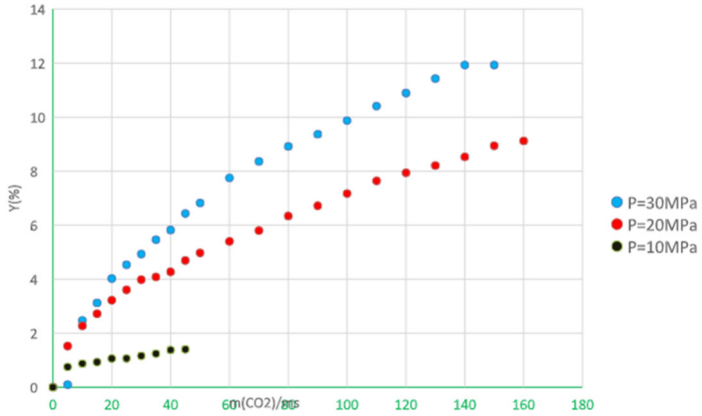

Figure 3. The dependence curves performed at a temperature of 40°C and at pressures of 10, 20 and 30 MPa

Figure 4 shows dependence curves for experiments performed at a pressure of 30 MPa and at temperatures of 40, 60 and 80°C. It can be seen that the highest yield was achieved at a temperature of 60°C.

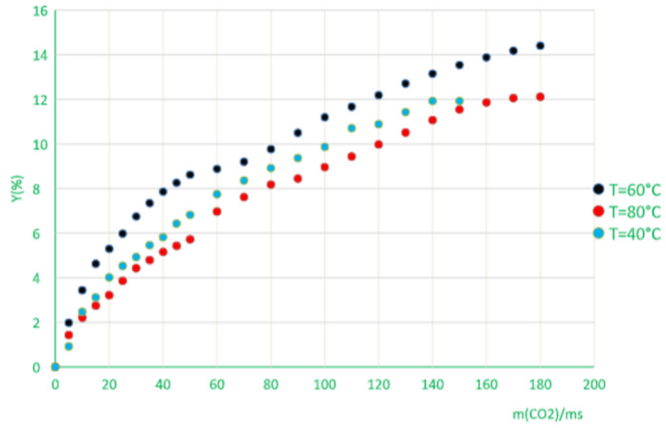

Figure 4. The dependence curves performed at a pressure of 30MPa and at temperatures of 40, 60 and 80°C

The best yield was achieved at a temperature of 60°C and a pressure of 30MPa, which can be clearly seen in Figure 5, which provides an overview of the results of all experiments.

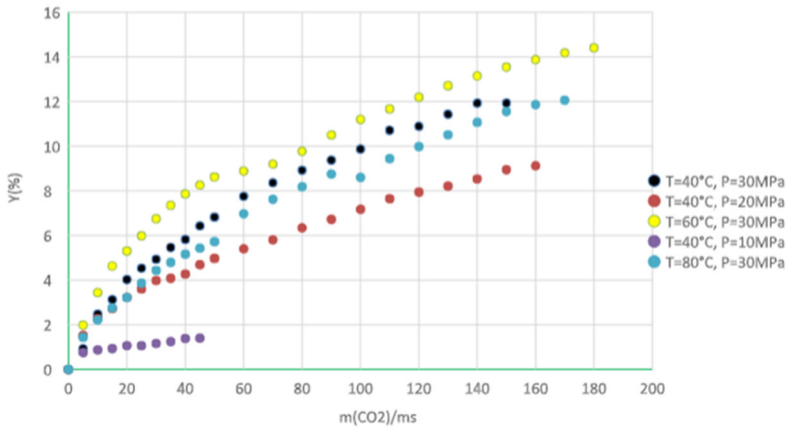

Figure 5. The dependence curves for different combinations of temperatures and pressures

Cannabis (*Cannabis sativa*) is a plant which is used as an industrial material, a therapeutic agent for pain relief, for obtaining food, oil, medical and cosmetic preparations. One of the main components of cannabis is cannabidiol (CBD). In experimental research, it has been shown to reduce inflammation and anxiety, as well as the growth of cancer cells. A level of a psychoactive substance called tetrahydrocannabinol (THC) in a plant which we used in our experiments is lower than 0,3%. [4]

Figure 6 shows the appearance of *Cannabis sativa*

Figure 6. The appearance of Cannabis sativa

In supercritical extraction experiments we used leaves and flowers of cannabis. Experiments were performed at temperatures of 20, 40 and 60℃ and pressures of 10, 20 and 30 MPa. Table 2 shows selected process parameters, obtained yield and density of carbon(IV)-oxide under these conditions.

T/p	p=10MPa	p=20MPa	p=30MPa
T=21°C	Y=3,03%, ρ=849kg/m3	/	/
T=40°C	Y=2,48%, ρ=628,6kg/m3	Y=3,82%, ρ=839,8kg/m3	Y=3,91%, ρ=909,9kg/m3
T=60°C	The pressure and temperature conditions are not adequate for the reaction. A negligible amount of extract is obtained , ρ=290 kg/m3	/	/

Table 2. Yields and CO_2 density at experimental conditions

Figure 7 shows the yield of the extract depending on the consumption of supercritical carbon(IV)-oxide per mass of the plant for experiments performed at a temperature of 40℃ and pressures of 10, 20 and 30 MPa.

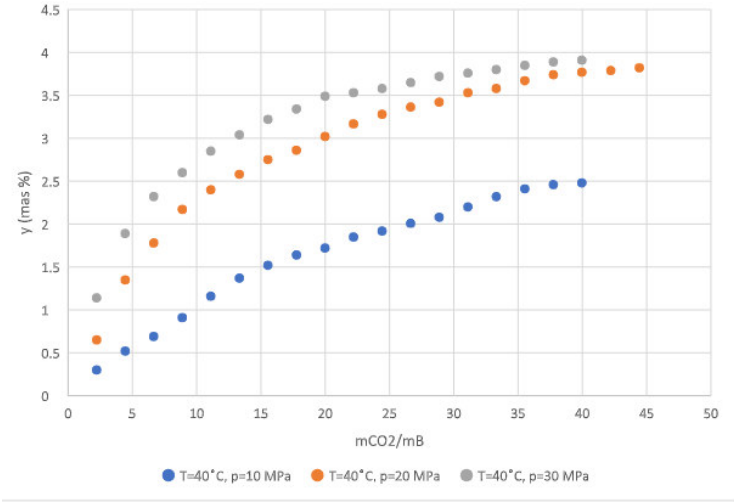

Figure 7. The dependence curves performed at a pressure of 40°C and at pressures of 10, 20 and 30MPa

From this diagram, it can be concluded that at the tested temperature, the yield of the extract increases as the pressure increases. This is due to the increase in the density of

carbon(IV)-oxide with increasing pressure. The highest yield (3.91%) achieved at a temperature of 40℃ is at a pressure of 30 MPa.

Figure 8 shows the extract yield depending on the consumption of supercritical carbon(IV)-oxide per mass of the plant for experiments performed at a pressure of 10 MPa and temperatures of 21, 40 and 60℃.

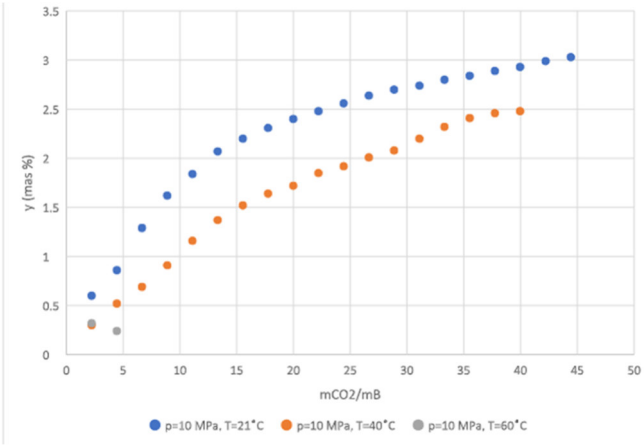

Figure 8. The dependence curves performed at a pressure of 10MPa and at temperatures of 21, 40 and 60°C

From this diagram, it can be concluded that at the tested pressure, the yield of the extract increases with decreasing temperature, which is a consequence of increasing the density of carbon(IV)-oxide with decreasing temperature.

The best yield was achieved at a temperature of 40°C and a pressure of 30MPa, which can be clearly seen in Figure 9, which provides an overview of the results of all experiments.

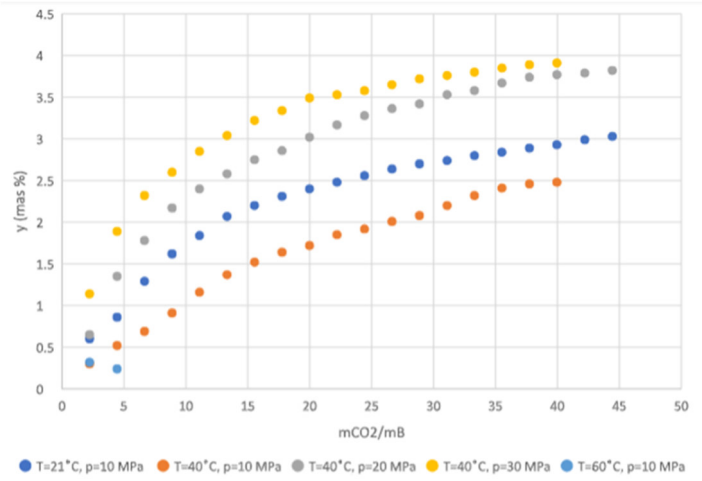

Figure 9. The dependence curves for different combinations of temperatures and pressures

Summary

From a lot of available literature data it can be concluded that supercritical extraction can overcome some limitations of traditional extraction methods like the use of organic solvents that are not good for the environment, the long process time and the degradation of some biologically active components due to working at high temperatures. The extract obtained using supercritical extraction does not need to be purified because it does not contain toxic organic solvents. In the future we are planning to perform supercritical extraction of dogwood (seeds and fruit). [1]

Cornus mas (dogwood) is traditionally used to treat asthma, bronchitis, chronic inflammation, diabetes and liver disease. Dogwood fruits have antimicrobial, antiallergic, and anticancer effects. The medical properties of this plant are attributed to the presence of polyphenols and iridoids, as well as anthocyanins. From available literature data we concluded that seeds of dogwoods are rich in fatty acids that are useful for human health, but also that there are not many papers published on this topic, so that additional research on dogwood seeds would contribute to science. [5]

References

[1] S. Milovanović, Impregnation of thymol on solid carriers using supercritical carbon dioxide, doctoral dissertation, University of Belgrade, Faculty of technology and metallurgy, Belgrade, Serbia, 2015.

[2] Z. Zhanga, S. Wang, H. Liu, B. Li and L. Che, Constituents and thermal properties of milk thistle seed oils extracted with three methods, College of Food Science and Technology, Henan University of Technology, Zhengzhou, China, 2020.

[3] H. T. Celik, M. Gürü, Extraction of oil and silybin compounds from milk thistle seeds using supercritical carbon dioxide, Gazi University, Engineering Faculty, Chemical Engineering Department, Ankara, Turkey, 2015.

[4] B. Koturević, A. Branković, Method for rapid extraction of cannabinoids from cannabis by microwave heating, University of criminal investigation and police studies, Belgrade, Serbia, 2014.

[5] B. Popović, B. Blagojević, D. Latković, D. Četojević-Simin, A. Kucharska, F. Parisi, G. Lazzara, A one step enhanced extraction and encapsulation system of cornelian cherry (Cornus mas L.) polyphenols and iridoids with β-cyclodextrin, LWT Food Science & Technology 141 (2021) 110884

Design of TiO_2-CeO_2 Based Catalysts for Dichloromethane Oxidation; from Powders Catalysts to Catalytic Foams by Using Subcritical Water Processing

Adéla Šlachtová[1], Michal Zym[1,2], Ivana Troppová[1], Lenka Matějová[1]

[1]Institute of Environmental Technology, CEET, VŠB – Technical University of Ostrava, 17. listopadu 15/2172, 708 00 Ostrava-Poruba, Czech Republic

[2]Faculty of Material Technology, VŠB – Technical University of Ostrava, 17. Listopadu 15/2172,708 00 Ostrava-Poruba, Czech Republic

adela.slachtova@vsb.cz

Introduction

Chlorinated volatile compounds (CVOC) such as dichloromethane (DCM) have been intractable environmental pollutants in air emission due to their chemical stability and harmful effect to human health due to their carcinogenicity and bioaccumulation [1, 2]. Dichloromethane is used as a raw material to produce a cellulose acetate film and as a solvent in the pharmaceutical and automobile industry [3]. There are many technologies for decomposing of DCM and other CVOCs, including recycling technology, destruction technology, photocatalytic oxidation, thermal combustion, and catalytic combustion. Catalytic combustion is an ideal method due to its low cost, less secondary pollution and high efficiency [2, 4]. Catalytic combustion (oxidation) can be used with many types of catalysts. One of many groups that can be used is noble metals (Pt, Pd, Ru) and the other group that can be used is transition metal oxides (TiO_2, CeO_x, MnO_x) or their mutual combination [2]. Noble metal catalysts are highly active for the oxidation of CVOCs. However, they are very sensitive to chlorine adsorption from the CVOCs oxidation process and are of high costs [4]. The deposition of noble metal on the transition metal oxide support can be applied to improve the catalytic efficiency of CVOCs oxidation [5]. Transition metal oxides are resistant to chlorine poisoning due to their chemical stability [6]. Transition metal oxides have been extensively investigated to be a better alternative to noble metals since they have achieved excellent catalytic performance even at low temperature [7]. The most important catalyst properties that play a key role in CVOCs catalytic combustion are active surface area, acidity and redox properties [4]. Acidity and reducubility of catalysts can be affected by acidification or using proper chemical precursors (*e.g.* titanyl sulphate [8] or sulftated iron titanate [4]) for catalyst synthesis. The

catalyst crystal structure and active specific surface area can be affected by post-treatment methods (calcination *versus* subcritical water crystallization). Moreover, there is a trend to transfer the pelletized powder form of catalysts to the monolithic form of catalysts (*i.e.* to deposit and crystallize the catalyst on the ceramic support) which is more economically and application attractive for industrial scale.

Objectives of the work

The goal of work is preparation of nanostructured TiO_2-CeO_2-based catalyst support (in various molar ratios of Ti:Ce) in powder form, impregnate it by Pt, investigate Pt/TiO_2-CeO_2 catalysts in dichloromethane oxidation and based on that to transfer the TiO_2-CeO_2 catalyst support on the VUKOPOR©A ceramic foam by using subcritical water processing. The effect of temperature and pressure or number of catalyst layer/s on the physico-chemical properties of TiO_2-CeO_2@VUKOPOR©A foams is investigated using nitrogen physisorption at 77 K, phase carbon determination and scanning electron microscopy with energy dispersive X-ray spectroscopy. The physicochemical properties of TiO_2-CeO_2@VUKOPOR©A foams prepared by subcritical water processing and calcination are compared and the benefits and disadvantages of subcritical water processing are evaluated and discussed.

Current results

It was revealed that the temperature significantly affects the porosity of pure VUKOPOR®A ceramic foams contrary to pressure which shows no effect. At a temperature of 200 °C and a pressure of 10 and 30 MPa during processing by subcritical water, the part of the Al^{3+} leaches out of the VUKOPOR®A ceramic foam. As a result the macroporosity of the VUKOPOR®A ceramic foam is formed and foam specific surface area increases 4 times from 0.29 $m^2 \cdot g^{-1}$ to 1.1 $m^2 \cdot g^{-1}$.

During the subcritical water processing of TiO_2-CeO_2@VUKOPOR®A foams a part of the TiO_2-CeO_2 catalyst layer is washed away and the complete removal of organic carbon from the catalyst layer/s is not achieved. This was proved by phase carbon determination. However, the catalyst layer is highly mesoporous and possesses the specific surface area of ~22-25 $m^2 \cdot g^{-1}$. The TiO_2-CeO_2 catalyst layer is a good protection against Al^{3+} leaching from VUKOPOR®A ceramic foams. A good reproducibility of the preparation of TiO_2-CeO_2 layers on VUKOPOR®A ceramic foam was reached.

Acknowledgment

The financial support of the project "COOPERATION" (project No. CZ.02.1.01./0.0/0.0/17_049/0008419) supported by ERDF is gratefully acknowledged. Experimental results were accomplished by using Large Research Infrastructure ENREGAT supported by the Ministry of Education, Youth and Sports of the Czech Republic under project No. LM2018098 and No. LM2023056.

References

1. Ying, Q.J., et al., The superior performance of dichloromethane oxidation over Ru doped sulfated TiO_2 catalysts: synergistic effects of Ru dispersion and acidity. Applied Surface Science, 2020. **515**.

2. Xu, S., et al., Catalytic oxidation of dichloromethane over CrFeO mixed oxides: Improved activity and stability by sulfuric acid treatment. Applied Catalysis a-General, 2022. **636**.

3. Huang, B.B., et al., Chlorinated volatile organic compounds (Cl-VOCs) in environment - sources, potential human health impacts, and current remediation technologies. Environment International, 2014. **71**: p. 118-138.

4. Xia, H.Q., et al., Oxidative decomposition of dichloromethane over sulfated iron titanate catalysts: Catalytic performance and reaction mechanism. Applied Catalysis a-General, 2021. **616**.

5. Shi, Y.J., J.L. Wang, and R.X. Zhou, Pt-support interaction and nanoparticle size effect in Pt/CeO_2-TiO_2 catalysts for low temperature VOCs removal. Chemosphere, 2021. **265**.

6. Sun, W., et al., CH_2Cl_2 catalytic oxidation over Ce-Ti-Zr mixed oxide catalysts. Applied Catalysis a-General, 2022. **629**.

7. Cao, S., et al., Catalyst performance and mechanism of catalytic combustion of dichloromethane (CH_2Cl_2) over Ce doped TiO_2. Journal of Colloid and Interface Science, 2016. **463**: p. 233-241.

8. Matejova, L., et al., Novel TiO_2 prepared from titanyl sulphate by using pressurized water processing and its photocatalytic activity evaluation. Materials Research Bulletin, 2017. **95**: p. 30-46.

Investigating Mixing Characteristics of Polymerization Reactors

Laura Ständecke, Markus Busch*

TU Darmstadt, Darmstadt/Germany, *markus.busch@pre.tu-darmstadt.de

Introduction

In polymerization processes, it is crucial to know the mixing behavior inside the reactors. Dependent on the reactor type and geometry as well as the respective operation conditions, various concentration and temperature profiles are observed in real reactors possibly leading to channelling, dead zones or short-circuiting. As this has a direct effect on polymer structure and properties, the hydrodynamic behavior has to be investigated in detail.[1, 3] Therefore, experimental model systems are most suitable since downtimes of the actual polymerization mini-plants and uncertainties of simulations can be prevented.[2] Furthermore regarding the high-pressure polymerization of polyethylene and to the thereby applied steel reactors, an insight into the reactor is enabled by the model system due to reconstructed transparent reactor mimics. The mixing investigations in the experimental model systems in this work serve for a more precise understanding of different polymerization processes of polyethylene under high temperatures and moderate to high pressures.[3]

Experimental

For investigating mixing characteristics of different mini-plant reactors in pulse experiments, the respective polymerization conditions are translated to a more simplified system at atmospheric pressure and room temperature. The conversions and the reaction viscosities are adjusted by water and water-glycerol mixtures. Due to its good solubility in water, blue ink is applied as tracer in the pulse experiments. These measurements are performed in transparent reactors to realize a visualization of the flow lines inside the reactor. When constructing the transparent reactors, the inner geometry resembles the geometry of the real steel polymerization autoclaves. Regarding the stirrers, the steel version is translated to a stable 3D printed version. Hereby again, attention is paid to the concept of transparency to ensure a focus on the flow lines. The measuring device for the pulse experiments is depicted in Figure 1.[3]

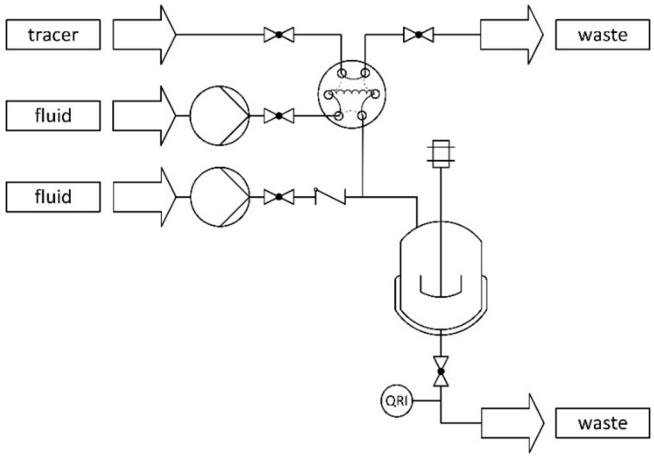

Fig. 1.: Measuring device for investigating mixing characteristics in pulse experiments [3].

A precise injection of the tracer is carried out by an electrically operated sample loop valve and a pulsation-free pump while the carrier stream of the fluid is dosed by another pump. Beneath the reactor, a colour sensor is sensitively detecting the tracer's concentration as function of time. The setup is designed for the investigations of the influences of the stirring frequency, the volume flow and the viscosity as well as the feed position on the mixing behaviour [3].

With the help of this setup, a large amount of data can be collected in a short time dependent on the research question. Generally, the video recorded flow lines of the blue ink inside the reactor are considered frame by frame and represent the basis for the validation of computational fluid dynamics (CFD) simulations. An example of the mixing behaviour of the 100 mL high-pressure reactor is shown in Figure 2. Thereby, the influence of the stirring frequency on the mixing behaviour becomes obvious. For a stirring frequency of 0 rpm, short-circuiting can be observed. From 100 rpm to 800 rpm, the mixing changes and the ink is mixed in from bottom to top much faster.

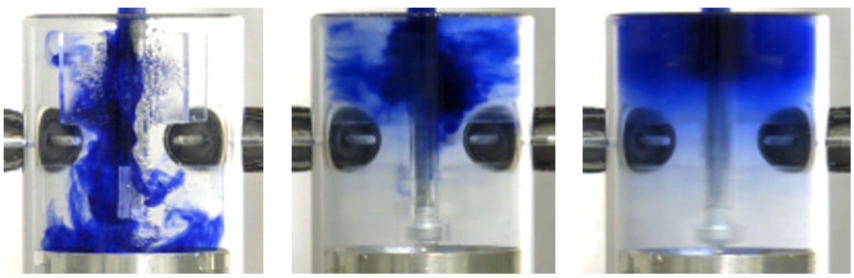

Fig. 2.: Mixing pictures at 2 s after the injection of blue ink for a stirring frequency of 0 rpm (left), 100 rpm (middle) and 800 rpm (right) [3]

The videos are further for the purpose of the determination of mixing time meaning the degree of homogeneity of the reactor. Next to this, the raw data of the color sensor provide additional results. The residence time distributions (RTD) and cumulative curves can be determined. Based on the RTD, the first moment can be calculated giving information on the mean residence time. With the second moment of the RTD, the variance or degree of dispersion can be evaluated. The skewness of the RTD is determined via the third moment of the RTD assessing the presence of channelling, dead zones or short circuiting in the reactor [4].

With these information different reactors are investigated. The validation of the setup is performed with a 100 mL high-pressure reactor. Besides, a study of side-feed injections is of key interest imitating further initiator or comonomer dosing in the actual polymerization system. For an upscaled reactor with a volume of 300 mL, the development of a stirrer can be implemented easier at the measuring device than in high-pressure polymerization plants. Further, the measuring device is used to investigate a reactor combination. Additionally, different conversions and reaction viscosities of the reactor are assessed for a solution polymerization system. All the collected data present a basis for the validation of CFD simulations [3]. The influence of different mixing behaviors during the polymerization process and on the resulting polymer properties is considered for an outlook.

Summary

The present work focusses on a measuring device designed for pulse experiments for the determination of the mixing behaviour for various reactors. The influence of the operation conditions such as stirring frequencies, volume flows, viscosities and feed positions are evaluated underlining the importance of knowing the mixing behaviour inside the reactor.

References

[1] M. Baerns, A. Behr, A. Brehm, J. Gmehling, K. O. Hinrichsen, H. Hofmann, R. Palkovits, U. Onken, A. Renken, Technische Chemie, Weinheim, **2013**.

[2] M. Busch, PhD Thesis, Georg-August-Universität zu Göttigen, **1993**.

[3] L. Ständecke, L. Gockel, M. Busch, *Chem. Ing. Tech.* **2023**.

[4] J. A. Conesa, *Chemical reactor design: Mathematical modeling and applications*, Wiley-VCH, Weinheim, **2020.**

Influence of Tannins Structure on the Formation of Coordination Compounds with Fe(II) Ions

Franjo Frešer[a], Urban Bren[a,b,c], Gregor Hostnik[a]

[a]Faculty of Chemistry and Chemical Engineering, University of Maribor,

[b]Faculty of Mathematics, Natural Sciences and Information Technologies, University of Primorska,

[c]Institute of Environmental Protection and Sensors,

franjo.freser@um.si

Introduction

Tannins are secondary plant metabolites found in various higher plants. They form important food constituents and present a significant proportion of polyphenols in the human diet [1]. Tannins' possible antioxidant, anticarcinogenic, antibacterial, and antiparasitic properties are among others being investigated in several studies [1][2]. Their aromatic rings and phenolic groups enable the formation of coordination compounds with metal ions [2][3]. Bacterial resistance to antibiotics is a growing problem; therefore, preventive usage of broad-spectrum antibiotics is being restricted. The addition of tannin extracts to animal feed presents one of the potential antibiotic substitutes [2]. Depletion of essential metal ions, such as Fe(II), from bacteria, which causes inhibition of their growth, is a proposed antibacterial mechanism [4]. Therefore, investigating the influence of different tannins on the concentration of iron ions in the medium is of crucial importance in developing more effective feed additives.

Experimental

The ability of the tannin hydrolysis product gallic acid (GA) [5] as well as ellagitannins (ETs) vescalin (VI), castalin (CI), vescalagin (VG), castalagin (CG), roburin-A (RO-A) and roburin-D (RO-A) (see Fig. 1), to form coordination compounds with Fe(II) ions was investigated, using the continuous variation method (Job plot) [6]. All ETs were isolated from chestnut wood using preparative HPLC chromatography and were later characterised by a comparison of retention times to retention times of standard compounds and NMR spectroscopy. For Job plot experiments the absorbances of solutions were measured with a Varian Cary 50 UV-Vis spectrophotometer and Cary 4000

UV-Vis Spectrophotometer. Both spectrophotometers were equipped with thermostated cuvette holders.

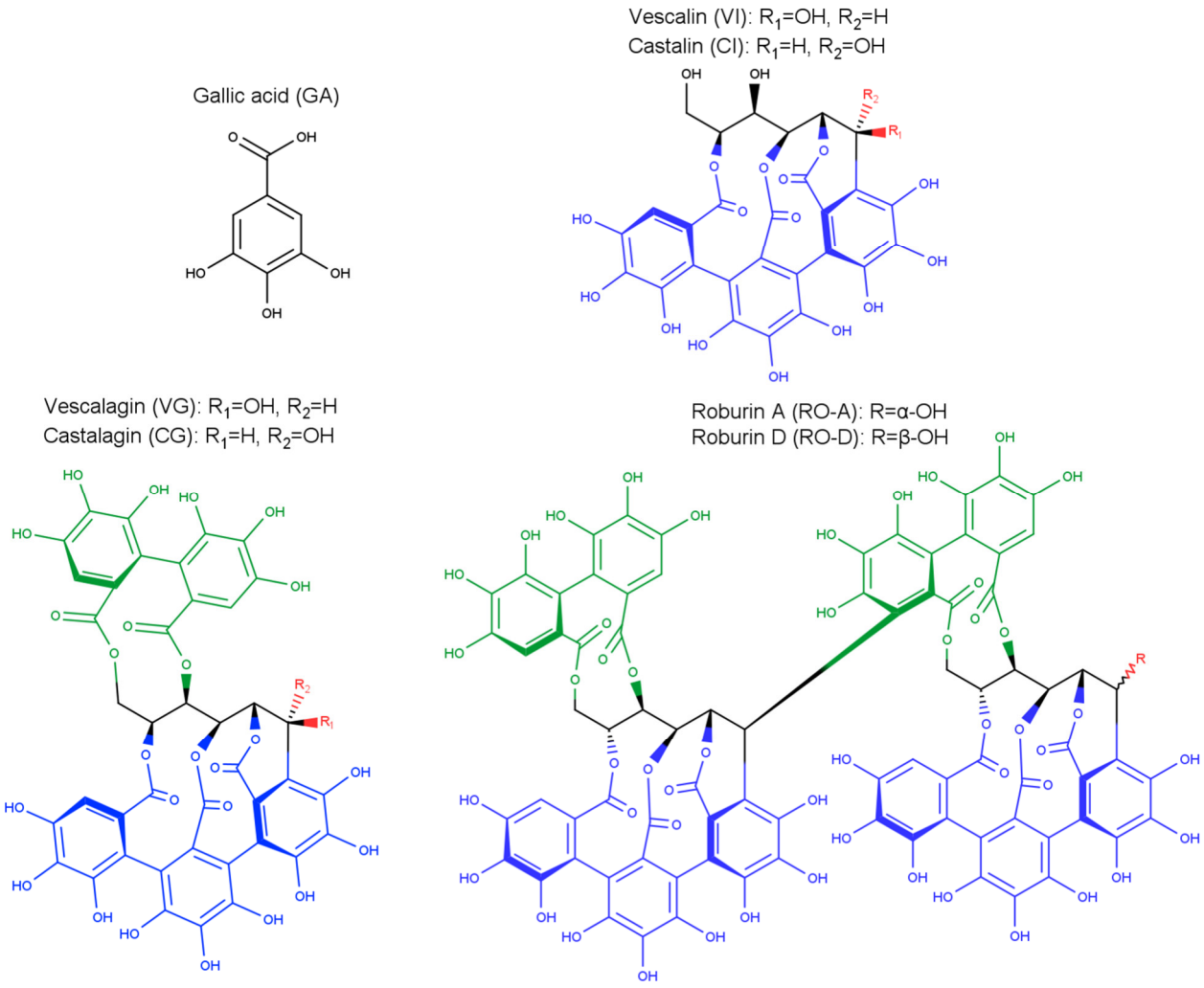

Fig. 1.: Chemical structures of investigated compounds. Red colour depicts different stereoconfiguration, while green and blue colour depicts HHDP and NHTP groups, respectively.

Ellagitannins isolation was carried out by performing several consecutive separation steps, using the preparative HPLC instrument PuriFlash 5.250 equipped with PDA and ELSD detectors. After every step of isolation, organic solvents were removed from the fractions obtained using a rotary evaporator, while water was removed using freeze drying. In the first step of isolation, 50 g of Sephadex LH-20 (25-100 μm) stationary phase was used, while the mobile phase consisted of type I water, methanol and acetone. Fractions rich with selected ETs, obtained from the first step, were further separated using C18 flash chromatography on column PF-50C18HP-F0025. The mobile phase consisted of 0.1 % formic acid (v/v) in water and 0.1 % formic acid (v/v) in acetonitrile. Fractions of ETs were purified using US10C18HQ-250/212 column. The mobile phase consisted of

0.1 % formic acid (v/v) in water and 0.1 % formic acid (v/v) in acetonitrile. Fig. 2 shows chromatograms for every step of CI isolation. By integrating the chromatographic peaks, the chromatographic purity of ETs was determined as 98 % in the case of VI, VG and CG, 97 % in the case of CI, and 96 % in the case of RO-A and RO-D.

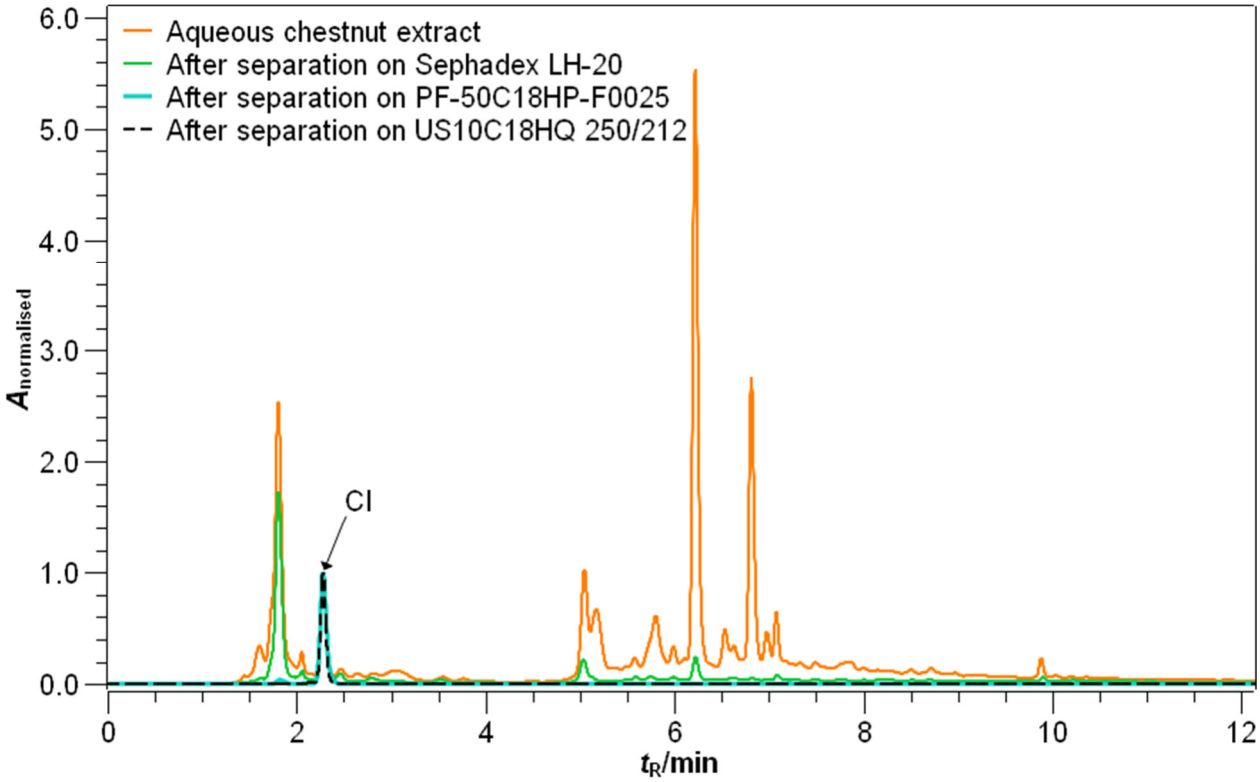

Fig. 2.: Chromatograms of aqueous chestnut abstract and fractions obtained after consecutive separations on Sephadex LH-20, PF-50C18HP-F0025 and US10C18HQ-250/212 column.

Job plot for the coordination compound formed by the reactions of each tannin with Fe(II) ions was constructed. Each tannin and Fe(II) ions sample was prepared in a 5,0 10^{-2} mol L^{-1} acetate buffer at a pH of 5.5. The concentration of tannin and Fe(II) ions in samples continuously varied in a way that the sum of concentrations of tannin and Fe(II) ions (c) was kept constant (in the case of GA c = 5,0·10^{-4} mol·L^{-1}, in the case of VI, CI, and CG c = 4,0·10^{-4} mol·L^{-1} while in the case of VG, RO-A and RO-D c= 2,0·10^{-4} mol·L^{-1}). For each sample, it was examined whether the system had already reached equilibrium by measuring a UV-Vis spectrum every five minutes until identical consecutive spectra were obtained. The stoichiometries of the formed coordination compounds were then determined from the position of the intersection of linear regression lines, that were fitted to the outermost points of the Job plots.

From Job plots (see Fig. 3) obtained values of linear regression line intersections (x) were 0.53 [5], 0.35, 0.34, 0.25, 0.27, 0.15, and 0.16 for GA, VI, CI, VG, CG, RO-A and

RO-D, respectively. Based on the obtained intercept values 1 mol of GA chelates 1 mol of Fe(II) ions, 1 mole of VI or CI chelate 2 mol of Fe(II) ions, 1 mol of VG or CG chelate 3 mol of Fe(II) ions and 1 mol of RO-A or RO-D chelate 6 mol of Fe(II) ions.

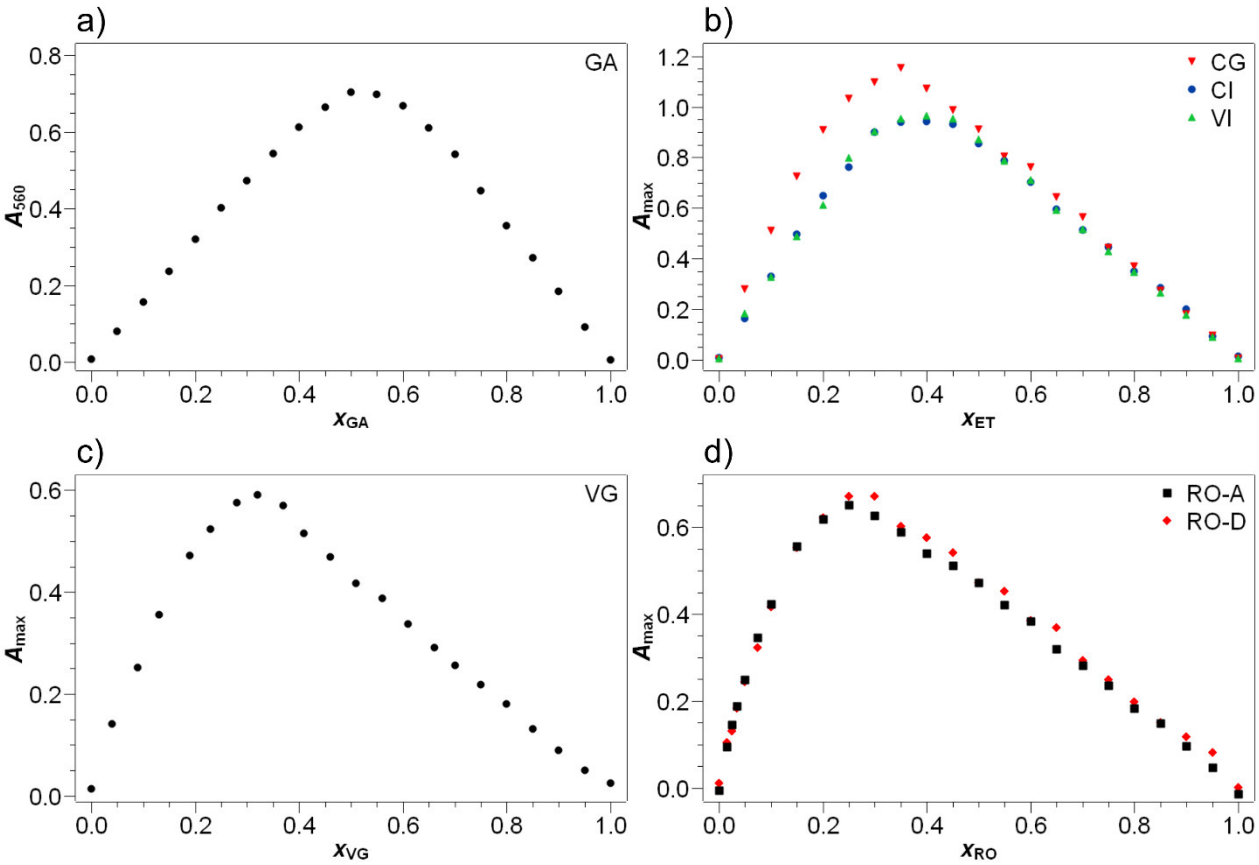

Fig. 3.: Job plots for the coordination compounds of Fe(II) ions and a) GA, b) VI, CI, CG, c) VG, d) RO-A, RO-D at pH = 5.5.

Summary

Six ellagitannins were isolated from the chestnut wood aqueous extract using preparative and semi-preparative HPLC. Afterwards, the ability of GA and isolated ETs to form coordination compounds with Fe(II) ions at the pH of 5.5 was investigated. It was shown that 1 mol of GA chelates 1 mol of Fe(II) ions, 1 mole of VI or CI chelate 2 mol of Fe(II) ions, 1 mol of VG or CG chelates 3 mol of Fe(II) ions and 1 mol of RO-A or RO-D chelate 6 mol of Fe(II) ions.

Acknowledgement

The authors thank the Slovenian Research Agency (ARRS), which supported this work through programme and project grants J1-2471, P2-0046, L2-3175, J4-4633, J1-4398, L2-4430, J3-4498, J7-4638, J1-4414, J3-4497, P2-0438, and I0-E015.

References

[1] Serrano J., Puupponen-Pimiä R., Dauer A., Aura A. M., Saura-Calixto, F. Tannins: Current knowledge of food sources, intake, bioavailability and biological effects. Mol Nutr Food Res, 53 (S2), S310-S329, 2009.

[2] Fraga-Corral M., García-Oliveira P., Pereira A. G., Lourenço-Lopes C., Jimenez-Lopez C., Prieto M. A., Simal-Gandara J. Technological application of tannin-based extracts. Molecules, 25 (3), 614, 2020.

[3] Okuda T., Ito H. Tannins of constant structure in medicinal and food plants—hydrolyzable tannins and polyphenols related to tannins. Molecules, 16 (3), 2191-2217, 2011.

[4] Akiyama H., Fujii K., Yamasaki O., Oono T., Iwatsuki K. Antibacterial action of several tannins against Staphylococcus aureus. J Antimicrob Chemother, 48 (4), 487 491, 2001.

[5] Frešer F., Hostnik G., Tošović J., Bren U. Dependence of the Fe (II)-Gallic Acid Coordination Compound Formation Constant on the pH. Foods, 10 (11), 2689, 2021.

[6] Renny J. S., Tomasevich L. L., Tallmadge E. H., Collum D. B. Method of continuous variations: applications of job plots to the study of molecular associations in organometallic chemistry. Angew. Chem. Int. Ed., 52 (46), 11998-12013, 2013.

Characterization of Cutin Monomers from Tomato Peel by Microwave-Assisted Basic Hydrolysis

María Constanza Maciel, María José Cocero Alonso, Rafael Bartolomé Mato Chaín

PressTech Group, Bioeconomy Research Institute, Chemical Engineering and Environment Technologies Department, University of Valladolid, Spain.

Email: mariaconstanza.maciel@uva.es

Introduction

Cutin can be found in the aerial part of fruits and vegetables as a major component of the plant cuticle structure. It is a three-dimensional biopolyester composed mainly of hydroxylated fatty acids of C16 and C18 chain lengths that are cross-linked by ester bounds giving rise to a very complex branched structure.[1] Due to this arrangement, little is yet known about its actual structure. Currently, long reaction times with many steps involved and expensive solvents and chemicals are used for its characterization, with the consequence of time and cost consuming[2]. The purpose of this work is to study the use of microwaves to reduce reaction times needed to complete cutin depolymerisation in order to characterize it and identify its monomer composition.

Experimental

First, the extractives from tomato peel were removed using cascade method with Soxhlet extraction using chloroform, methanol, and water[3]. After this, the extract free biomass (EFB) was dried overnight in an oven at 50°C and then manually grinded. Microwave-assisted basic hydrolysis (BHMW) was performed using a single mode microwave Monowave 300 (Anton Paar). Also, conventional basic hydrolysis for comparison was performed in a silicon bath (BHSB). The vessel was stirred, and the area not covered by the bath was insulated to homogenise the temperature. In both cases, 0.02 g of EFB per ml of 1M NaOH and 600 rpm of stirring were used. Temperature used were 100°C and 120°C with BHSB and 120°C for BHMW. Between 10 and 120 min of reaction time were evaluated in both cases. After each reaction, the system was immediately cooled down with compressed air in the case of microwaves and with cold water for silicon bath experiments.

The results were analysed by gravimetry (see figure 1) to control the hydrolysis ratio with non-hydrolysed residue and acid precipitation, Fourier Transform Infrared Spectrometry (FTIR) for characterization and gas chromatography-mass spectrometry (GC-MS) to determine fatty acid composition. The main monomers were identified by mass spectra analysis and Kovats Index calculation, as well as comparison with NIST library and literature of previous works.

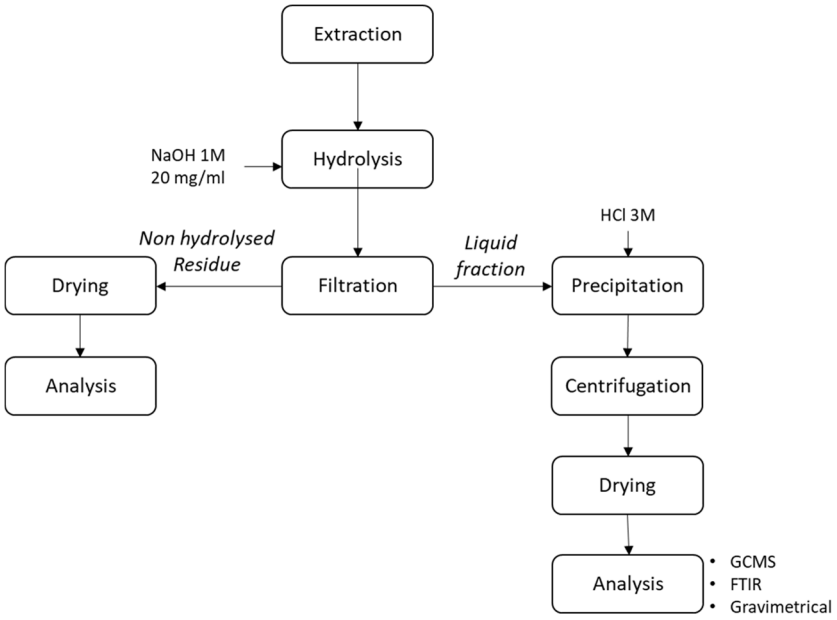

Figure 1: Processes diagram

Summary

In both methods the complete hydrolysis of the ester bounds can be achieved at 60 min with 120°C using sodium hydroxide at 1 molar concentration. But the main difference between them is 25% more conversion of the main monomer can be obtained with BHMW. As we are getting more monomers, we can think that may be microwaves are improving the depolymerisation ratio by helping to cleave the ester bound. But most importantly, reaction times can be reduced, thus saving time and energy.

Acknowledgment

This work was supported by Ministry of Science and Innovation & FEDER for funding the project PID2019-105975GB-I00 and the Regional Government of Castilla y León & FEDER for funding the program CLU-2019-04. C. Maciel thanks to Ministry of Science and Innovation for her predoctoral contract.

References

1. Fich, E. A., Segerson, N. A. & Rose, J. K. C. The Plant Polyester Cutin: Biosynthesis, Structure, and Biological Roles. *Annual Review of Plant Biology* vol. 67 207–233 (2016).
2. Heredia-Guerrero, J. A. *et al.* Cutin from agro-waste as a raw material for the production of bioplastics. *J. Exp. Bot.* **68**, 5401–5410 (2017).
3. Sluiter, A. *et al.* Determination of Ash in Biomass. *Lab. Anal. Proced.* **36**, 302–305 (2008).

Continuous Electroreduction of Compressed CO_2 to CO

Stephan Heuser[1,2], Lucas Hoof[3], Eduardo García Alanís[2], Michael Prokein[2], Andreas Kilzer[1], Ulf-Peter Apfel[3,4], Marcus Petermann[1]

[1]Institute for Particle Technology, Ruhr University Bochum, NRW, Germany

[2]Product Development, Fraunhofer Institute for Environmental, Safety and Energy Technology, Oberhausen, NRW, Germany

[3]Electrosynthesis, Fraunhofer Institute for Environmental, Safety and Energy Technology, Oberhausen, NRW, Germany

[4]Inorganic Chemistry I, Ruhr University Bochum, NRW, Germany

Introduction

In the future, achieving carbon cycle closure in the production of fuels and essential chemicals will be a significant challenge. To address this challenge, there is a growing emphasis on processes like Carbon Capture and Utilization, which involve capturing and reusing carbon dioxide (CO_2). These innovative methods utilize CO_2 as a raw material, along with renewable energy sources, to generate carbon-based energy and important chemicals.[1–3] Initially, valuable feedstocks can be obtained by effectively harnessing CO_2 emissions from fossil power plants. However, the long-term objective is to directly capture CO_2 from the atmosphere or from biomass, thus enabling a closed carbon cycle.[1–4]

Electrochemical CO_2 reduction (CO_2R) is a highly promising approach for utilizing captured CO_2, as it enables the conversion of CO_2 into valuable carbon-based energy sources and chemical feedstocks. This process relies on volatile renewable power sources like wind or solar power plants to effectively harness peak power generation, playing a crucial role in the overall process.[5, 6] A particular focus is given to the conversion of CO_2 into carbon monoxide (CO), which is widely used in combination with hydrogen to form syngas. Currently, the market price of CO is $0.8 per kilogram, and it has an existing sales market valued at $3 billion.[7] By integrating with processes such as Fischer-Tropsch synthesis, the resulting syngas can be used to produce high-value hydrocarbons like kerosenes, alcohols, and synthetic fuels.[8, 9] Industrial-scale CO_2R to CO using zero-gap technology, which is well-known from water electrolysis, has demonstrated continuous and scalable performance metrics that are relevant to industry. Despite these promising outcomes, this technology is still in the early stages of development, and it is crucial to enhance the long-term stability, scalability, energy efficiency, and revenue of these systems.[10, 11]

In zero-gap electrolyzers various types of membranes can be utilized, including cation exchange membranes (CEMs), bipolar membranes (BPMs), and commonly used anion exchange membranes (AEMs). The choice of membrane is vital as it governs the ion transport processes between the electrodes and influences the chemical environment at the membrane-catalyst interfaces. CEMs facilitate the migration of cations, particularly H^+ ions, from the anode to the cathode. Conversely, AEMs enable the transport of anions such as OH^-, CO_3^{2-}, and HCO_3^- from the cathode to the anode. BPMs consist of both an AEM and a CEM, resulting two different types of ion conduction.[12, 13] In the reverse BPM (r-BPM) configuration, the CEM is positioned at the cathode side while the AEM is located at the anode side. In this arrangement, water dissociates at the membrane junction, causing OH^- ions to migrate towards the anode and H^+ ions towards the cathode. When the membrane order is reversed, known as forward BPM (f-BPM), H^+ ions move from the anode, while OH^-, CO_3^{2-}, or HCO_3^- ions from the cathode transport to the membrane junction, thereby maintaining ion conduction.[12, 14]

Currently, in zero-gap electrolyzers, AEMs are commonly used to create an alkaline environment that favors CO_2R over the parasitic hydrogen evolution reaction (HER).[15, 16] However, the application of AEMs presents several challenges, including CO_2 crossover, carbonate formation, and cathode flooding. Overcoming these obstacles is crucial to improve the efficiency and stability of CO_2 electrolysis.[17]

CEMs and r-BPMs create highly acidic conditions at the cathode catalyst layer due to proton transport from the anode to the cathode, unintentionally promoting the parasitic HER.[15, 16, 18] Nevertheless, studies have indicated lower Faraday efficiencies for CO (FE_{CO}) in zero-gap electrolyzers that employ f-BPMs. The exact cause of this phenomenon remains uncertain, but it is likely related to challenges in accurately monitoring local pH levels.[19, 20] Additionally, the use of f-BPMs poses significant challenges due to the transport of protons and carbonate ions, leading to the generation of water and CO_2 within the membrane, which can cause physical separation and eventual mechanical failure.[12] Furthermore, BPMs require a significant membrane potential, resulting in increased voltage requirements for electrolysis and reduced overall energy efficiency.[19, 21] Despite these drawbacks, BPMs offer several advantages over monopolar ion exchange membranes. They allow the use of two distinct electrolyte solutions while maintaining a consistent pH gradient across the membrane. BPMs also exhibit reduced product crossover compared to monopolar membranes and allow the elimination of additional acids and bases.[22]

The implementation of differential pressure between the cathode and anode offers a promising strategy to improve CO_2 electrolysis. Applying increased pressure to the cathode side brings about mechanical, electrochemical, and thermodynamic benefits.[23] This approach is particularly advantageous for integration into process chains, as higher gas pressure facilitates transportation and allows downstream processes like Fischer-Tropsch synthesis to be conducted under pressure as well.[24] The application of pressure in CO_2 electrolysis yields positive effects, including enhanced CO_2 conversion and reduced cell voltage.[23, 25, 26] Studies on the electrolysis of CO_2 under differential pressure have highlighted the significant influence of pressure on key parameters such as Faraday efficiency, cell voltage, and conversion rate. However, there is still a research gap in this area, particularly in the emerging field of bipolar CO_2 electrolysis.

In order to fill this research gap, we have developed a continuous high-pressure reactor with a zero-gap design, allowing for increased CO_2 pressure. Notably, the bipolar system employed in our study eliminates the need for humidifying the CO_2 stream and utilizes ultrapure water as a proton source. The application of pressure led to significant enhancements in Faraday efficiency for CO (FE_{CO}) at current densities relevant to industrial applications, accompanied by a substantial reduction in cell voltage by several hundred millivolts. The highest selectivity for CO and the lowest cell voltage were observed at the maximum tested differential pressure of 20 bar(g). At a current density of 100 mA cm^{-2}, an average FE_{CO} of 76 % and a cell voltage of 2.6 V were consistently maintained over a duration of 95 minutes. These findings highlight the immense potential of differential pressure electrolysis.

Experimental

Measurement setup

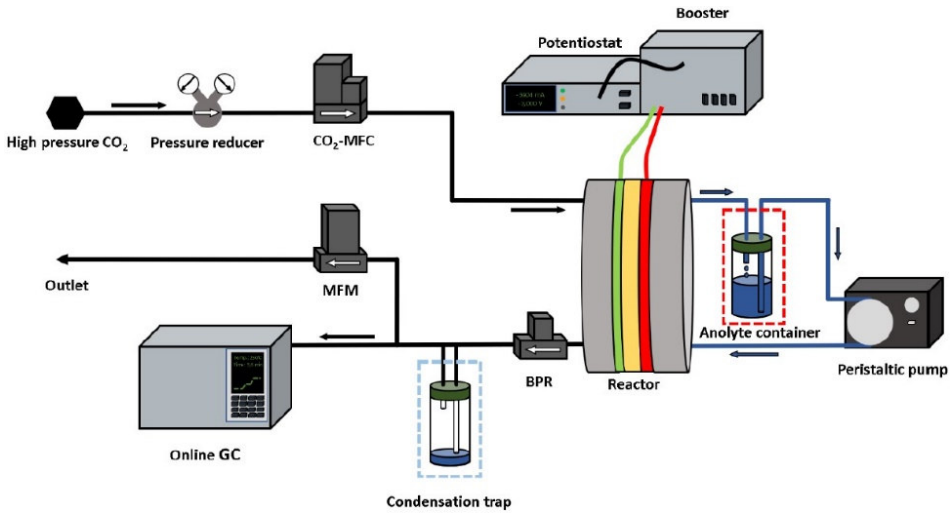

Fig. 1: Simplified schematic layout of the test stand

The experiments were carried out using a high-pressure test rig, illustrated in **Fig. 1**. The CO_2 was sourced from a tank and compressed to a maximum of 200 bar(g). It underwent an initial expansion to approximately 50 bar(g) before being controlled by a mass flow controller (MFC) to maintain a constant mass flow rate of 300 mln min^{-1}. The CO_2 then entered the reactor and flowed through the cathode flow field of the electrolyzer. Downstream of the electrolyzer, a back pressure regulator (BPR) was employed to regulate the CO_2 pressure. To achieve this, a dome pressure was applied to the BPR using nitrogen from a gas cylinder. Following the BPR, a cold trap was used to separate water and potential liquid products. Subsequently, the gas passed through a mass flow meter. A gas chromatograph (GC) was connected after the separator via a three-way valve, allowing for periodic analysis of the gaseous product stream using online gas chromatography.

In the anode section of the setup, there was an anolyte tank that held 500 ml of ultrapure water (Mili-Q). This ultrapure water was continuously circulated at a flow rate of 4.8 L/h using a peristaltic pump. The temperature of the water was measured just before it entered the electrolytic cell and was found to be 53 °C. To compensate for any temperature losses, the ultrapure water in the tank was heated to a temperature of 63 °C using a heating plate.

Fabrication of the membrane electrode assemblies

The catalyst and ionomer layers are applied using a spray coating technique. For the bipolar membrane, a solution containing 1.25 wt % PiperION ionomer in ethanol is sprayed onto a Nafion 117 membrane using a spray gun (Iwata Takumi Eclipse) at a temperature of 80 °C until the desired loading is achieved. Subsequently, the membranes are hot-pressed at 80 °C for a duration of 3 minutes.

The catalyst layers (CL) utilize ionomer-based inks consisting of a catalyst, an ionomer, and a solvent. The ionomer plays a vital role in providing ionic conductivity and binding the catalyst to the electrode. To prepare the ink, the catalyst is dispersed with the ionomer in a mixture of isopropanol and water with a ratio of 7:3. To ensure thorough mixing of the components, the ink is subjected to an ultrasonic bath for 15 minutes, followed by mixing with a disperser at a speed of 13,000 min^{-1} for 90 seconds.

At the cathode, silver nanoparticles (Alfa Aesar) combined with varying amounts of PiperION ionomer are sprayed onto a carbon cloth (CT W1S1010) at a temperature of 80 °C, achieving a loading of 2.5 mg cm^{-2}. At the anode, iridium oxide powder (Alfa Aesar) blended with 15 wt % Nafion D2020 ionomer is sprayed onto a titanium felt (Bekaert-2GDL40) at a temperature of 90 °C, resulting in a loading of 0.85 mg cm^{-2}.

Electrochemical measurement results

As shown in **Fig. 2**, the impact of pressurizing the CO_2 feed was investigated within the range of 0 to 60 bar(g) on electrolysis efficiency and the suppression of the HER.

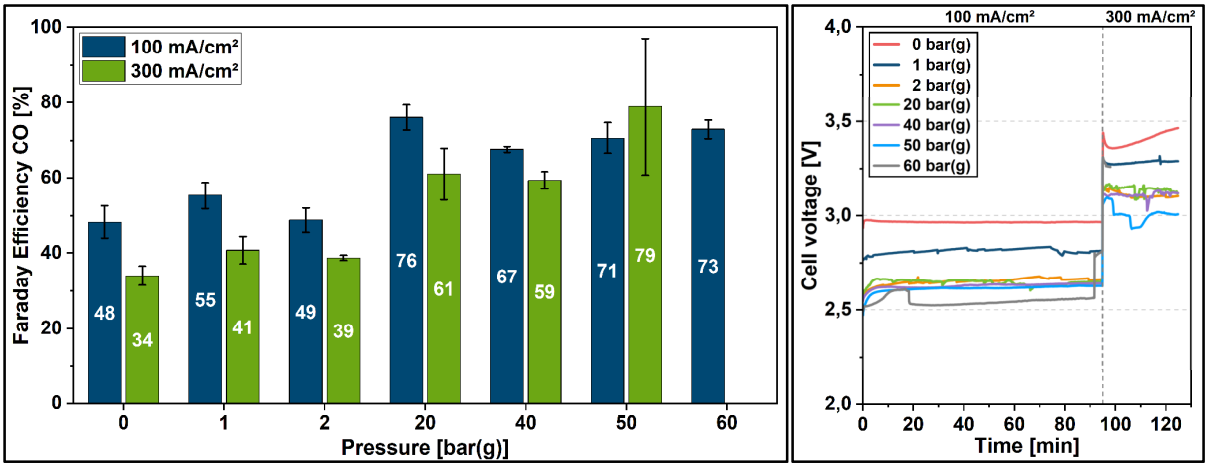

Fig. 2: FE_{CO} (left) and cell voltage (right) at a current density of 100 and 300 mA·cm-2 and a pressure of 0 to 60 bar(g). Measurements were taken after 30, 60, 90 and 120 minutes of electrolysis. The graph show the average FE_{CO} over the measurement points. Every experiment was carried out twice.

The process of electrolysis was performed using a chronopotentiometric technique. Initially, a constant current density of 100 mA cm^{-2} was applied for a duration of 95 minutes. This was followed by a subsequent period of 30 minutes during which the current density was increased to 300 mA cm^{-2}. Upon examining both current densities, it is observed that the FE_{CO} in the low pressure range (0 – 2 bar(g)) is lower, approximately 50 % and 40 % respectively, compared to the high pressure range (20 – 50 bar(g)), where FE_{CO} reaches approximately 70 % and 60 % respectively. This finding suggests that the CO_2R is favored in the high pressure range due to the increased availability of CO_2 molecules, consequently leading to the suppression of the HER. Additionally, a notable decrease of approximately 200 mV in cell voltage is observed within the lower pressure range (0 to 2 bar(g)). This decrease in cell voltage may be attributed not only to the improved availability of CO_2 but also to a better electrode contact pressure resulting from the pressurization. Interestingly, further increases in pressure do not yield significant drops in cell voltage. Remarkably, the membrane ruptured after 100 minutes of electrolysis when subjected to a differential pressure of 60 bar(g), indicating that this level of differential pressure exceeds the operational limit of the system.

Summary

We established a new test setup and constructed a zero-gap high-pressure reactor to facilitate continuous CO_2 electrolysis at pressures of up to 60 bar(g). Additionally, the

membrane electrode assembly was adapted by incorporating a BPM instead of the commonly used AEM in research. It was observed that cathode-side pressure application had a significant effect on improving efficiency and product selectivity. Impressive FE_{CO} of up to 80 % and current densities reaching 500 mA cm^{-2} were achieved, representing substantial progress towards achieving industrially relevant process parameters.

Acknowledgment

Funded by the Deutsche Forschungsgemeinschaft (DFG, German Research Foundation) under Germany's Excellence Strategy - EXC-2033 – 390677874 - RESOLV.

References

1. Meinshausen, M., Meinshausen, N., Hare, W., Raper, S.C.B., Frieler, K., Knutti, R., Frame, D.J., and Allen, M.R. (2009). Greenhouse-gas emission targets for limiting global warming to 2 degrees C. Nature *458,* 1158–1162.
2. Hepburn, C., Adlen, E., Beddington, J., Carter, E.A., Fuss, S., Mac Dowell, N., Minx, J.C., Smith, P., and Williams, C.K. (2019). The technological and economic prospects for CO2 utilization and removal. Nature *575,* 87–97.
3. Gao, W., Liang, S., Wang, R., Jiang, Q., Zhang, Y., Zheng, Q., Xie, B., Toe, C.Y., Zhu, X., and Wang, J., et al. (2020). Industrial carbon dioxide capture and utilization: state of the art and future challenges. Chemical Society reviews *49,* 8584–8686.
4. Okesola, A.A., Oyedeji, A.A., Abdulhamid, A.F., Olowo, J., Ayodele, B.E., and Alabi, T.W. (2018). Direct Air Capture: A Review of Carbon Dioxide Capture from the Air. IOP Conf. Ser.: Mater. Sci. Eng. *413,* 12077.
5. Barnhart, C.J., Dale, M., Brandt, A.R., and Benson, S.M. (2013). The energetic implications of curtailing versus storing solar- and wind-generated electricity. Energy Environ. Sci. *6,* 2804.
6. Saadi, F.H., Lewis, N.S., and McFarland, E.W. (2018). Relative costs of transporting electrical and chemical energy. Energy Environ. Sci. *11,* 469–475.
7. Shin, H., Hansen, K.U., and Jiao, F. (2021). Techno-economic assessment of low-temperature carbon dioxide electrolysis. Nat Sustain *4,* 911–919.
8. Krylova, A.Y. (2014). Products of the Fischer-Tropsch synthesis (A Review). Solid Fuel Chem. *48,* 22–35.

9. Henrici-Olivé, G., and Olivé, S. (1976). Die Fischer-Tropsch-Synthese: Molekulargewichtsverteilung der Primärprodukte und Reaktionsmechanismus. Angew. Chem. *88,* 144–150.
10. Chang, F., Zhan, G., Wu, Z., Duan, Y., Shi, S., Zeng, S., Zhang, X., and Zhang, S. (2021). Technoeconomic Analysis and Process Design for CO 2 Electroreduction to CO in Ionic Liquid Electrolyte. ACS Sustainable Chem. Eng. *9,* 9045–9052.
11. Rabiee, H., Ge, L., Zhang, X., Hu, S., Li, M., and Yuan, Z. (2021). Gas diffusion electrodes (GDEs) for electrochemical reduction of carbon dioxide, carbon monoxide, and dinitrogen to value-added products: a review. Energy Environ. Sci. *14,* 1959–2008.
12. Vass, Á., Kormányos, A., Kószó, Z., Endrődi, B., and Janáky, C. (2022). Anode Catalysts in CO2 Electrolysis: Challenges and Untapped Opportunities. ACS catalysis *12,* 1037–1051.
13. Blommaert, M.A., Sharifian, R., Shah, N.U., Nesbitt, N.T., Smith, W.A., and Vermaas, D.A. (2021). Orientation of a bipolar membrane determines the dominant ion and carbonic species transport in membrane electrode assemblies for CO2 reduction. Journal of materials chemistry. A *9,* 11179–11186.
14. Oener, S.Z., Foster, M.J., and Boettcher, S.W. (2020). Accelerating water dissociation in bipolar membranes and for electrocatalysis. Science (New York, N.Y.) *369,* 1099–1103.
15. Larrazábal, G.O., Strøm-Hansen, P., Heli, J.P., Zeiter, K., Therkildsen, K.T., Chorkendorff, I., and Seger, B. (2019). Analysis of Mass Flows and Membrane Cross-over in CO2 Reduction at High Current Densities in an MEA-Type Electrolyzer. ACS applied materials & interfaces *11,* 41281–41288.
16. Delacourt, C., Ridgway, P.L., Kerr, J.B., and Newman, J. (2008). Design of an Electrochemical Cell Making Syngas (CO+H[sub 2]) from CO[sub 2] and H[sub 2]O Reduction at Room Temperature. J. Electrochem. Soc. *155,* B42.
17. Lees, E.W., Mowbray, B.A.W., Parlane, F.G.L., and Berlinguette, C.P. (2022). Gas diffusion electrodes and membranes for CO2 reduction electrolysers. Nat Rev Mater *7,* 55–64.
18. Hori, Y., Ito, H., Okano, K., Nagasu, K., and Sato, S. (2003). Silver-coated ion exchange membrane electrode applied to electrochemical reduction of carbon dioxide. Electrochimica Acta *48,* 2651–2657.

19. Ge, L., Rabiee, H., Li, M., Subramanian, S., Zheng, Y., Lee, J.H., Burdyny, T., and Wang, H. (2022). Electrochemical CO2 reduction in membrane-electrode assemblies. Chem *8,* 663–692.
20. Li, Y.C., Zhou, D., Yan, Z., Gonçalves, R.H., Salvatore, D.A., Berlinguette, C.P., and Mallouk, T.E. (2016). Electrolysis of CO 2 to Syngas in Bipolar Membrane-Based Electrochemical Cells. ACS Energy Lett. *1,* 1149–1153.
21. Vargas-Barbosa, N.M., Geise, G.M., Hickner, M.A., and Mallouk, T.E. (2014). Assessing the utility of bipolar membranes for use in photoelectrochemical water-splitting cells. ChemSusChem *7,* 3017–3020.
22. Ramdin, M., Morrison, A.R.T., Groen, M. de, van Haperen, R., Kler, R. de, Irtem, E., Laitinen, A.T., van den Broeke, L.J.P., Breugelmans, T., and Trusler, J.P.M., et al. (2019). High-Pressure Electrochemical Reduction of CO 2 to Formic Acid/Formate: Effect of pH on the Downstream Separation Process and Economics. Ind. Eng. Chem. Res. *58,* 22718–22740.
23. Endrődi, B., Kecsenovity, E., Samu, A., Darvas, F., Jones, R.V., Török, V., Danyi, A., and Janáky, C. (2019). Multilayer Electrolyzer Stack Converts Carbon Dioxide to Gas Products at High Pressure with High Efficiency. ACS Energy Lett. *4,* 1770–1777.
24. Bachmann, M., Völker, S., Kleinekorte, J., and Bardow, A. (2023). Syngas from What? Comparative Life-Cycle Assessment for Syngas Production from Biomass, CO 2 , and Steel Mill Off-Gases. ACS Sustainable Chem. Eng. *11,* 5356–5366.
25. Gabardo, C.M., Seifitokaldani, A., Edwards, J.P., Dinh, C.-T., Burdyny, T., Kibria, M.G., O'Brien, C.P., Sargent, E.H., and Sinton, D. (2018). Combined high alkalinity and pressurization enable efficient CO 2 electroreduction to CO. Energy Environ. Sci. *11,* 2531–2539.
26. Dufek, E.J., Lister, T.E., Stone, S.G., and McIlwain, M.E. (2012). Operation of a Pressurized System for Continuous Reduction of CO 2. J. Electrochem. Soc. *159,* F514-F517.

Modelling the High-Pressure Process of Ethylene-Methyl Acrylate Copolymerization

Joshua Stahl, Nicola Schreiner, Markus Busch*

TU Darmstadt, Darmstadt/Germany, *markus.busch@pre.tu-darmstadt.de

Introduction

Polymers, such as low-density polyethylene (LDPE), represent one important class of base materials with applications ranging from products for day-to-day life to highly specific industrial applications. The individually required polymer attributes are determined by the chemical structure of the polymer chain, which in turn can be controlled through the reaction conditions and the introduction of comonomers. Therefore, it is important to obtain further understanding on the industrial production process of LDPE and its comonomers. Modelling is used in this context as a toolbox and can also be employed in the prediction of polymer properties.[1] The description of the high-pressure polymerization process requires extensive kinetic data on the individual reactions, which are already well established in literature for the LDPE homopolymerization. However, the addition of a comonomer requires additional consideration for the cross-reactions between the monomers. In this work, the literature kinetic coefficients on the free-radical polymerization of methyl acrylate (MA) and its copolymerization with ethylene are summarized, re-evaluated and extended for usage in a deterministic model using the software Predici®.

Modelling

In the first step, the available literature data on the different kinetic coefficients is summarized. For the evaluation, the data points are grouped by their determination method and respective reaction conditions, which are then visualized in Arrhenius plots. For the homopropagation of methyl acrylate, the data points show a dependency on whether the experiment was conducted in solution or in bulk phase. With the approach of covariance ellipses [2], a possible correlation between the fits is investigated and matching data combined into a single Arrhenius fit equation. This procedure is repeated for all coefficients, where sufficient data is available.

In addition, the significance of more stable tertiary mid-chain radicals, which occur when MA is involved in the polymerization, is investigated. These radicals are formed following the transfer to polymer and backbiting reactions (Figure 1).

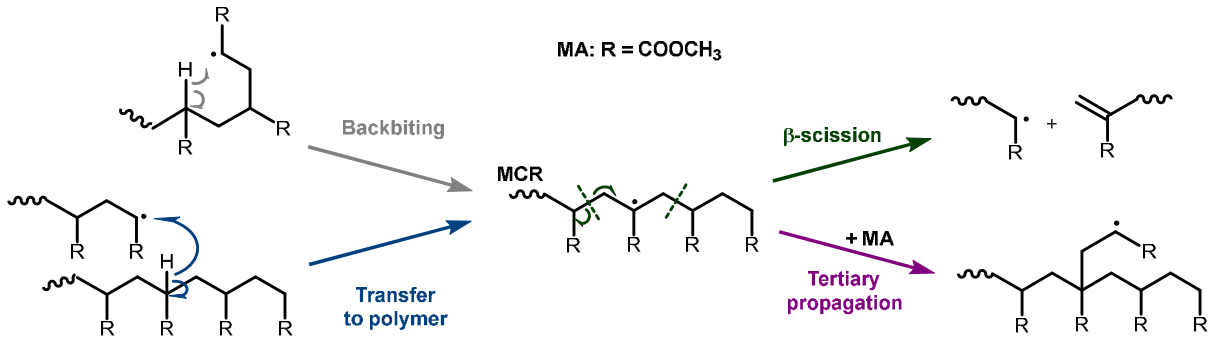

Figure 1: Reactions leading to a tertiary mid-chain radical and the possible follow-up reactions in a MA homopolymerization.

In literature, the propagation rate of tertiary MA radicals is estimated to be about one thousandth of the standard rate of secondary propagation.[3] The effect of more stable tertiary MA radicals as well as the backbiting of acrylate chain ends[4] was not included a previous deterministic Predici® model, based on the data by van Boxtel,[5, 6] and is added to the used set of kinetic coefficients.

The effect of the updated set of kinetic coefficients on process and product properties is investigated on a model tubular reactor, created by Pflug[7] for LDPE, which is expanded towards EMA. As the separate consideration of the tertiary propagation influences the molecular weight and branching values, experimental molecular weight distributions (MWD) from experiments in a 100 ml miniplant autoclave are used to validate the approach in the simulation. It was found that the new kinetic coefficients need to be adapted in order to match the experimental MWD. In this context, the previous β-scission rate coefficient showed increased values in comparison to the kinetic data of other acrylates. As a result, the β-scission coefficient is varied to compensate the propagation of tertiary MA radicals. The deterministic model is able to depict the experimental MWD and the results are confirmed by simulations without the separate consideration of tertiary radicals and a subsequent stochastic Monte Carlo simulation in both cases.

Summary

In this work, a deterministic model for the ethylene-methyl acrylate copolymerization is set up and the underlying kinetic system investigated. Available data from literature on the kinetic coefficients of the ethylene-methyl acrylate copolymerization are summarized and re-evaluated. The additional influence of slower propagating, more stable tertiary mid-chain MA radicals is included in the model as well. The results are investigated in a model tubular reactor and the implementation of the kinetics confirmed using experimental results obtained in a 100 ml miniplant reactor setup.

References

[1] K. M. Zentel, M. Busch, *Macro Reaction Engineering*, **2022**, *16*, 2100027.

[2] E. Nowottny, *unpublished dissertation*, Technical University Darmstadt, **2023**.

[3] C. Barner-Kowollik, S. Beuermann, M. Buback, P. Castignolles, B. Charleux, M. L. Coote, R. A. Hutchinson, T. Junkers, I. Lacík, G. T. Russell et al., *Polym. Chem.*, **2014**, *5*, 204–212.

[4] H. Kattner, M. Buback, *Macromolecules*, **2018**, *51*, 25–33.

[5] K. Becker, *Dissertation*, Technical University Darmstadt, **2010**.

[6] H. C. M. van Boxtel, *Dissertation*, Georg-August-Universität Göttingen, **2000**

[7] K. M. Pflug, M. Busch, *Chemie Ingenieur Technik*, **2016**, 88, 1665–1675.

Supercritical Carbon Dioxide as a Solvent in Graphene Production via Ultrasound Assisted Exfoliation with Intercalating Compounds

Małgorzata Djas[1,2], Marek Henczka[2], Przemysław Rakowski[1,2*]

[1]Łukasiewicz Research Network – Institute of Microelectronics and Photonics, al. Lotników 32/46, 02-668 Warsaw, Poland

[2]Faculty of Chemical and Process Engineering, Warsaw University of Technology, Waryńskiego 1, 00-645 Warsaw, Poland

*corresponding author: przemyslaw.rakowski.stud@pw.edu.pl

Introduction

There are multiple methods of producing graphene, in which top-down and bottom-up approaches can be distinguished. The first group of methods aim to break down bulk structures of carbon (like graphite) to obtain graphene. Bottom-up methods are synthetizing graphene from molecules using different materials as carbon source (methane [1], acetylene [2], carbon monoxide [3] etc.). Each of these approaches has its advantages and disadvantages, but none is ideal. In this work the focus was laid on exfoliating raw graphite to graphene (top-down approach) using liquid exfoliation coupled with ultrasounds. This process traditionally takes place in toxic, high-boiling liquids such as N-Methyl-2-pyrrolidone [4] or N,N-Dimethylformamide [5]. There have been made attempts to instead use low-boiling points solvents (chloroform, isopropanol [6] and 1-propanol [7]), so as to remove the solvent more easily from obtained product. However, those methods are not providing satisfactory results regarding quality and quantity of graphene. Recently supercritical carbon dioxide ($scCO_2$) [8] has been used as a solvent. It is nontoxic, environmentally friendly solvent, obtained by compressing carbon dioxide to pressure and temperature above its critical points (respectively 73.8 bar and 31 °C). Its properties, e.g. low surface tension, high diffusivity, low kinematic viscosity, allow effective exfoliation of graphite. Additional factor that causes exfoliation (apart from ultrasounds) is rapid depressurization procedure – intercalated CO_2 expands and pushes graphene layers apart. But even those two factors put together are not enough to effectively exfoliate graphite, that's why improvements to this method are needed. Exfoliation efficiency may be increased by addition of intercalating compounds e.g. pyrene-polymers [9]. In this work vanillin and 2-naphthol were used as intercalating compounds to improve efficiency of graphene production using $scCO_2$.

Experimental

In this work the following materials were used: natural graphite NO. 635 (Asbury Carbons, USA), vanillin (pure p.a. POCH, Poland), 2-naphthol (pure p.a., Chempur, Poland), carbon dioxide (purity > 99.996%, Linde Gaz, Poland), ethyl alcohol 96% (pure p.a., Chempur, Poland).

The initial load of a high-pressure reactor is: raw graphite, intercalating compound and (optionally) ethanol. Then CO_2 is pumped into the vessel and process conditions are achieved by precise pressure and temperature control. After experimental setup is finished, ultrasonics treatment begins. It consists of low amplitude short pulses to promote intercalation (when intercalating compound is used) and one hour long, high amplitude, constant sonication. The process is conducted in experimental system shown in Fig. 1.

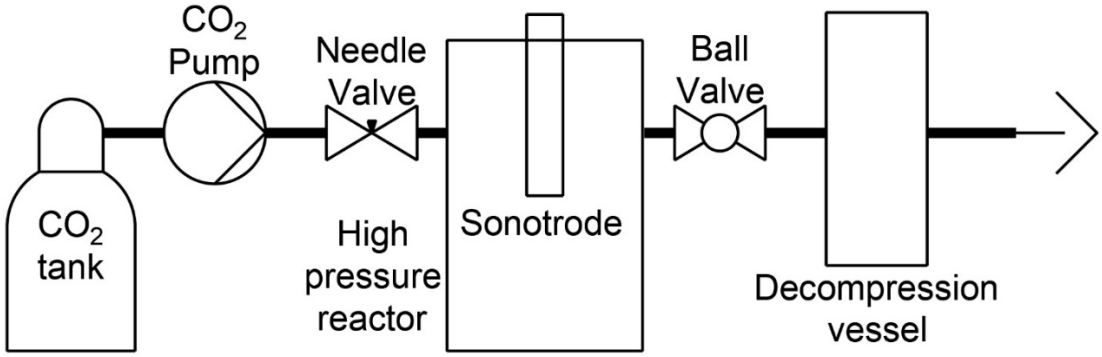

Fig. 1.: Scheme of experimental system.

After ultrasound treatment the reactor is rapidly depressurized. Obtained material is purified and investigated using scanning electron microscope (SEM).

Results

SEM image of raw graphite is presented in Fig. 2. and SEM images of material after experimental process are presented in Fig. 3.

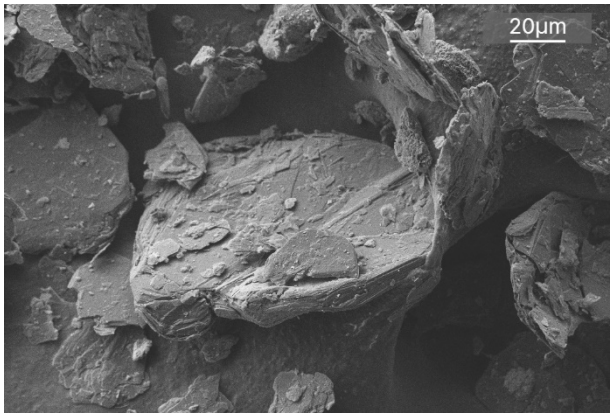

Fig. 2.: SEM image of raw graphite before process.

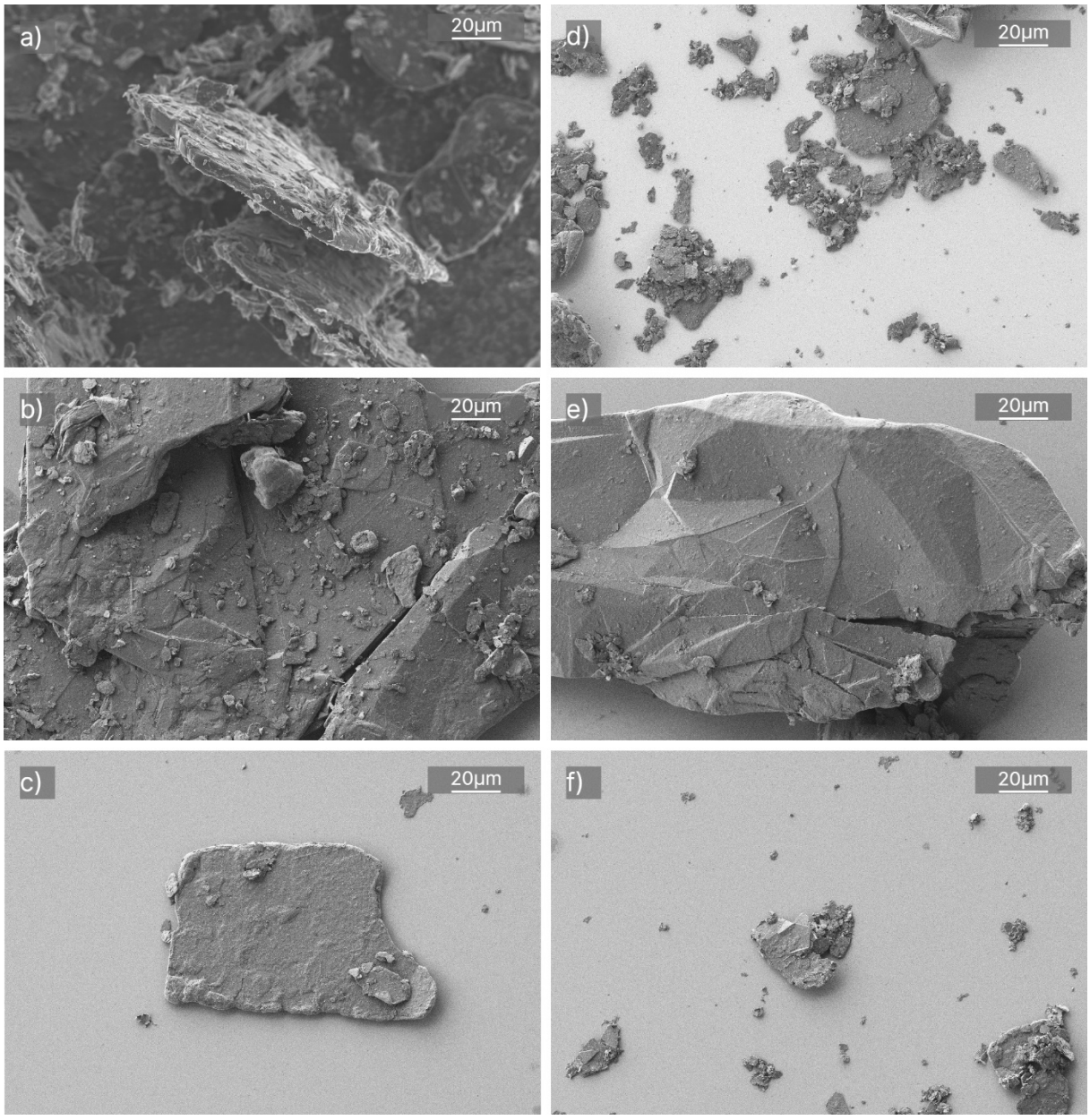

Fig. 3.: SEM images of material after experimental process:
without cosolvent: a) ultrasounds (US); b) US & vanillin; c) US & 2-naphthol and
with cosolvent d) US & EtOH; e) US & EtOH & vanillin; f) US & EtOH 2-naphthol.

Summary

Ultrasounds treatment on its own in supercritical carbon dioxide is not able to thoroughly exfoliate graphite. Multiple flakes of similar size as source material are visible (Fig. 3a). The surface of the flake is ragged, but thinner flakes are not detached from main flake. By adding vanillin (Fig. 3b) flake size was not reduced and there are many residues visible on the surface. Better result was obtained with addition of 2-naphthol (Fig. 3c). Apart from large piece of graphite, smaller flakes are also visible. Additionally, flake surface is relatively smooth.

Addition of ethanol to experimental system visibly increases effects of ultrasounds (Fig. 3d). Comparing with process carried out without cosolvent flakes are crumbled although some flakes still reassemble source material. Process carried out with vanillin and cosolvent (Fig. 3e) was not able to reduce size of flake, however surface of the flakes is smooth, much more than in Fig. 3c. The most promising results were obtained with 2-naphthol and cosolvent (Fig. 3f). Sizes of flakes have been drastically reduced and there are tiny pieces of material, which may be flake graphene.

Acknowledgment

The research was funded by National Science Centre, Poland – grant “Identification of mechanisms and investigations of flake graphene production by direct exfoliation using supercritical carbon dioxide”, project number 2019/35/D/ST8/02977.

References

[1] Pham TT, Huynh TH, Do QH, Ngo TKV. Optimum reproduction and characterization of graphene on copper foils by low pressure chemical vapor deposition. Materials Chemistry and Physics 2019;224:286–92. https://doi.org/10.1016/j.matchemphys.2018.12.009.

[2] Singh S, Chen X, Zhang C, Gautam RK, Tyagi R, Luo J. Nickel-catalyzed direct growth of graphene on bearing steel (GCr15) by thermal chemical vapor deposition and its tribological behavior. Applied Surface Science 2020;502:144135. https://doi.org/10.1016/j.apsusc.2019.144135.

[3] Kim C-D, Min B-K, Jung W-S. Preparation of graphene sheets by the reduction of carbon monoxide. Carbon 2009;47:1610–2. https://doi.org/10.1016/j.carbon.2009.02.025.

[4] Hernandez Y, Nicolosi V, Lotya M, Blighe FM, Sun Z, De S, et al. High-yield production of graphene by liquid-phase exfoliation of graphite. Nature Nanotech 2008;3:563–8. https://doi.org/10.1038/nnano.2008.215.

[5] Zhu L, Zhao X, Li Y, Yu X, Li C, Zhang Q. High-quality production of graphene by liquid-phase exfoliation of expanded graphite. Materials Chemistry and Physics 2013;137:984–90. https://doi.org/10.1016/j.matchemphys.2012.11.012.

[6] O’Neill A, Khan U, Nirmalraj PN, Boland J, Coleman JN. Graphene Dispersion and Exfoliation in Low Boiling Point Solvents. J Phys Chem C 2011;115:5422–8. https://doi.org/10.1021/jp110942e.

[7] Choi E-Y, Choi WS, Lee YB, Noh Y-Y. Production of graphene by exfoliation of graphite in a volatile organic solvent. Nanotechnology 2011;22:365601. https://doi.org/10.1088/0957-4484/22/36/365601.

[8] Pu N-W, Wang C-A, Sung Y, Liu Y-M, Ger M-D. Production of few-layer graphene by supercritical CO2 exfoliation of graphite. Materials Letters 2009;63:1987–9. https://doi.org/10.1016/j.matlet.2009.06.031.

[9] Zheng X, Xu Q, Li J, Li L, Wei J. High-throughput, direct exfoliation of graphite to graphene via a cooperation of supercritical CO2 and pyrene-polymers. RSC Adv 2012;2:10632. https://doi.org/10.1039/c2ra21316h.

Dosing of Powder by Vibration Stimulation

Roland Gall

Institute of Chemical Engineering and Environmental Technology, Graz University of Technology, r.gall@student.tugraz.at

Introduction

The applications of active pharmaceutical ingredients are becoming more and more specific and increasingly also individually tailored to the patient. The goal here is to achieve maximum therapeutic effect with minimum use of active pharmaceutical ingredients. For this purpose, individual dosages in very small batches of a few tablets are required, which must nevertheless be produced in compliance with the highest quality standards. To achieve this, powder must be weighed in reproducibly and with economically justifiable effort. [1] The powders to be weighed in are active ingredients and excipients required for tabletting.

Experimental

Content of the task is the investigation for powder dosing of an experimental setup by using Vibration Stimulation. Different pharmaceutical powders shall be dosed to investigate the possibilities of the system which is shown in Fig. 1.

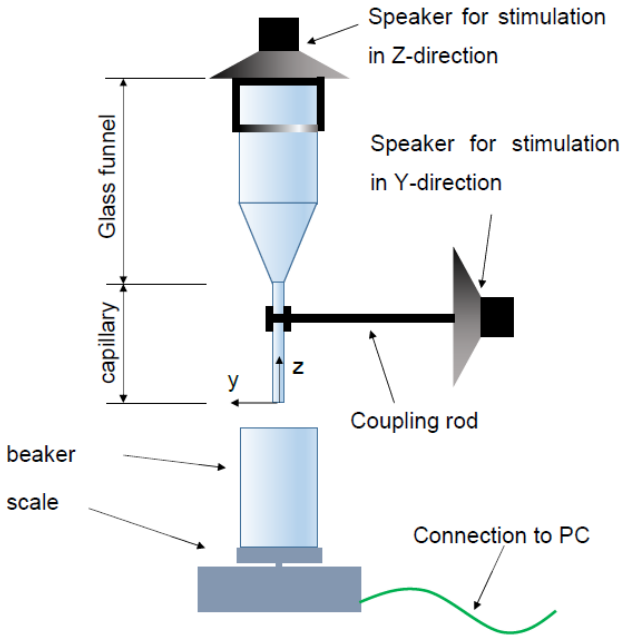

Fig. 1: Experimental setup

Due to the behaviour of the investigated powders, the dosing system was changed to a syringe and different cannulas but the principle stayed the same.

SEM-recordings of the investigated powders can be seen in Fig. 2, Fig. 3 and Fig. 4. It can be seen that the shape of the single particles is quite different which makes it challenging to dose these different powders with the same system.

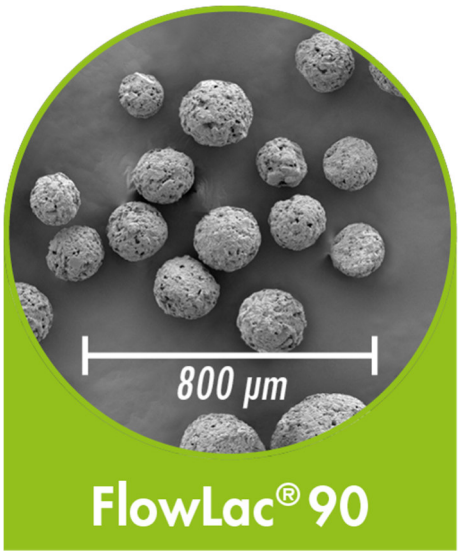

Fig. 2: SEM-recording of FlowLac 90 [2]

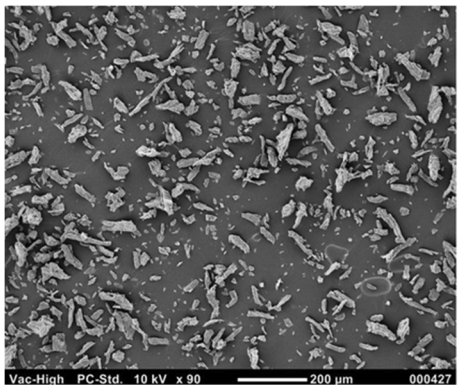

Fig. 3: SEM-recording of Avicel PH 101 [3]

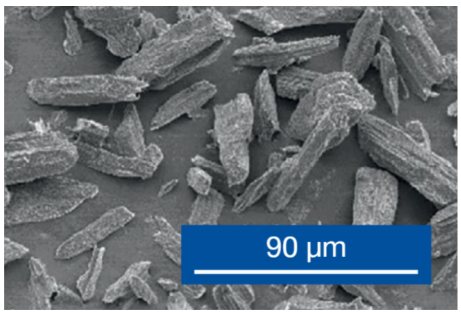

Fig. 4: SEM-recording of Ibuprofen 25 [4]

Dosing tests were carried out using a scale. The linearity of dosing behaviour, the dosing rate in respect to frequency and amplitude as well as the possibility to dose powder according to the measured dosing rate were investigated.

For example, in Fig. 5 the mass of dosed powder over time for different pairs of frequency and amplitude is shown.

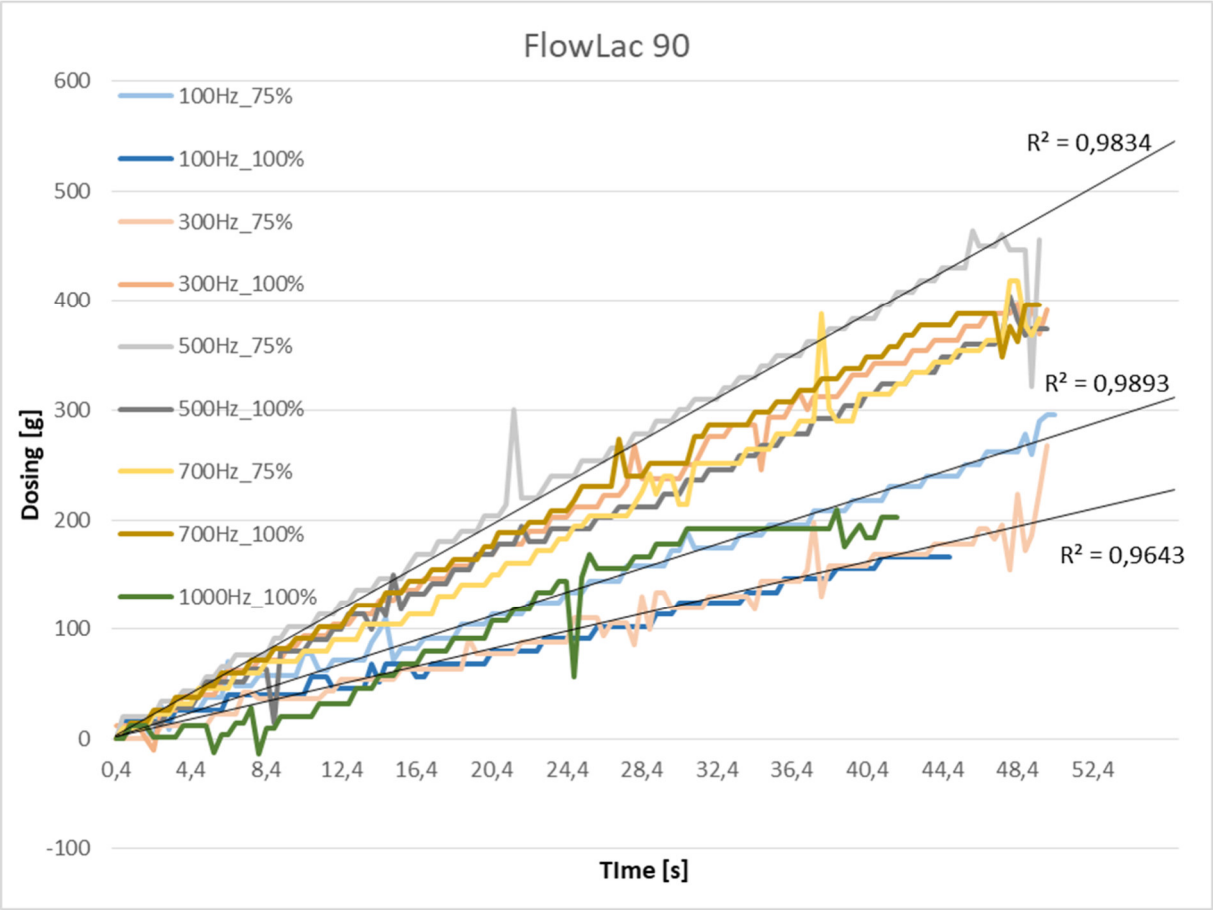

Fig. 5: Dosing of FlowLac 90 at different parameters for frequency and amplitude

Finally, 230 mg of Avicel PH 101 were dosed with a reproducibility of nearly 10%, which just fulfils the requirements of the European pharmacopoeia. On the other hand, dosing of FlowLac 90 and Ibuprofen 25 was not possible. Together with a control loop the reproducibility can be increased in future.

Summary

To meet the more specific requirements of personalised pharmaceuticals, it is mandatory to be able to dose powders accurate and economical on small batches. Therefore, powder should be dosed by using vibration stimulation and a capillary.

It was found the powder dosing is with well-chosen diameters of the canullas and parameters for vibration is possible, but the precision can be increased.

References

[1] A. Eckhardt *et al.*, *Personalisierte Medizin*. vdf Hochschulverlag AG, 2014. doi: 10.3218/3592-6.

[2] MEGGLE GmbH & Co. KG, “REM Aufnahme von FlowLac 90,” Oct. 19, 2021. https://www.cphi-online.com/flowlac-90-spraydried-lactose-prod022563.html (accessed Oct. 19, 2021).

[3] Gregory Thoorens, “REM Aufnahme von Avicel PH 101.” Gregory Thoorens (accessed Oct. 19, 2021).

[4] BASF Corporation, “Technical Information Ibuprofen 25.” [Online]. Available: www.pharma.basf.com

Data-Driven Scale-up of High Performance Supercritical CO_2 Drying Processes

Dennis Arigbe, Alberto Bueno, Pavel Gurikov, Irina Smirnova

Institute of Thermal Separation Processes, Hamburg University of Technology,

dennis.arigbe@tuhh.de

Introduction

Aerogels are highly porous materials (porosity up to 99 %), which show promising properties for various applications due to their high specific internal surface areas (1200 m^2/g), as well as their low thermal conductivities and densities (< 0.1 g/cm^3).

To maintain mesoporous structures (which are necessary for the characteristic properties) of aerogels during the drying process, it is necessary to work in the supercritical phase. With this type of drying, capillary forces are avoided and, in contrast to freeze-drying, no macro pores are formed. Supercritical drying is usually carried out with CO_2 as the drying fluid. The disadvantages of this method are currently the high time and energy requirements, which inhibit the commercialization of supercritical dried aerogels. The aim of this work is therefore to optimize supercritical drying and to minimize the required energy input.

So far, there are no facilities on a scale between laboratory autoclaves and fully integrated pilot/demonstration plants, which limits/hinders the transfer of knowledge from lab-scale to industrial scale.

Therefore, a pilot scale plant was developed at TUHH (figure 1), which offers a high flexibility in terms of process parameters to be set (temperature and pressure, 16 Raman probes for composition determination, flow controller) in order to achieve a large number of different process conditions and to determine ethanol/CO_2 inline and in every part of the setup.

Fig.1: AeroKinetics Plant

In order to reduce the number of experiments, a process model is additionally developed which covers and simulates the previously mentioned aspects of the plant. This includes drying (continuous and batch), drying kinetics, and especially recycling and purification of the CO_2/solvent mixture, which have a large impact on energy consumption.
Thus, the still existing lack of reliable process data, which are required for the development and scale-up of continuous and discontinuous supercritical CO_2 drying processes can be addressed.

Experimental

The AeroKinetics plant was designed to be Industry 4.0 compatible, allowing the flawless handling of data. This allows a real-time access to the enormous amount of data generated during the operation of the equipment which can be fed, analysed by flowsheet simulators, surrogate and artificial intelligence models.

First flowsheet simulations were carried out in order to determine the temperature and pressure influence of the separation of the CO_2 and solvent mixture (Figure 2).

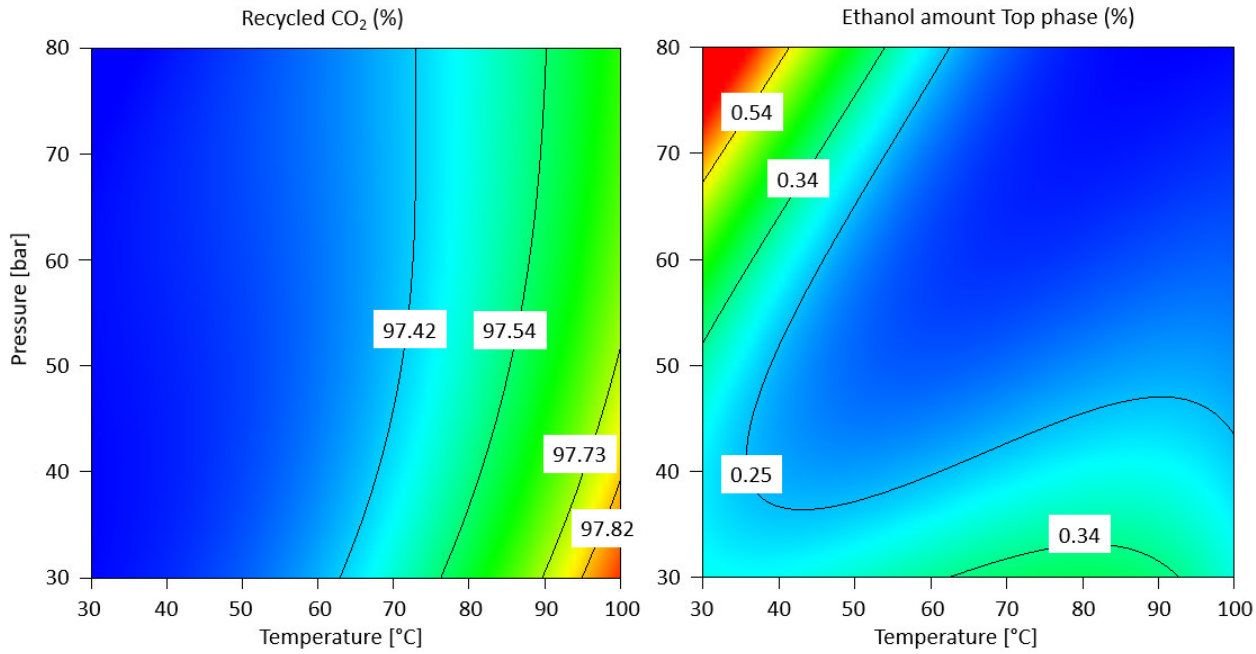

Fig. 2: Resulting variables (recycled CO2 in % and residual ethanol content in recycled CO2 in %) as a function of pressure and temperature.

Figure 2 shows two different parameters exemplary (amount of recycled CO_2 and Ethanol concentration in the CO_2 rich phase). With these sensitivity analysis approaches, it is possible to evaluate the effect, which each sub process has on the stability, performance and energy efficiency of the overall process.

The validation and parametrization of these models will open the opportunity not just to properly size the required equipment but also to develop the most energy efficient drying profile, allowing an agile transition of aerogel products from the lab to the commercialization.

Summary

As there is still a lack of reliable data for supercritical drying of aerogels in the industry scale, the existing potential of aerogels can't be exploit yet. Therefore, this project is about analyzing drying data and kinetics in an experimental and simulative way to get a better understanding of the overall aerogel drying process. A pilot plant scale-drying column is being used to generate missing data and kinetics required to design and scale-up continuous and batch supercritical CO_2 drying processes. Additionally a Flowsheet model will be established to handle these data and evolve the scale-up step of the aerogel production.

Acknowledgment

The AeroKinetics plant is part of the Project network „AeroKinetics – Energieeffiziente Aerogelsysthese durch Bestimmung der Trocknungs- und Alterungskinetik von Aerogelen“

References

[1] Bueno, A. et al., *Ind. Eng. Chem. Res.* ***2018****, 57, 26,* 8698–8707

[2] Bueno, A. et al*. J Mater Sci* ***56****, 18926–18945 (****2021****)*

Solubility of NO from Combustion Gases in Amine Solutions

Castro-Ferro, N., Vaquerizo, L.

BioEcoUva, Bioeconomy Research Institute, PressTech Group, University of Valladolid.

Corresponding author email: luis.vaquerizo@uva.es

Introduction

NOx gases are the product of different anthropogenic activities related to energy production, leading to significant emissions, and making NOx one of the major contributors to global warming, smog, and acid rain[1]. Due to the impending increase in power requirements and the efforts to avoid and control the negative environmental impacts that power production could have, nowadays two leading technologies are used to control NOx emissions: selective catalytic reduction (SCR) and selective non-catalytic reduction (SCNR). The main drawbacks of these technologies are the high capital cost (SCR), high operative cost (SCR/SCNR), and the possibility of ammonia slip (SCR/SCNR)[2].

One of the most common absorption processes that can be found at industrial scale is the amine scrubbing used for CO_2 removal. The amine scrubbing uses mainly primary amines. However, tertiary amines are also being studied due to their resistance to thermal degradation[3]. One of the biggest advantages of using tertiary amines for NO absorption is their limited capacity to form nitrosamines, which are toxic sideproducts[4]. Moreover, the affinity of NO for the alcohol groups[5] is one opportunity to evaluate the absorption of NO using amino alcohols.

To achieve a more effective media for controlling NOx emissions, different approaches must be deemed to find better alternatives to the existing ones. Therefore, in this research, the NO solubility has been measured in primary amines (AMP) and tertiary amines (TEA, MDEA) to determine whether they can be used as an efficient alternative medium for NOx control. The three types of amines used in the experiment belong to the amino alcohol group as shown in Figure 1.

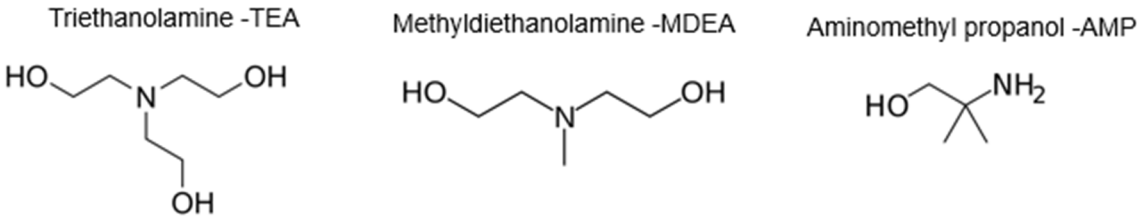

Figure 1. TEA, MDEA and AMP structure

Experimental

Primary amines (Aminomethyl propanol -AMP) and tertiary amines (Triethanolamine- TEA, Methyl diethanolamine- MDEA) at 40% w/w concentration were used as absorbent media and 15 ml of each amine solution were placed in a reactor with a total volume of 28.7 ml. The reactor has a temperature controller and a manometer for pressure measurement. Before the experiment, the amine contained in the reactor was degassed using liquid nitrogen and vacuum. After two repetitions, it was assumed that the absorbent liquid was fully degassed. The reactor was preheated at 35°C and once the temperature was stable different pressures were evaluated (1, 3, 5, and 7 bar). The pressure decay inside the reactor was monitored until it became stable. Using the ideal gas law and the difference between initial and final pressure, the amount of NO solubilized in the absorbent liquid was determined.

Summary

The NO solubility results for the evaluated amines are AMP: $3.61 \times 10^{-3} \frac{mol}{atm\ L}$, TEA: $3.31 \times 10^{-3} \frac{mol}{atm\ L}$ and MDEA: $2.28 \times 10^{-3} \frac{mol}{atm\ L}$. . The results obtained are higher than the NO absorption in water[2] $1.90 \times 10^{-3} \frac{mol}{atm\ L}$ but lower compared to the CO_2 absorption in MDEA[3] $6.54 \frac{mol}{atm\ L}$. According to Fine, N. et al, for tertiary amines (TEA and MDEA) the absorption of NO is in form of nitrate and nitrite and for primary amines (AMP) the reaction will form unstable nitrosamines which will ready deaminate into a carbonization and nitrogen gas. Because of the facility to create nitrosamines rather than nitrate and nitrite[8], the highest absorption was found by AMP. Further analysis will be performed to verify that the adsorption in AMP is giving unstable nitrosamines or whether there is some absorption as nitrate and nitrites. To find comparable results for solubility of NO with solubility for CO_2 in

amines other types of absorbent liquids such as alcohols and sulfites will be tested to determine which could be the better option for NO solubility.

Acknowledgment

This work/project was supported by the Regional Government of Castilla y León and the EU-Feder program (CLU-2019-04)

References

[1] Lasek. J, Lajnert. R. Appl. Sci.12(20). 2022

[2] Y. Su, Zhao. B and Demg, W. Fuel.170, 9–15. 2016

[3] Rochelle. G. Curr Opin Chem Eng. 1(2), 183-190. 2012

[4] Fine. N, M. Rochelle. Energy Procedia. 63, 830 – 847. 2014

[5] Krantz. J. J Am Pharm Assoc. 22 (3), 318-220. 1933

[6] Zacharia. I, Deen. W. Ann Biomed Eng. 33, 214-222. 2005

[7] Jou. F, Mather. A, Otto. F. Ind. Eng. Chem. Process Des. Dev. 21, 539-544. 1982

[8] Fine. N, Goldman. M and Rochelle. G. Environ. Sci. Technol. 48, 8777–8783. 2014

Ionic Liquid Pre-Treatment of Waste Biomass for Subsequent Extraction of Biologically Active Compounds

Marcell Gyurkač, Taja Žitek, Maša Knez Marevci

Faculty of Chemistry and Chemical Engineering, University of Maribor, SI-2000 Maribor, Slovenia, marcell.gyurkac@student.um.si

Introduction

The central goal of the present project is to create new ways for the circular bioeconomy and thereby reduce CO_2 emissions in addition to numerous positive environmental aspects. The use of ionic liquids (ILs) is intended to facilitate the extraction and production of products from various biomass raw material sources or the utilization of various biomass waste streams. The production of essential oils, phyto-pharmaceutical active ingredients, dietary supplements, and phyto-biocides from plants such as hemp, star anise, coffee, medicinal mushrooms or chrysanthemums is also planned. In addition to classical ILs, new ones will be synthesized which are produced from cations and/or anions of natural origin. These bio-based ionic liquids would contain choline-based cations or amino acid-based anions, which also occur in human metabolism. Bio-based ionic liquids have advantages over conventional ionic liquids such as better compatibility with biochemical processes (e.g. downstream enzymatic or microbial conversion steps of the isolated biomass fractions, safety of residual traces in food or pharmaceuticals, excellent biodegradability, high safety and easy disposal (Penín et al., 2020).

Various plants will be examined as potentially valuable raw materials for bio-based products. Examples of this would be flowers from hemp or chrysanthemums to extract the contained valuable substances. In the case of hemp, the focus would be on CBD oil as a valuable substance. Furthermore, pyrethrins can be obtained from chrysanthemum flowers, which are used as natural insecticides. In addition, other plants are to be examined, preferably those that contain active ingredients or valuable substances that are of interest to end customers and can be profitable (e.g., essential oils, pharmaceutical active ingredients, phytopharmaceuticals, dietary supplements.

One way of product recovery could be via distillation after complete dissolution of the biomass. Since ionic liquids have negligible vapor pressure (Kalb et al., 2017), it is possible to investigate whether volatile substances from biomass/IL mixtures can be obtained in a pure form using fractional distillation methods. Due to the lack of vapor pressure of ionic liquids, all distillation methods are possible in principle, since even under

ultra-high vacuum, evaporation of the IL is impossible. As a prominent example, hemp flowers should be dissolved in ionic liquids in order to be able to win volatile substance classes step by step by distillation. The individual fractions are then analysed for biologically active substances (terpenes, CBD derivatives, etc.). In this approach, individual products are selectively separated from a complex product mixture based on their different boiling points.

Another way of extracting the nonpolar volatile products would be to re-extract them with supercritical carbon dioxide (Kornpointner et al., 2021).

Ionic liquids are by no means as established in the field of extraction of pharmaceutical active ingredients (phytopharmaceuticals) or essential oils. Here, competing technologies (such as CO2 extraction or the use of “chilled ethanol”) are more common for the extraction of valuable substances. Rather than competing with those technology, a combined IL-treatment and CO_2-extraction approach would be beneficial.

The idea here is to open up the plant cells with IL-pre-treatment and then re-extract valuable components with environmentally benign solvent such as supercritical CO_2.

Experimental

Following protic ionic liquids were synthesized and tested:

- Triethylammonium formiate
- Triethylammonium methansulfonate
- Dimethylbuthylammonium hydrogensulfat
- Dibuthylammonium formiate
- Pyrrolidinium acetate
- Pyridinium formiate
- Pyridinium acetate
- 2-Picolinium formiat

Briefly a biomass loading of 2.5 wt% of hemp material was be applied and different temperatures and time were tested. After extraction, solid/liquid separation and washing with deionized water followed. The washed pre-treated biomass was then subjected to supercritical fluid extraction to obtain the target molecules (predominantly terpenes and CBD derivatives). The filtrate was analysed on its ionic liquid composition. Recycling rate and reusability of the ionic liquids were investigated.

Summary

8 different protic ionic liquids were synthesized. Hemp stalks were subjected to ionic liquid pre-treatment at different temperatures for 45 minutes. After filtration, the residual biomass was washed with deionized water and the biomass subjected to supercritical carbon dioxide extraction. Oil products were collected and stored until analysis.

Acknowledgment

I would like to thank Maša Knez Marevci and Taja Žitek for the opportunity to collaborate in the topic of combined ionic liquid a supercritical fluid extraction. Also big thanks to the proionic GmbH team for the provided ionic liquids for research.

References

Kalb, R. S., Damm, M., & Verevkin, S. P. (2017). Carbonate Based Ionic Liquid Synthesis (CBILS®): Development of the continuous flow method for preparation of ultra-pure ionic liquids. *Reaction Chemistry and Engineering*, *2*(4), 432–436. https://doi.org/10.1039/c7re00028f

Kornpointner, C., Sainz Martinez, A., Schnürch, M., Halbwirth, H., & Bica-Schröder, K. (2021). Combined ionic liquid and supercritical carbon dioxide based dynamic extraction of six cannabinoids from: Cannabis sativa L. *Green Chemistry*, *23*(24), 10079–10089. https://doi.org/10.1039/d1gc03516a

Penín, L., López, M., Santos, V., Alonso, J. L., & Parajó, J. C. (2020). Technologies for Eucalyptus wood processing in the scope of biorefineries: A comprehensive review. *Bioresource Technology*, *311*, 123528. https://doi.org/https://doi.org/10.1016/j.biortech.2020.123528

Modelling Mixing Characteristics in a Mini-Plant Polymerization Reactor using Computational Fluid Dynamics Simulation

Emil Schwarz, Markus Busch*

TU Darmstadt, Darmstadt/Germany, *markus.busch@pre.tu-darmstadt.de

Introduction

The mixing behaviour in a polymerization reactor is of great importance for the overall reaction control since the reactive species have to interact spatially with each other. Knowledge of these mixing processes is therefore crucial in terms of understanding and modelling the entire process. In stirred autoclaves, this mixing process is largely determined by the stirrer and the viscosity and density of the fluid. The study of mixing behaviour allows the identification of effects such as bypassing, dead zones, and channelling, all of which affect mixing and therefore the residence time. Consequently, parameters such as reactor temperature, conversion, and product properties such as number and weight average molar mass are dependent on this behaviour. Since knowledge of these product properties is of particular interest in polymerisation processes, the mixing behaviour can be investigated by simulation. Computational fluid dynamics (CFD) is a suitable method for modelling this behaviour, as it provides spatially resolved information about the fluid.

Modelling

The basis of any CFD simulation is the geometry in which the fluid is located. In this work, the geometry of the simulation is based on a laboratory autoclave in which the catalytic polymerization of ethene is studied. The used catalyst system is known from literature and the kinetic data for this system were determined and published by Mehdiabadi and Soares[1,2]. Typical reaction conditions of the laboratory experiments which are used to validate the model are in the range of 120 °C and 130 bar at stirrer speeds of 550 rpm.

In the CFD model the heating jacket of the autoclave is simplified by assuming isothermal reactor walls. The rotation of the stirrer is modelled using the multiple reference frame (MRF) concept, where the stirrer can also be considered stationary by considering its relative speed to the reactor wall. The thermophysical properties of the fluid such as viscosity, density, thermal conductivity and heat capacity are adjusted over the course of the simulation depending on temperature, pressure and polymer properties.

During a CFD simulation, the balance equations for mass, energy and momentum are solved. The mass balance includes a slightly simplified kinetic mechanism (Tab. 1.) of the catalytic polymerization. In order to also obtain information about the polymer properties, the method of moments is used[3]. This requires three equations for the moments of the active polymer chains and a further three equations for the moments of the inactive polymer chains in order to determine the number and mass average molecular weights as well as the PDI from the simulation.

Tab. 1.: Simplified kinetic mechanism of the catalytic polymerization.

Initiation	$C^* + M \xrightarrow{k_p} P_1^*$	β-hydride Elimination	$P_s^* \xrightarrow{k_{\beta h}} P_s + C^*$
Propagation	$P_s^* + M \xrightarrow{k_p} P_{s+1}^*$	Transfer to Monomer	$P_s^* + M \xrightarrow{k_{tr,M}} P_s + P_1^*$
Deactivation	$P_s^* \xrightarrow{k_d} P_s + C$ $C^* \xrightarrow{k_d} C$	Transfer to Hydrogen	$P_s^* + H_2 \xrightarrow{k_{tr,H_2}} P_s + C^*$

For the comparison with the experimental data the reactor is simulated in a steady state simulation and the amount of catalyst is set in order to meet the experimental conversion. This results in an overestimation of the mass and number average molecular weight of 9 % and 33 % respectively. Further it is possible to vary the stirrer rotation in the simulation and observe the conversion, reactor temperature and the mass and number average molecular weights at the reactor outlet. This indicates that the reactor is homogenously mixed at 550 rpm. For stirrer frequencies below 200 rpm effects on the observed quantities become clearly visible.

Summary

In this work, the catalytic polymerisation of ethene is investigated by means of CFD simulations. For this purpose, a reactor model based on a laboratory autoclave is set up and the polymerization kinetics are implemented using the method of moments. The comparison with the experiment shows that the number- and mass-average molecular weights can be represented with satisfactory accuracy by the simulation. Furthermore, by varying the stirrer speed, it can be concluded that the reactor is nearly homogeneously mixed.

Acknowledgment

The authors gratefully acknowledge the computing time provided to them on the high-performance computer Lichtenberg at the NHR Centers NHR4CES at (National High Performance Computing Center for Computational Engineering Science) TU Darmstadt. This is funded by the Federal Ministry of Education and Research, and the state governments participating on the basis of the resolutions of the GWK for national high-performance computing at universities.

References

[1] S. Mehdiabadi, J. B. P. Soares, D. Bilbao, J. L. Brinen, *Macromolecular Reaction Engineering* **2011**, 5, 418–430.

[2] S. Mehdiabadi, J. B. P. Soares, D. Bilbao, J. Brinen, *Macromolecules* **2013**, 46, 1312–1324

[3] E. Mastan, S. Zhu, *European Polymer Journal* **2015**, 68, 139–160.

Thermosetting Polymer Waste Valorization by Sub- and Supercritical Water

Petra Kántor, János Béri, Edit Székely

Department of Chemical and Environmental Process Engineering, Faculty of Chemical Technology and Biotechnology, Budapest University of Technology and Economics, Műegyetem rkp. 3., H-1111 Budapest, Hungary

petra.kantor@edu.bme.hu

Introduction

In addition to the increasingly widespread use of thermosetting polymers, the number of end-of-life products also shows an increasing trend. Unlike thermoplastics, they cannot be remelted or converted back into the original monomer. However, thermosetting polymers are used in fiber-reinforced composites because of their beneficial properties. Their lower viscosity enables faster production, in addition to having better impregnation, adhesion and mechanical properties. Carbon, glass, and aramid fibers are usually used in the matrix of fiber-reinforced composites, so the product, which is inherently difficult to recycle, presents additional challenges to the waste management.

The most common method of thermosetting polymer waste valorization is incineration. Incineration is a form of energy recovery; only a reduced amount of waste must be landfilled. However, it is only on the low level of waste handling hierarchy. In respect of circular economy material recovery, recycling is more beneficial; typical methods are summarized in Tab. 1. Various physical, thermal and chemical recycling methods can be found in the literature, but occasionally in industrial practice as well. In the case of physical methods, after grinding the composite, fibrous and powdered fillers can be used in new products, but typically of lower quality only. In the case of thermal methods, we encounter different possibilities. In addition to the fluidization process, pyrolysis is also a common method. The advantage of these methods is that the fibers can also be recovered, but they require extensive additional cleaning in both cases.

At the dawn of the 21st century, a third method family became a popular research area, which implements recycling with the help of chemical solutions, mainly presenting solvolysis processes. During the solvolysis processes (mostly hydro-, alcoho-, and aminolysis), the main aim is the liquefaction of the polymer matrix with selective chemical bond cleavages and the recovery of the fibers used for reinforcement. [1][2]

Tab. 1.: Comparison of the methods

	Physical methods	Thermal methods	Chemical methods
Recovery	Grinded reinforcing material and the polymer matrix.	Energy, heating oil, the reinforcing material, sometimes petrochemical feedstock.	Monomers, oligomers and the reinforcing material.
Pretreatment	Usually long pretreatment procedures.	In some cases, pretreatment may be required.	In some cases, pretreatment may be required.
Solvents and catalyst	-	No solvents needed, catalysis for special processes.	They require a solvent, and it is also possible to use catalyst.
Change of properties	In general, a drastic deterioration of the mechanical properties.	Mechanical properties generally deteriorate.	The deterioration of the mechanical properties is usually the smallest.
Emission	Minimal.	Carbon dioxide, carbon monoxide and VOCs.	Depends on the technology.
Scale up	Usually simple to implement.	Usually simple to implement.	They are generally difficult to scale up and industrialize.

Our research primarily aims to develop a hydrolysis method for termosetting polimers with sub- and supercritical water, using its benefits. In addition to adjustable solvent properties, the great advantage of using water is that it is cheap, easily accessible, non-toxic and environmentally friendly. In experiments with composites, we use a semi-continuous operation flow reactor, because although solvolysis processes have promising prospects,

they almost always require harsh conditions. The dense and stable three-dimensional network structure of the matrix can justify this. However, with the help of the flowing environment, the mass transfer of the reaction reagents in the resin matrix can be improved, so the operational time is reduced by using the advantages of continuous technologies.

Hydrolysis

Thermal hydrolytic processes are primarily carried out in sub- and supercritical water, apart from alkaline hydrolysis. The critical temperature of water is 374℃ and the pressure at the critical point is 21.7 MPa. Properties of supercritical fluids fall between gases and liquids in terms of their transport and physical properties and may therefore they may be favorable environment over the use of a liquid or gaseous medium. Their outstanding solvent properties include a high heat capacity, ensuring efficient heat transfer, and an outstanding diffusivity, which allows rapid mass transfer of sub- and supercritical media. [3] [4] These advantages can also be exploited for solvolysis processes as well.

At temperatures below 300℃, in liquid phase water is practically incompressible, which means that pressure has little effect on its physical properties such as viscosity or density if it is high enough to maintain the water in a liquid state. [3]

However, as we start to approach the Widom-region at higher temperatures, properties become affected by pressure, therefore allowing fine-tuning through pressure regulation, without changing the solvent or chemical composition. And beyond the critical temperature and pressure of the solvent in the reaction mixture, there is a single phase, the fluid phase, eliminating the limitation of mass transfer between phases, the interface diffusion control. Furthermore, the concentration of gas reactants in supercritical solvents can be much higher than in a liquid phase reaction media, where their solubility in the liquid limits the maximum available concentration. Their use may also simplify product separation, as often the desired reaction product can be separated from the supercritical reaction medium under sub-critical conditions. In these cases, separation of the product from the solvent is easier than in conventional liquid phase processes where distillation or extraction may be required. [3][4]

Water is an important reaction media because it is safe, non-toxic, readily available, cheap and environmentally friendly. The use of pressurized water at temperatures above its normal boiling point and supercritical water can also have potential applications. The properties of water change significantly with increasing temperature. As it approaches

supercritical temperature, it behaves more and more like a polar organic solvent. The dielectric constant of water is about 80 at room temperature but decreases to about 20 at 300 ℃ in the liquid phase when the temperature is raised. The decrease in dielectric constant is caused by the breakdown of the hydrogen network at high temperatures. A solvent is considered to be apolar if its dielectric constant is less than 15, making it suitable for dissolving small organic molecules in high temperature, near-apolar applications of water. In addition to the change in dielectric constant, high temperature also promotes the dissolution of substances with high dissolution enthalpy [4][5].

Several studies have shown that the combined effects of high temperature and H+ or OH- concentration, as well as catalysis by the water molecules themselves, are probably responsible for the reactivity observed in the absence of added acid or base. Experiments in supercritical media have also demonstrated the role of water using deuterated water, convincing that it can be an excellent reagent for the degradation of plastic waste [6]

Introduction of the device

To perform the solvolysis experiments, we designed the apparatus shown in Fig.1.

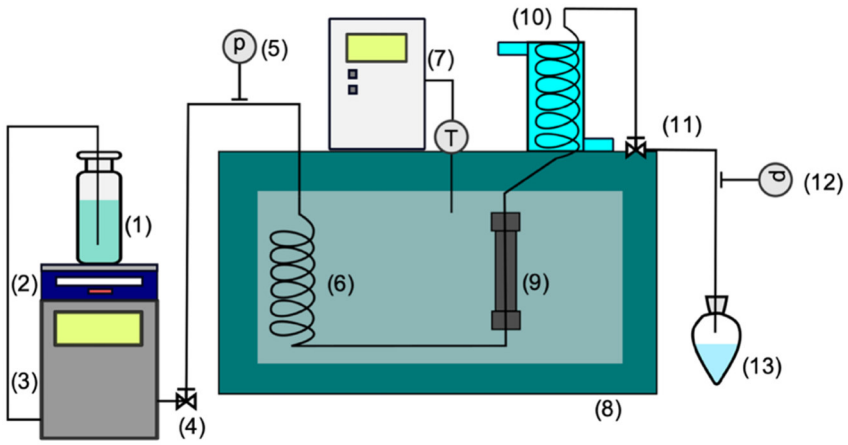

Fig. 1.: Schematic illustration of the device

The water is transferred from the glass vessel (1) via an HPLC pump (3). The amount of water used can be checked during the measurement by using a scale. A valve (4) is located at the downstream of the pump for pressure control. The pressure of the liquid entering the tempered chamber (8) is checked by a manometer (5). The air thermostat in the tempering chamber is controlled by a PID controller (7).

The water is fed from the pump to the reactor through 1/8" steel piping made by Swagelok. From the point of entry into the heated space, it passes through a long preheater section,

indicated by the number (6) in Fig. 1. After the preheating section, the heated water enters the reactor (9). The Swagelok 1/2" steel tube reactor is filled with the desired amount of material to be hydrolysed before the measurement is started. The liquid stream leaving the reactor exits the tempered chamber through a 1/16" Swagelok steel tube into the quench cooler (10), which is tempered with tap water.

A needle valve (11) was installed to the downstream of the cooler to allow manual control of the pressure during measurement, which can be checked with a manometer (12). The liquid product is collected in a flask (13).

Summary

For fiber reinforced polymer composites, several recycling solutions can be found in the literature. In addition to the widespread thermal and physical methods, the implementation of chemical methods is a promising field. Solvolysis processes are found to include hydrolysis, alcoholysis and aminolysis. Because of the green nature of hydrolysis and the outstanding solvent properties of subcritical water, we have designed a measurement method in which various polymer composite wastes can be degraded. The main aim is the recovery of both the fibers used for reinforcement and the monomers.

Acknowledgment

Project no. 2019-1.3.1-KK-2019-00004 has been implemented with the support provided by the National Research, Development and Innovation Fund of Hungary, financed under the 2019-1.3.1-KK funding scheme.

The European Summer School in High Presssure Technology" is available by the ERASMUS+ BIP funding. Project number: 2022-1-AT01-KA131-HED-000052815

References

[1] Pickering, S. J. (2006). Recycling technologies for thermoset composite materials — current status. 37, 1206–1215. https://doi.org/10.1016/j.compositesa.2005.05.030

[2] dos Passos, J. S., Glasius, M., & Biller, P. (2020). Screening of common synthetic polymers for depolymerization by subcritical hydrothermal liquefaction. *Process Safety and Environmental Protection*, *139*, 371–379. https://doi.org/10.1016/j.psep.2020.04.040

[3] Simsek Kus, N. (2012). Organic reactions in subcritical and supercritical water. *Tetrahedron*, *68*(4), 949–958. https://doi.org/10.1016/j.tet.2011.10.070

[4] Duan, J., Shim, Y., & Kim, H. J. (2006). Solvation in supercritical water. *Journal of Chemical Physics*, *124*(20), 1–16. https://doi.org/10.1063/1.2194012

[5] Savage, P. E. (2009). A perspective on catalysis in sub- and supercritical water. *Journal of Supercritical Fluids*, *47*(3), 407–414. https://doi.org/10.1016/j.supflu.2008.09.007

[6] Tagaya, H., Katoh, C., Katoh, K., & Kadokawa, J. (1999). *The Reaction of Model Compounds of Plastics in Sub- and Supercritical D_2O*.

Modelling and Simulation of Heat Transfer in Solid-State Bioreactors

Mahdi Miravandi

Chemical and Process Engineering, University of Padova,

mahdi.miravandi@studenti.unipd.it

Introduction

One of the problems in biological systems is the accumulation of heat generated during growth. This issue becomes particularly problematic in cases such as solid-state fermentation where the growth medium is not aqueous. To address this problem, one can utilize bioreactor modelling and find a solution by observing the effects of various variables. Among the variables that can aid in heat transfer in biological reactors, the inlet air velocity for ventilation and bed porosity hold great importance. In this study, the growth conditions of Aspergillus niger fungus in a solid-state fermentation bioreactor have been simulated using COMSOL Multiphysics version 5.6 software, and the impact of the mentioned variables on improving heat transfer has been investigated. Solid-state fermentation is a process in which microorganisms grow on solid substrates without the presence of free liquid. The substrates used in solid-state fermentation have low thermal conductivity, leading to heat accumulation and inadequate heat dissipation. Therefore, heat removal is one of the key issues in this type of fermentation. Research indicates that when the desired temperature for growth exceeds the maximum limit, fungal activity decreases exponentially. The investigated reactor in this study has a diameter of 0.2m and a height of 0.3m, considering Aspergillus niger as the microorganism. A moist substrate, along with the fungus, is placed in the bioreactor at time zero. Water flow is used to remove the heat generated around the reactor wall through convection. Ambient air is drawn from beneath the reactor to remove the generated heat through forced convection, subsequently reducing the temperature along the bioreactor. The bed is assumed to be fixed throughout the experiment.

Experimental

Experimental data for validating the modelling have been obtained from the studies of Glidyal and Saxoudo-Castanda. In this study, we were inspired by the Mitchell and Sargossark heat transfer model, with the difference that their model was a two-dimensional model with a constant air velocity profile, while in our model, we aimed to

investigate heat transfer in two dimensions with a variable air velocity. Therefore, the model presented in this study is significantly more complex and advanced than the previous model. To solve this problem, we have utilized three physics: "Laminar flow," "Transport diluted species in porous media," and "Heat transfer in porous media" in COMSOL, as the mentioned problem is a time-dependent problem and needs to be solved transiently and non-stationarily. However, it should be noted that the aeration is done uniformly, so it is better to solve this physics in a steady state as it is independent of time. The governing energy equation of the model is expressed as Eq.1:

$$\rho_b C_{pb}\left(\frac{\partial T}{\partial t}\right) + \rho_a C_{pa} V_z\left(\frac{\partial T}{\partial z}\right) = \left[\frac{K_b}{r}\frac{\partial T}{\partial r} + K_b\frac{\partial^2 T}{\partial r^2}\right] + K_b\left(\frac{\partial^2 T}{\partial z^2}\right) + Q \qquad (1)$$

In this equation, the term inside the brackets represents radial conduction, and the second term on the right-hand side represents axial conduction. On the left-hand side, convective and evaporative terms can be observed. The combined evaporative term assumes that the saturated air remains saturated throughout the flow within the bed. Therefore, evaporation always occurs inside the bioreactor. Another important point is the calculation of Q, which is referred to as metabolic heat. In fact, the removal of this heat is the main concern in heat transfer within SSF systems. It is assumed that the production of metabolic heat is directly proportional to the production of new cellular mass, and the energy associated with maintenance metabolism is neglected. This heat is defined as follows:

$$Q = YX \qquad (2)$$

Several models have been proposed for modeling X and its variation during the process, with the logistic model being the most comprehensive among them, as shown in Eq.3:

$$\frac{dX}{dt} = \mu \emptyset X\left(1 - \frac{X}{X_m}\right) \qquad (3)$$

In this model, we assumed that the fungi grow at an optimal specific growth rate, as research in this field has shown that up to 90% of the specific growth rate remains at the optimum temperature. Additionally, the maximum temperature considered for the Mitchell model does not exceed the optimal temperature. Therefore, our assumption is reasonable. To solve this problem, COMSOL automatically uses the finite element method, which we

often utilize in heat transfer problems. In this approach, small control volumes within the bioreactor are considered, which have defined distances from each other in the longitudinal and transverse directions. The more of these small control volumes we have, the more accurate our calculations will be. However, the volume of these calculations increases, and it may take a long time for COMSOL to perform these calculations.

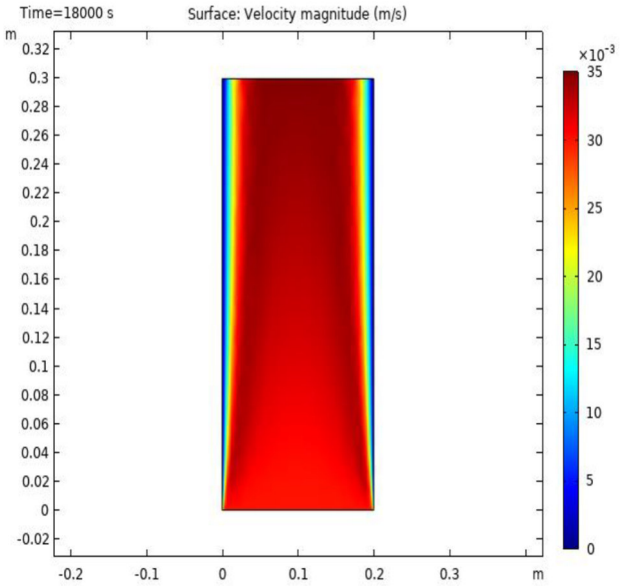

Fig.1 The fluid velocity profile after 50 hours from the start of fermentation.

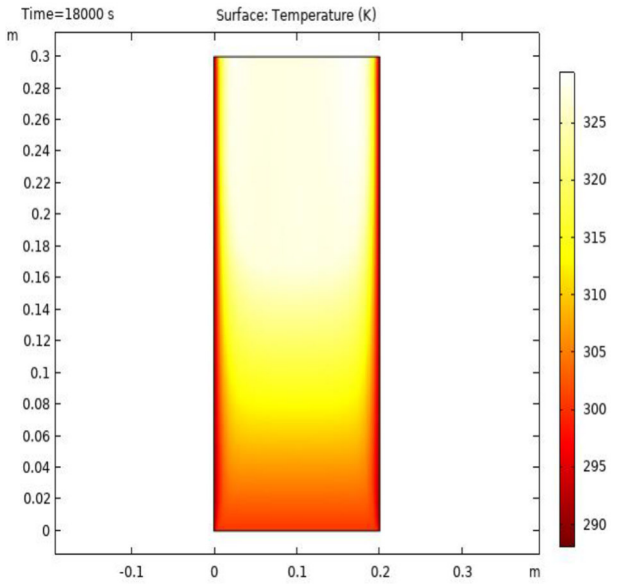

Fig.2 Temperature profile after 50 hours from the start of fermentation with air velocity 0.03

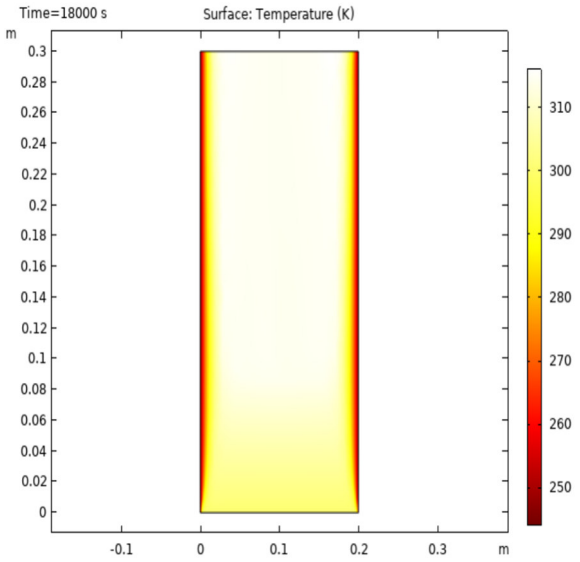

Fig.3 Temperature profile after 50 hours from the start of fermentation with air velocity 0.06

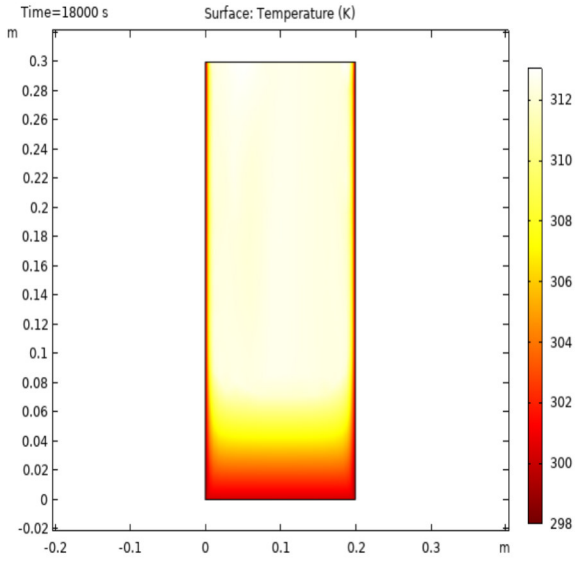

Fig.4 Temperature profile after 50 hours from the start of fermentation with air velocity 0.1

As observed in Figure 1, the velocity profile in this modelling includes both vertical and horizontal components for all points. However, in Mitchell's modelling and his colleagues,

the velocity profile is assumed to be constant and linear. On the other hand, as we approach the reactor outlet and connect to atmospheric pressure on one side and undergo heat exchange on the other side, the air velocity at the reactor outlet decreases throughout. With the movement in reactor height, the temperature increases. This is similar to the results obtained by Mitchell. The reason for this is the reduction in the effect of the velocity profile, as discussed earlier. In the reactor height, the velocity profile becomes more tranquil, and consequently, with the decrease in the convection term, the heat transfer rate decreases in this regard. Additionally, although metabolic heat is a time-dependent term, after 50 hours, the reactor temperature approximately remains the initial temperature, which means that the conduction and convection heat transfer terms have been able to successfully transfer the metabolic heat from the reactor so that microorganisms can continue to reproduce and grow. It was expected that increasing the air velocity would improve the convection heat transfer rate. Therefore, air velocities of 0.06 and 0.1 meters per second were also applied in the reactor modelling. By comparing Figures 2 to 4, it can be observed that increasing the air velocity resulted in a decrease in temperature at various points. The reason for this is clearly stated in the energy equation, as the convective heat transfer term on the right side of the equation increases with an increase in the velocity profile. Consequently, a greater amount of heat is transferred from inside the reactor.

Summary

The model we simulated includes many assumptions and simplifications to enable successful simulation. One of the most important assumptions is neglecting the increase in bed porosity over time. It is evident that with the growth of fungi in the inter-particle spaces, the bed porosity significantly decreases, leading to an increase in pressure drop within the bed. To prevent this issue and ensure effective heat transfer and heat removal through forced convection, the air pressure needs to continuously increase during the fermentation process. Otherwise, the pressure drop within the bed increases, resulting in a decrease in the airflow rate in the bioreactor. Nowadays, plug flow bioreactors are used to prevent this problem by inducing intermittent mixing, which maintains the bed porosity considerably and avoids excessive pressure drop. Intermittent mixing also helps to create temperature uniformity and prevent excessive temperature in certain areas of the bed, which can lead to the death of microorganisms. However, it should be noted that mixing causes the disruption and loss of filamentous structures, so careful consideration is

required when selecting the type of blades. The most important aspect to consider in the development of this model is the water balance in the bed. Adequate moisture content is necessary for the proper growth of microorganisms in the substrate, but it is anticipated that a significant amount of water evaporates from the evaporation column. In practice, to continuously compensate for this evaporated water, as mentioned before, it is advisable to incorporate holes in the bioreactor through which water droplets can be sprayed inside the bioreactor.

In conclusion, we observed that increasing the air velocity improves the heat removal process. Therefore, we were able to address one of the major issues in solid-state fermentation, which is the lack of heat dispersion. Additionally, based on laboratory studies, by using air supply, we can fulfill the process's oxygen demand and facilitate the removal of carbon dioxide. This itself has positive implications for energy and cost savings and plays a significant role in optimizing the problem. If the mentioned improvements are considered, this model can be regarded as a comprehensive and accurate model for solid-state fermentation (SSF).

References

- Kadam, Avinash A., et al. "Heat transfer modeling in solid-state fermentation: a review." Critical Reviews in Biotechnology 34.2 (2014): 173-187.
- Subramanian, Rajagopal, and Balamurugan Subramanian. "Heat transfer in solid-state fermentation systems: A review." Chemical Engineering Communications 206.12 (2019): 1561-1582.
- Negi, Pradeep S., et al. "Modeling and simulation of heat transfer in solid-state fermentation: A comprehensive review." Critical Reviews in Food Science and Nutrition 57.9 (2017): 1889-1905.
- Paul, Sanjoy K., and Mainak Banerjee. "Heat transfer in solid state fermentation: basic concepts and applications." Advances in applied microbiology 78 (2012): 81-141.
- Pandey, Ashok, and Carlos Ricardo Soccol. "Advances in solid-state fermentation." Springer, 2008.

Xanthohumol Extraction from Spent Hops

Aleksandra Modzelewska

Faculty of Chemistry,

Department of Micro, Nano and Bioprocess Engineering,

Wrocław University of Science and Technology, Poland

aleksandra.modzelewska@pwr.edu.pl

Introduction

Production of beer has been known for millennia, currently reaching over 33 million litres in Europe per year. Beer production is a multi-stage process requiring the usage of four main ingredients: water, brewing malt, hops, and yeast. To produce beer, ground barley malt undergoes mashing – it is mixed with water, which causes the conversion of the starches contained in the malt into fermentable sugars. The obtained mixture of wort (liquid phase) and brewer's spent grain (solid phase) is later filtered – in this step, spent grain particles are usually used as the filtrating medium. The wort then can be enriched with bittering and aroma substances from hops during the hopping stage, where hop extracts, pellets, or cones are added to the boiling mixture. Solid remains are filtered, the wort is cooled down, and the fermentation stage can be initiated by the addition of yeast culture. After fermentation, the beer is again filtered and can undergo the finishing steps, such as pasteurization, bottling, increasing the CO2 level, etc. The process is inevitably connected to the production of large quantities of brewing waste – spent grain, hops, and yeast (Fig. 1).

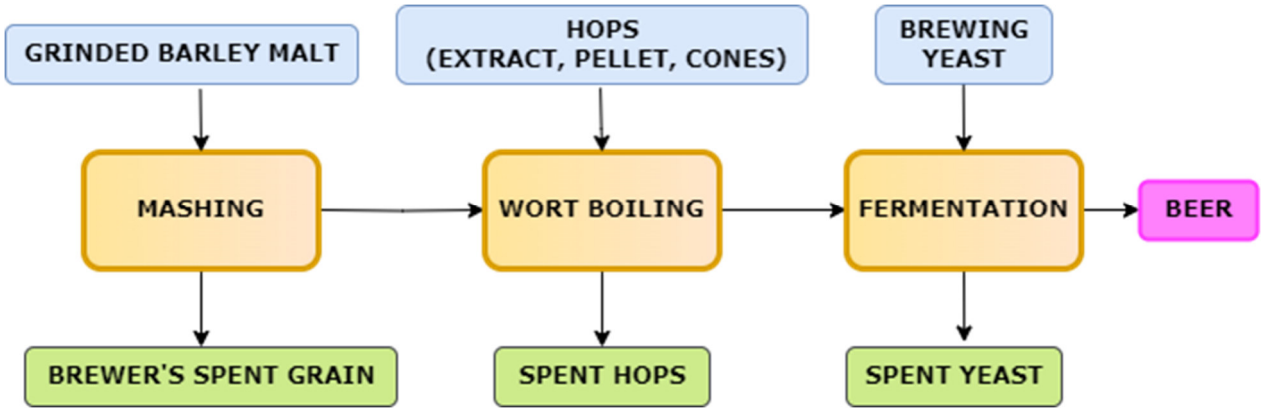

Fig. 1: Beer production steps with the indication of substrates and by-products

The brewing waste is a valuable material that, despite already having provided all the substances required for the beer production process, is still rich in components of high value (Table 1).

Table 1. Waste produced during the brewing process, their valuable components and current applications [1, 2, 3]

Waste	Components of high value present in the waste	Current application examples
Brewer's spent grain (BSG)	Proteins, fibre, carbohydrates	Animal feeds
Spent hops	Hop acids, xanthohumol proteins	Cannot be used as animal feed (high bitterness) - utilization
Spent yeast	B12 vitamins, proteins	Reusing for the next beer batches

Utilization of spent hops is problematic because, unlike brewer's spent grain, they cannot be used as an animal food additive in quantity exceeding 5% of the mixture [4]. Therefore alternative applications of this waste material are necessary for improving the overall sustainability of the brewing industry.

Nowadays, many researchers are trying to approach the extraction of xanthohumol (XN) from fresh hops and hop pellets, as this natural chalcone shows high bioactivity and several beneficial health effects. Extraction of XN from hops is possible using numerous procedures, such as extraction with organic solvents with or without intensification (microwave, ultrasonication), deep eutectic solvents (DES), and supercritical CO2 [2], and the application of those methods in spent hops extraction is a topic worth further investigation. This preliminary research proved that simple extraction of spent hops using Soxhlet apparatus allows obtaining more than half of XN compared to the same process where fresh hop pellets were used.

Experimental

Hop pellet samples (Hallertau tradition) were used in laboratory-scale hopping processes. Three hopping regimes: hopping for aroma (15 minutes in boiling water), hopping for bitterness (1h boiling), and dry hopping (72 hours in cold water) were applied to obtain spent hop samples. The material was later dried, and extraction using Soxhlet apparatus was performed, using isopropanol as the solvent (time:180min). For the comparison, fresh H. Tradition pellet underwent the same extraction process using the same dry mass: solvent volume ratio (5g:350ml).

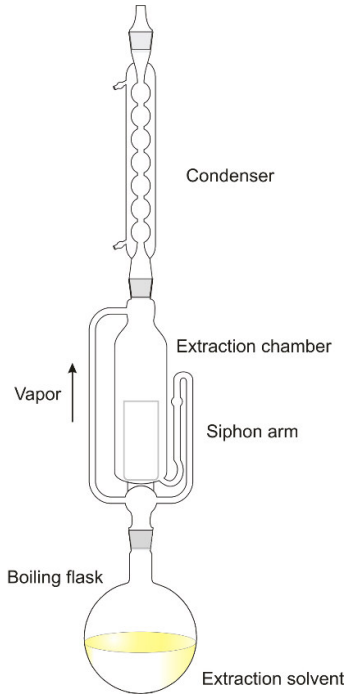

Fig. 2: Soxhlet apparatus scheme [5]

The concentration of XN (Tab. 2) was later measured using HPLC (column: 5µm Fortis C18, 250x4.6mm; flow: 0.8 mL/min; λ 370 nm; mobile phase: methanol: water with formic acid (pH=2.6) 85:15, analysis time: 20 min).

Results

The results are presented in Table 2 and show that spent hops still contain a significant amount of XN - according to the results of the applied extraction method, over 50% of XN remains in the waste compared to fresh pellets.

Table 2. The concentration of XN in obtained extracts (column 2) and referring to the dry mass of spent hops/hop pellets (column 3).

sample	XN [mg/L]	XN [mg/g $_{\text{dry mass}}$]	% of XN obtained compared to extraction from fresh pellets
Bitterness hopping (1h)	12.922	0.903	40.87
Aroma hopping (15min)	16.302	1.137	51.45
Dry hopping	15.920	1.113	50.35
Fresh hop pellet	31.902	2.210	-

Summary

Extraction of XN from spent hops is a wide topic worth further investigation, as it might be of great value due to the constantly increasing production of brewing by-products, along with the search for their optimal utilization methods. The research shows promising results for Soxhlet extraction. However, applying novel extraction methods - including supercritical fluid extraction and other high-pressure processes - could have the potential to obtain an even higher yield. Therefore, further research is going to concern these methods.

References

[1] Jackowski, M.; Niedźwiecki, Ł.; Jagiełło, K.; Uchańska, O.; Trusek, A. Brewer's Spent Grains—Valuable Beer Industry By-Product. *Biomolecules,* 2020, *10*, 1669 DOI: 10.3390/biom10121669

[2] Gerbson Vicente de Andrade Silva, Giordana Demaman Arend, Acácio Antonio Ferreira Zielinski, Marco Di Luccio, Alan Ambrosi, Xanthohumol properties and strategies for extraction from hops and brewery residues: A review, Food Chemistry, 2023, Volume 404, Part B, 2023, 134629, ISSN 0308-8146, DOI: 10.1016/j.foodchem.2022.134629.

[3] Jacob, F.F.; Striegel, L.; Rychlik, M.; Hutzler, M.; Methner, F.-J. Spent Yeast from Brewing Processes: A Biodiverse Starting Material for Yeast Extract Production. *Fermentation,* 2019, *5*, 51. DOI: 10.3390/fermentation5020051

[4] Mirosław, A, Anna Żołnierczyk. Extraction of Spent Hops Using Organic Solvents, Journal of the American Society of Brewing Chemists, 2008, 66:4, 208-214, DOI: 10.1094/ASBCJ-2008-0818-01

[5] Fig. 2: Soxhlet apparatus scheme, E. Generalic, https://glossary.periodni.com/glossary.php?en=Soxhlet+extractor

Modeling of the High-Pressure Separator in the LDPE Polymerization Process

Anne Rott, Markus Busch*

TU Darmstadt, Darmstadt/Germany, *markus.busch@pre.tu-darmstadt.de

Introduction

Nowadays, plastics are a vital part of life. Next to others, it is used as package material and for construction. The diversity in which plastics can be applied as well as the ease of processing and their light weight lead to the plastics industry being one of Europe's biggest industry sectors. With about 30 % of all produced polymers, polyethylene is the most widely used polymers. With different polymerization routes leading to different microstructures of the polymer and therefore different properties, polyethylene itself has widespread applications.[1–3]

Low-density polyethylene (LDPE) is produced at high pressures and high temperatures. For process design and optimization, modeling of polymerization processes has become more and more important. Process simulations can replace time consuming and expensive experiments. When modeling polymerization processes, the focus of modeling is often on the reactor. If the entire process is to be modeled, not only the reactor, but also the recycle stream and therefore the separation process needs to be included in the model. A schematic flowsheet of the LDPE polymerization process is shown in Figure 1.

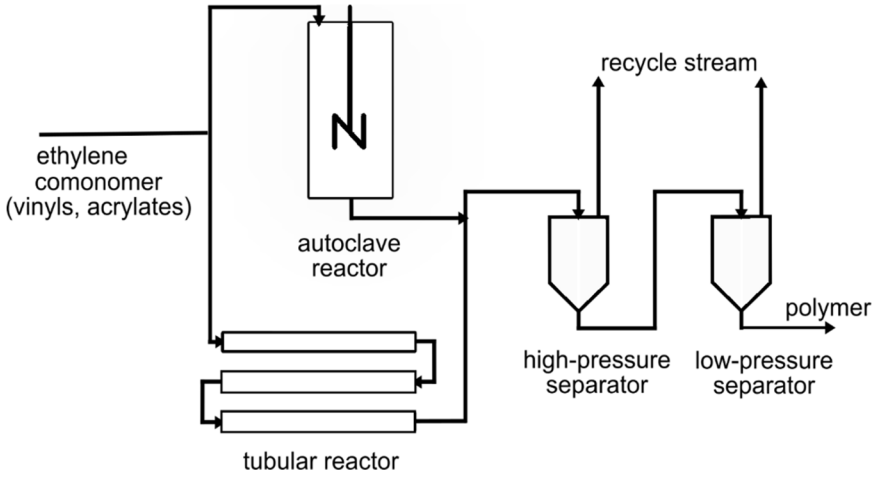

Fig. 1: Schematic representation of the LDPE polymerization process. The polymerization itself can be carried out either in an autoclave or a tubular reactor. After the polymerization, the residual monomer is separated in two consecutive flash separation units.

Modeling Approach

For modeling the separation process, an equation of state can be applied. This approach, however, is only valid if a thermodynamic equilibrium is reached in that unit. Buchelli et al.[4] used an equation of state approach to model both flash separation units. They found that only the low-pressure separator could be described accurately, while the modeling results for the high-pressure separator deviated from the experimental data. As a result, a mechanism for the separation process outside the thermodynamic equilibrium was proposed. This mechanism consists of four steps which occur during the initial pressure decrease as shown in Figure 2.

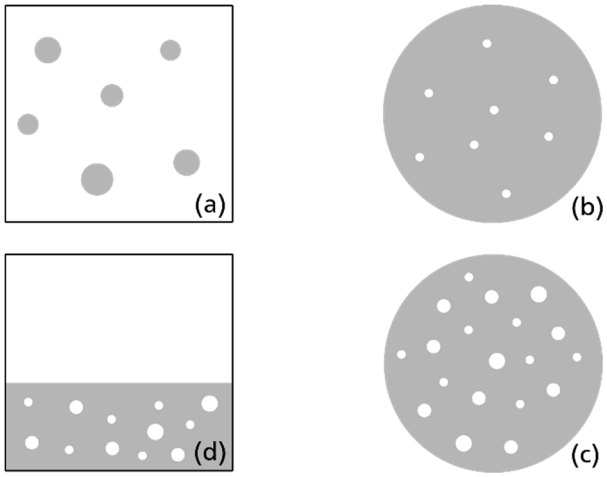

Fig. 2: Mechanism of the separation process as proposed by Buchelli. In the first step, polymer droplets are formed in the monomer-rich phase (a). Further pressure decrease leads to formation of monomer bubbles inside the polymer droplets (b) which expand as the pressure decreases further (c). The last step describes the coalescence of the polymer droplets to a polymer-rich phase (d). The polymer-rich phase is shown in grey, while the monomer-rich phase is shown in white.[4]

Buchelli et al. successfully modeled the separation process using industrial data for comparison. However, if no industrial data is available, another modeling approach has to be taken.

In this work, a two-step modeling approach is applied to the mechanism proposed by Buchelli for modeling the high-pressure separator. In a first step, an equation-of-state modeling approach is used to model steps (a) and (d). The formation of monomer bubbles inside the polymer network (step (b) and (c) in Figure 2) is described using molecular dynamics simulations. A time-dependent pressure gradient is used to model the pressure

drop between the reactor and the high-pressure separator. The results of these simulations are then used to determine formation, growth, and movement of monomer bubbles inside the polymer network by determination of volumetric regions exhibiting a locally light density which may subsequently be used to describe the separation process outside of thermodynamic equilibrium conditions.

Summary

For modeling the entire LDPE polymerization process, not only knowledge about the reactor but also of the separation process is needed. Since the high-pressure separator does not operate at thermodynamic equilibrium conditions, an equation of state approach is not sufficient to accurately represent this separator. Using molecular dynamics simulations, time-dependent bubble growth phenomena can be described. The results of these simulations may then be used to determine the residual amount of monomer in the polymer phase after the high-pressure separator.

The authors gratefully acknowledge the computing time provided to them on the high-performance computer Lichtenberg at the NHR Centers NHR4CES at TU Darmstadt. This is funded by the Federal Ministry of Education and Research, and the state governments participating on the basis of the resolutions of the GWK for national high performance computing at universities (www.nhr-verein.de/unsere-partner).

References

[1] S. K. Nayak, S. Mohanty, L. Unnikrishnan, *Trends and applications in advanced polymeric materials*, John Wiley & Sons, Hoboken, NJ **2017**.

[2] PlasticsEurope, *Plastics - the Facts. An analysis of European plastics production, demand and waste data* **2020**.

[3] G. Luft, *Chemie in unserer Zeit* **2000**, *34*, 190.

[4] A. Buchelli, M. L. Call, A. L. Brown, C. P. Bokis, S. Ramanathan, J. Franjione, *Ind. Eng. Chem. Res.* **2004**, *43*, 1768.

PMMA Foaming with $SCCO_2$ and Water

Redondo, A.[1*], García, P. [1], Martín-de-León, J.[2], Cantero, D.[1].

[1] BioEcoUva, Research Institute on Bioeconomy, High Pressure Processes Group, Department of Chemical Engineering and Environmental Technology, University of Valladolid, Valladolid, 47011, Spain.

[2] Cellular Materials Laboratory (CellMat), Condensed Matter Physics Department, University of Valladolid, Valladolid, 47011, Spain.

*Corresponding author: aranzazu.redondo@uva.es

Introduction

Poly(methyl methacrylate) (PMMA) is a synthetic and amorphous polymer that belongs to the acrylate family. It is an optically clear polymer with a glass transition temperature range of 100ºC to 130ºC. It presents high resistance to sunshine exposure, high impact strength, high scratch and shatter resistance, good optical properties, good degree of compatibility with human tissue, is a lightweight and exhibits favorable processing conditions and a reasonable resistance to chemicals. For all these properties, PMMA is known for being used in contact lenses, bone prostheses and high-strength insulation panels. A summary of these applications appears in Figure 1 [1].

Figure 1. PMMA applications.

Very promising application have been developed with PMMA in recent years through the polymer foaming with CO_2. The produced foams present very low thermal conductivity, which make them a great insulation material [2].

Experimental

PMMA Plexiglas® 7N was supplied by EVONIK in the form of pellets. CO_2 grade 99,999% was from Linde. Ultrapure water (18.2 MΩ·cm, collected from a Milli-Q® water purification system) was used.

Foaming was carried out in High-Pressure foaming unit HPF-700. System set up is shown in the figure 2.

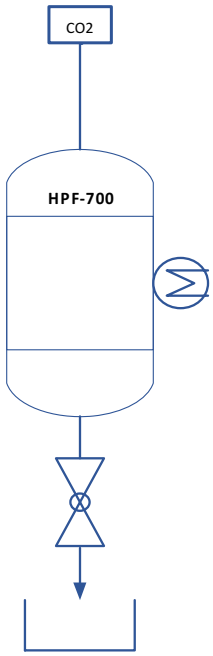

Figure 2. HPF-700 set up.

A given amount of PMMA was placed in a 65 mL high pressure tube autoclave. CO_2 was also introduced in the system by pneumatically driven gas booster and the temperature was controlled by a PID loop connected to a jacket heater. The experiments were done at different pressures, temperatures and times conditions. Also, different water/polymer ratios were selected to do the assays to avoid pellets agglomeration. The system was depressurized by pneumatic ball valve. The products were recollected from the expansion vessel. Comparison between raw material and products obtained can be observed in figure 3. Significant shape and transparency loss, volume increase and macrostructure change were visually observed.

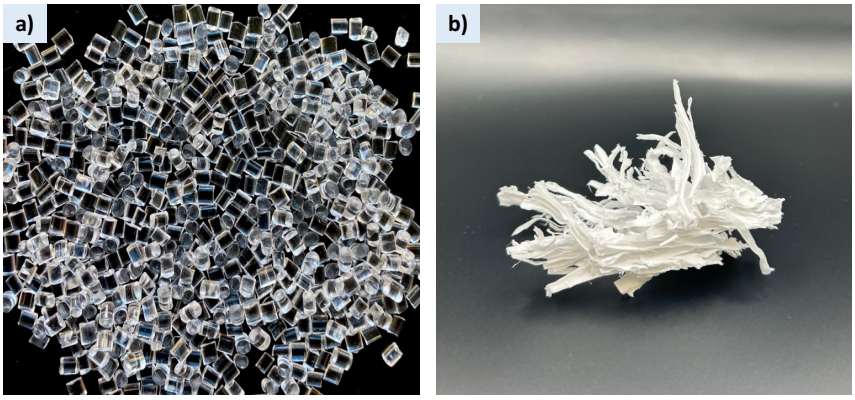

Figure 3. a) Original PMMA in pellets; b) PMMA foaming product.

Apparent density was measured after milling the product to homogenize the particle size. Then, an amount of the product was placed in a 10 mL test tube and weight was measured. Results from six samples are shown in Table 1.

Table 1. Apparent density.

Sample	ρ apparent
A	0,085
B	0,060
C	0,112
D	0,066
E	0,047
F	0,044

Foam density and other parameters were studied from the SEM images with ImageJ software [3]. Foaming was confirmed with this analysis. Figure 4 shows the difference between original PMMA and one of the products. Analysis results from same six samples are in Table 2.

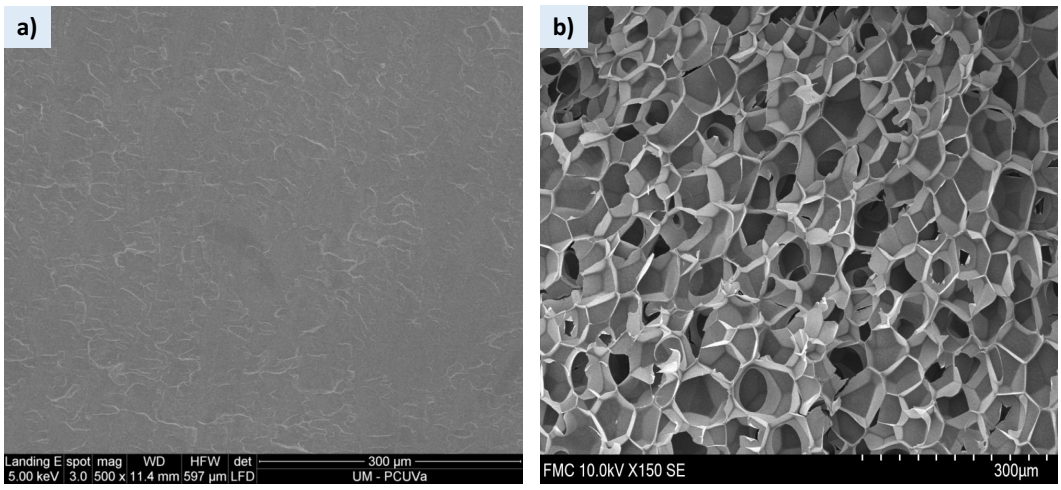

Figure 4. a) Original PMMA image from SEM; b) SEM image from one of the products at the same magnification.

Table 2. Relative density, foam density and expansion of six of the foamed products.

Sample	ρR	ρfoam/ g·cm3	Expansion
PMMA	1,19	1	1
A	0,307	0,365	2,7
B	0,260	0,310	3,2
C	0,604	0,719	1,4
D	0,275	0,328	3,1
E	0,332	0,395	2,5
F	0,295	0,351	2,9

Summary

It has been found that exist PMMA foaming under aqueous media. Different conditions were carried out in that part of the study with promising results. Nevertheless, further experiments will be conducted to carry on this study to achieve the best conditions and to understand the process.

Acknowledgment

The authors acknowledge the Agencia Estatal de Investigación for the financial support given in Project PID2020–119249RA-I00. This work was supported by the Regional Government of Castilla y León (Spain) and the EU-FEDER program (CLU-2019-04). Danilo Cantero is funded by Spanish Ministry of Science, Innovation and Universities ("Beatriz Galindo" fellowship BEAGAL18/00247).

References

[1] *U. Ali, K.J.B. Abd Karim, N.A. Buang, Polymer Reviews 2015, 55 (4), 678.*

[2] *J.Martín-de León, M.Jiménez, J.L. Pura, V. Bernardo, M.A. Rodríguez-Pérez, Polymer 2021, 236, 124298*

[3] *Pinto, J.; Solorzano, E.; Rodriguez-Perez, M. a.; de Saja, J. a. Characterization of the cellular structure based on user-interactive image analysis procedures. Journal of Cellular Plastics 2013, 49, 555–575.*

High Pressure Phase Equilibrium Measurements of Methyl Acetate and Carbon Dioxide

Ghazwan S. Ahmed, Edit Székely

Department of Chemical and Environmental Process Engineering, Faculty of Chemical Technology and Biotechnology, Budapest University of Technology and Economics, Műegyetem rkp. 3., H-1111 Budapest, Hungary

Email: ghazwansalehahmed@edu.bme.hu

Introduction

The current energy system for transportation is still based on fossil fuels whose utilisation is not sustainable in the long term due to limited resources and the negative impact on climate change related to the accumulation of CO_2 in the atmosphere. For these reasons, fossil fuels must be gradually substituted by other CO_2-neutral renewable energetic sources. In this context, biodiesel can be an interesting renewable alternative to fossil diesel as it has similar performances but lower emissions of particulate matter and greenhouse gases. The conventional industrial route to biodiesel (fatty acid methyl esters or FAME) production is by transesterification of triglycerides (TG) contained in fatty feedstocks, such as vegetable oils or animal fats, with excess methanol. Recently, prospective studies have described the use of dimethyl carbonate and methyl acetate or ethyl acetate as reactants to transform TG into biofuel through an interesterification reaction. The interesterification route excludes the glycerol formation and does not need methanol, having the two major drawbacks of the conventional process. The interesterification reaction yields valuable by-products such as glycerol carbonate and triacetin. Compared to alcohols, an attractive advantage of these reactants is that they synthesise biofuel and biofuel additives simultaneously [1-3].

This study is aimed to produce biodiesel in a supercritical continuous process using an interesterification reaction with biocatalysis. In order to avoid the degradation of the fatty acids the temperature needs to be limited, which is the advantage of any biocatalytic route. In the case of biocatalysis, however, mass transfer is often the rate-limiting step; thus, CO_2 expanded liquid is intended to accelerate the reaction rate. To ensure a homogeneous phase for the reaction, equilibrium measurements have been performed using a variable volume view cell (methyl acetate + CO_2, Oil + CO_2 and methyl acetate + Oil + CO_2). Binary phase

equilibrium data is available to certain extent in the literature, thus experimental results is compared to those and are the bases of modelling.

Experimental

In this study, the phase equilibrium measurements are carried out using view cell apparatus and the detailed description of the apparatus configuration was showed in literature [6] and our experimental procedure for methyl acetate + CO_2 system is as follow:

The required amount of methyl acetate was measured and inserted in the cell, the temperature was set at the required temperature. The required amount of CO_2 was measured using special pump (ISCO 260 D syringe pump) and inserted in the cell to get the required mole fraction between CO_2 and methyl acetate. We let the system under mixing at required temperature for some time where we get homogeneous phase inside the cell. After that, we start measuring phase equilibrium by reducing the pressure (increasing volume using movable piston) until phase separation (cloud point) inside the cell was visible, the phase separation conditions are recorded using sensible device and the results are preserved directly on a computer. This procedure is repeated at least five times at the same mole fraction and taking the average as one point. After that, the cell opened and cleaned for other measurement with new mole fraction.

Results and discussions

In this study, view cell used to get phase equilibrium and compare the results with literature. For methyl Acetate +CO_2 system, we measured cloud points at 25 and 40 °C at different mole fractions. The results and the comparison with the literature can be shown in Fig 1.

Detailed evaluation of the literature data in [4] and [5] in comparison with our own cloud point measurements showed that there is a significant difference between the published results and our measurements correlate well with the data in [4] (Fig 2.).

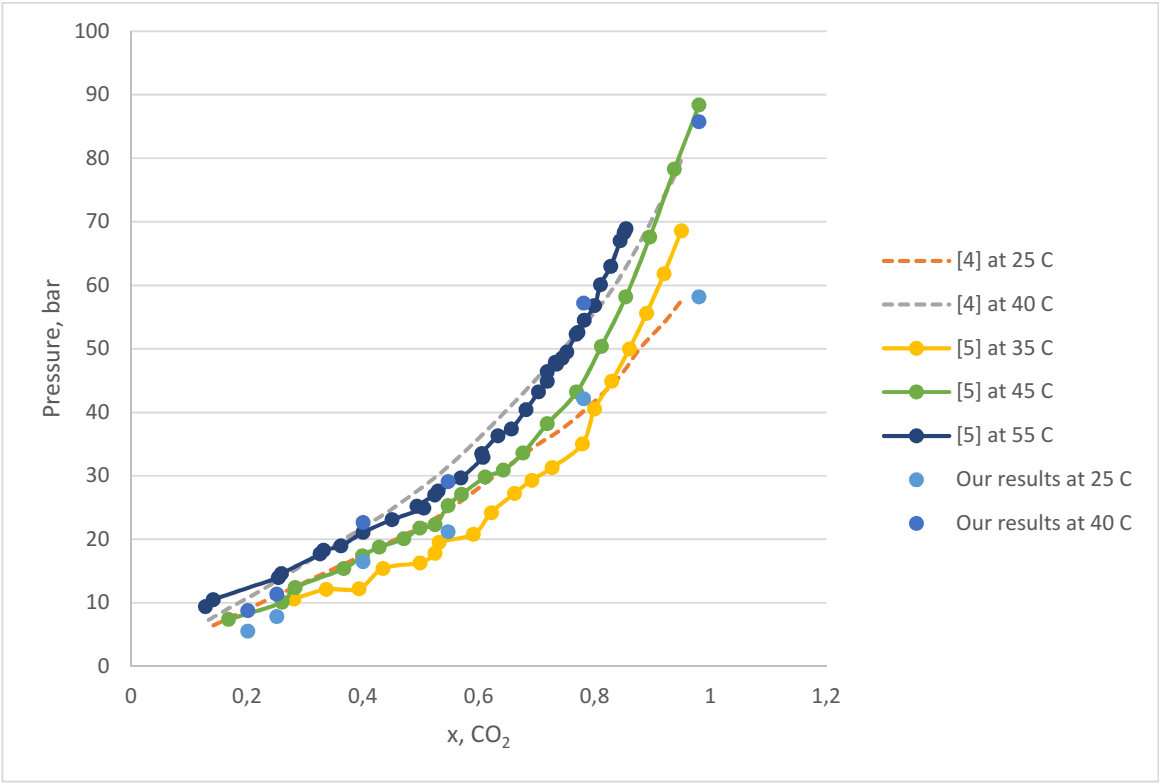

Fig. 1 Methyl acetate + CO_2 liquid phase boundary

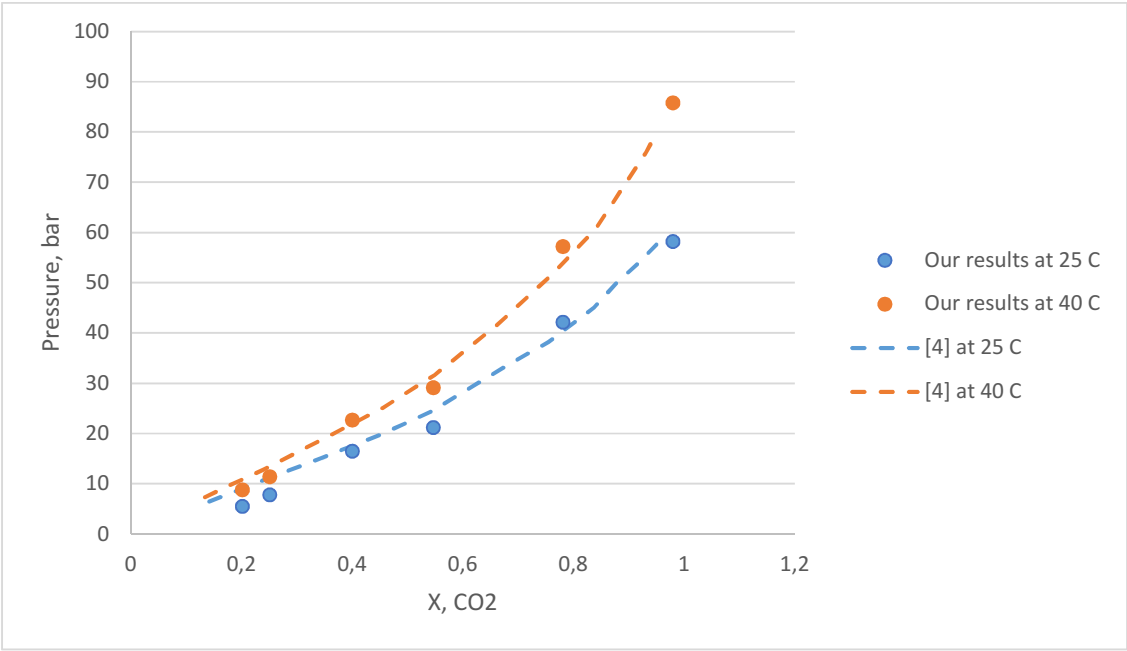

Fig. 2 Comparison of our methyl acetate + CO_2 results with the data available in [4] at 25°C and 40°C.

Summary and outlook

The phase equilibrium measurements of methyl acetate with carbon dioxide at 25°C and 40°C using a cloud point method were in good agreement with the literature results of [4] while deviating from [5]. However, from the point of view of the biocatalytic reactor design the phase equilibrium studies confirmed low miscibility pressures, which is promising and expectable. Further studies will involve the experimental and simulation-based investigation of oil – carbon dioxide and oil – methyl acetate pseudo-binary mixtures and of the oil – methyl acetate – carbon dioxide pseudo-ternary mixture to support the design of the parameter space of the biocatalytic studies.

Acknowledgements

The research is related to the Project no. TKP2021-EGA-02, which has been implemented with the support provided by the Ministry of Culture and Innovation of Hungary from the National Research, Development and Innovation Fund, financed under the TKP2021-EGA funding scheme. G.S.A thanks the support of Stipendium Hungaricum Program of Hungary and of the Green Chemical Engineering Network towards upscaling sustainable processes (CA18224) – GREENERING project funded by COST (European Cooperation in Science and Technology).

References

[1] Goembira F. and Saka S. “Effect of Additives to Supercritical Methyl Acetate on Biodiesel Production”, Fuel Processing Technology,125, 114-118, (2014).

[2] Komintarachat C., Sawangkeaw R. and Ngamprasertsith S. “Continuous Production of Palm Biofuel under Supercritical Ethyl Acetate”, Energy Conversion and Management, 93, 332-338, (2015).

[3] Marx S. “Glycerol-free Biodiesel Production Through Transesterification: A review”, Fuel Processing Technology, 151, 139-147, (2016).

[4] Ohgaki K., Katayama T. “Isothermal Vapor-liquid Equilibria for Systems Ethyl Ether-Carbon Dioxide and Methyl Acetate-Carbon Dioxide at High Pressure”, Journal of Chemical and Engineering Data, 20(3), 264-267, (1975).

[5] Schwinghammer S., Siebenhofer M. and Marr R. “Determination and Modelling of High-Pressure Vapor-liquid Equilibrium Carbon Dioxide-Methyl Acetate”, The Journal of Supercritical Fluids, 38, 1-6, (2006).

[6] Kőrösi M. “Enhancing the enantiomeric purity of scalemic mixtures by gas antisolvent fractionation”, PhD thesis, Budapest University of Technology and Economics, (2020).

Oxidative Desulfurization of Carbon Dioxide Rich Gas Streams

Abhinav Chandrasekar Nagarajan, Thomas Ernst Müller

Carbon Sources and Conversion, Ruhr-Universität Bochum

nagarajan@ls-csc.ruhr-uni-bochum.de

Introduction

The current global industry is carbon intensive as it strongly depends on fossil-based sources for both energy generation and raw materials. These fossil-based sources are limited and upon their combustion lead to global warming, the effect of which is felt by countries across the world [1]. In order to make the global economy more sustainable, the dependence on fossil-based sources for raw material needs to be reduced and alternate production processes need to be developed and CO_2 emissions need to be mitigated. Valorisation of biomass through gasification and fermentation yielding syn-gas and biogas respectively presents a robust alternative to replace some of the fossil fuel-based energy supply [2]. The composition of biomass however, plays a major role in the quality of the biogas/syngas produced. The gas usually contains 30 - 35% (vol) CO_2 and 0.5 - 2 % (vol) H_2S. Thanks to recent advances in CO_2 utilization and the emerging power-to-X processes, Carbon dioxide rich waste gas streams are now considered a valuable raw material [3]. Power-to-X processes combined with bioenergy plants enables cleaner chemicals and energy production by reducing the dependency on fossil raw materials and pre-emptively removing CO_2 from the atmosphere. However, H_2S hinders the further valorisation of CO_2, as it is a catalyst poison, corrosive and toxic to the environment, therefore, its separation from the CO_2 rich waste gas streams is necessary.

Approach

The removal of H_2S from CO_2 rich gas streams can be carried out through various processes. The selection of a suitable process depends on the sulphur content in the gas stream and its mass flow (see Figure 1) [4]. Considering the case of a bioenergy plant, which produces CO_2 rich waste gas streams with low mass flow and low concentration of H_2S, the suitable process window lies in ambit of the liquid redox processes (see Figure 1). Liquid redox processes are less energy intensive and easy to handle compared to existing processes such as acid gas enrichment followed by Claus

process. Redox liquids such as Ferric sulphate ($Fe_2(SO_4)_3$) and Potassium permanganate ($KMnO_4$) have been widely studied for the oxidative desulphurisation of sewer gas and wastewater streams. In comparison, Hydrogen peroxide is cleaner due to the formation of water as a non-toxic by-product as described in eq (1) and (2) [5].

$$H_2S\,(aq) + H_2O_2(aq) \rightarrow S\,(s) + H_2O\,(l) \quad (1)$$

$$H_2S\,(aq) + 4H_2O_2(aq) \rightarrow SO_4^{2-}(aq) + 4H_2O\,(l) + 2H^+(aq) \quad (2)$$

This simplifies the downstream processing and H_2O_2 can be produced readily through the recombination H_2 and O_2 obtained from the electrolysis of H_2O in the presence of a catalyst [6].

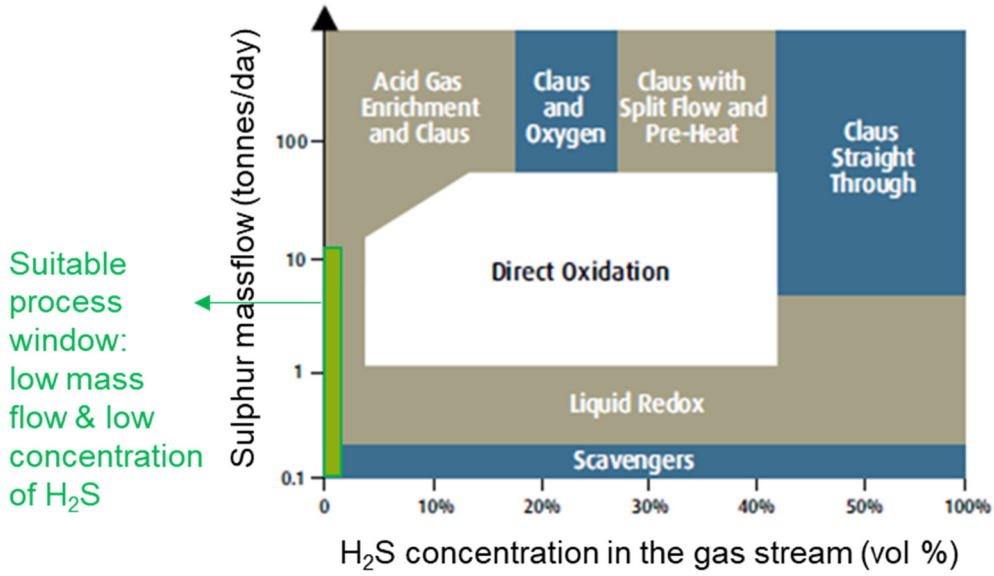

Figure 1: Processes for H_2S separation from CO_2 rich gas streams [3]

Experimental

The performance of H_2O_2 as a desulfurization reagent was tested under the following conditions in a semi-batch reactor with continuous gas flow and a constant volume liquid batch:

i. Temperature range: 25 – 60 °C
ii. Pressure range: 1 – 5 bar

The composition of the gas phase was 1% (vol) H_2S in CO_2, with a flow rate of 200 ml(N)/min. The composition of liquid phase was 3% (wt) H_2O_2 in water with a total volume of 700 ml. The composition in the gas phase was monitored using an in-line micro gas-chromatograph while the reaction mixture was analysed in-situ using pH cum redox potential probe and conductivity probe. The temperature within the reactor was monitored and controlled using a thermostat coupled to an in-situ sensor. The

pressure was set using a back-pressure regulator and recorded using an in-situ pressure sensor. The process control was realised through the LabVIEW software.

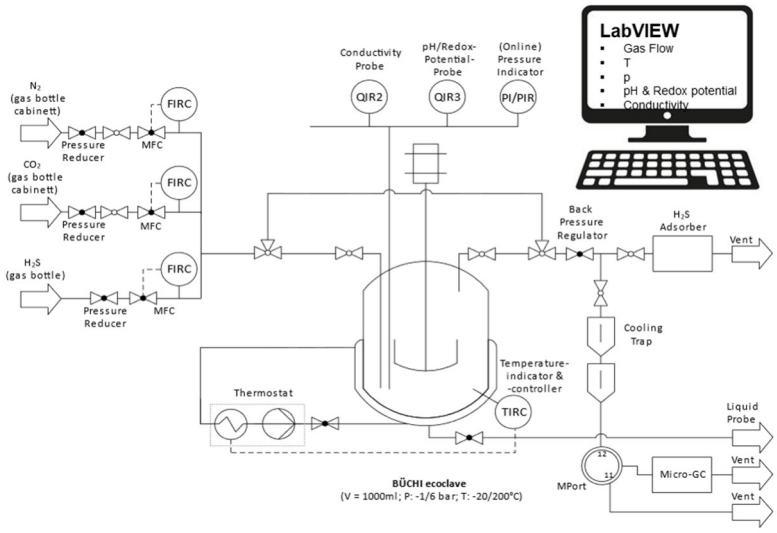

Figure 2: P&ID of the experimental setup

Results and Discussion

The results of the experiment are shown in Figure 3 using the H_2S removal plot for reactions carried out at different temperatures and pressures. The results highlight the effect of temperature and pressure on the reaction: higher temperatures and pressures enhance the removal of H_2S.

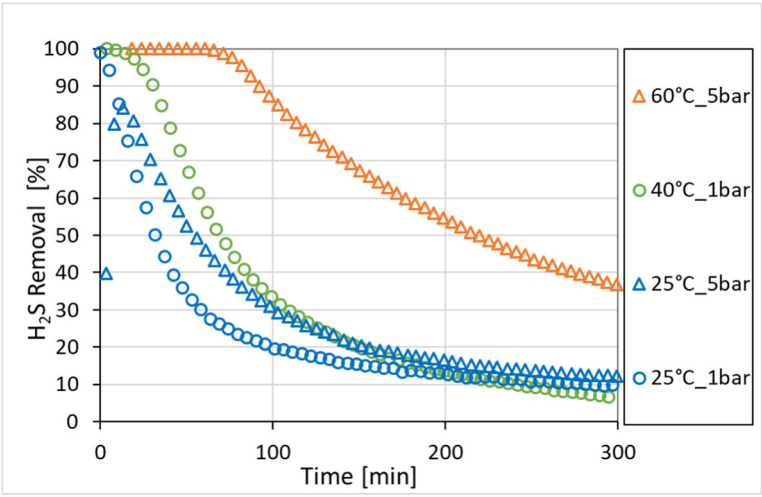

Figure 3: H_2S removal at different temperatures and pressures

The pH-value data is an indicator for the selectivity of the reaction as sulphate formation is the only source of proton generation once the dissolution equilibrium is obtained (see Figure 4). The pH progression highlights the effect of pressure and temperature on the selectivity: higher pressures favour a lower sulphate selectivity and

higher temperatures favour a higher sulphate selectivity. The increase in sulphate selectivity with increase in temperature could be related to a lower activation energy of sulphate formation and increase in sulphur selectivity with increase in pressure could be related to the thermodynamic favourability of sulphur when the ratio of H_2S to H_2O_2 is increased as per Le Chatelier's principle.

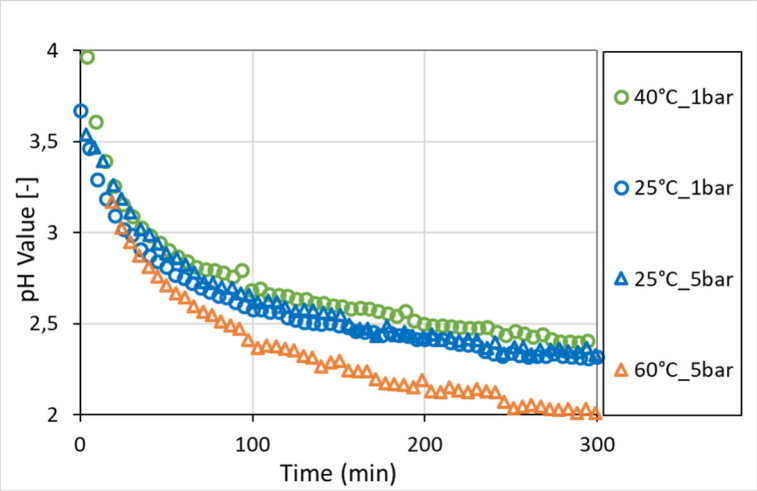

Figure 4: pH plot of the different reactions

Summary and Outlook

Increase in both temperature and pressure enhanced the removal of H_2S from the gas phase. Nevertheless, sulphur selectively is an issue. Increasing pressure alone leads to more sulphur formation whereas increasing temperature alone leads to more sulphate formation. Thus, within the conditions explored formation of sulphate is both thermodynamically and kinetically favoured over sulphur formation. To further substantiate the conclusions made above, investigation of the reaction kinetics is necessary.

Acknowledgement

Abhinav Chandrasekar Nagarajan would like to thank the partners involved in the ECO_2Feed project and the colleagues Wiebke Saß, Julius Schmitt and Dr.-Ing. Kirsten Grübel for their discussions.

The financial support of the Bundesministerium für Bildung und Forschung (BMBF) for the project ECO_2Feed (grant number 03EE5126B) is acknowledged. This research was made possible by funding of the state of North Rhine-Westphalia, RWE Power AG, and the Faculty of Mechanical Engineering of Ruhr-Universität Bochum as part of the endowed chair CSC.

References

1. IPCC, 2018: Global Warming of 1.5°C. An IPCC Special Report on the impacts of global warming of 1.5°C above pre-industrial levels and related global greenhouse gas emission pathways, in the context of strengthening the global response to the threat of climate change, sustainable development, and efforts to eradicate poverty [Masson-Delmotte, V., P. Zhai, H.-O. Pörtner, D. Roberts, J. Skea, P.R. Shukla, A. Pirani, W. Moufouma-Okia, C. Péan, R. Pidcock, S. Connors, J.B.R. Matthews, Y. Chen, X. Zhou, M.I. Gomis, E. Lonnoy, T. Maycock, M. Tignor, and T. Waterfield (eds.)]. Cambridge University Press, Cambridge, UK and New York, NY, USA, pp., 616. https://doi.org/10.1017/9781009157940.001
2. FNR. (2019). Bioenergy in Germany. Facts and Figures 2020. Fachagentur Nachwachsende Rohstoffe (Agency for Renewable Resources). https://www.fnr.de/fileadmin/allgemein/pdf/broschueren/broschuere_basisdaten_bioenergie_2020_engl_web.pdf
3. Rego de Vasconcelos, B. and Lavoie, J.M., 2019. Recent advances in power-to-X technology for the production of fuels and chemicals. Frontiers in chemistry, 7, p.392. https://doi.org/10.3389/fchem.2019.00392
4. Linde Group. (2021, November 25). “Sulphur Process Technology”. https://www.linde-engine-ering.com/en/images/Sulfur%20Process%20Technology_tcm19-111155.pdf
5. Cadena, F. and Peters, R.W., 1988. Evaluation of chemical oxidizers for hydrogen sulfide control. Journal (Water Pollution Control Federation), pp.1259-1263 https://www.jstor.org/stable/25043633
6. Menegazzo, F., Signoretto, M., Ghedini, E. and Strukul, G., 2019. Looking for the “dream catalyst” for hydrogen peroxide production from hydrogen and oxygen. Catalysts, 9(3), p.251. https://doi.org/10.3390/catal9030251

Bark Bio-Refinery using Supercritical Carbon Dioxide

Stefano Barbini, Antje Potthast

Institute of Chemistry of Renewable Resources,

Department of Chemistry, BOKU University, Vienna

s.barbini@natex.at

Introduction

Cellulose obtained from trees (40-50%) is used in many applications: from cheap commodities such as kitchen and toilet paper to regenerated cellulosic fibres used to produce cloths. However, the tree is also composed of lignin and so-called extractives, which are present in higher amounts in the bark. Until now, no high-value applications of tree bark have been discovered, except tannins and antioxidant compounds extracted with polar solvents such as water, i.e., Pycnogenol (condensed tannins) obtained from the maritime pine bark. However, the lipophilic part contained in the bark (4-5%), which is composed of fatty acids, resin acids, steroids, sterol esters, wax esters, and acyl glycerides, among others, is still mainly overlooked. During this research, we have aimed to selectively extract different classes of compounds from bark using different extraction conditions of $scCO_2$ (i.e., pressure, temperature, % of EtOH as co-solvent). Characterization of the obtained extracts with a new analytical method called Ultra-Performance Convergence Chromatography (UPC^2) connected with a high-resolution mass spectrometer Quadrupole-Time of flight (QTof-MS) was compared with the conventional technique based on gas chromatography (GC-MS/FID).

Experimental

Seven conditions of extraction were used to fractionate sequentially pine bark using $scCO_2$. Starting from liquid CO_2, a first extract was obtained, followed by three isothermal steps at 40°C at increasing pressure: 10, 20, and 30 MPa. Once the maximum pressure was reached, two isobaric extractions were carried out at increasing temperatures: 62.5°C and 85°C. Lastly, 6.5% wt of EtOH was incorporated as co-solvent in the stream of $scCO_2$ at 30 MPa and 85°C, obtaining the seventh fraction. These fractionations were characterized by GC-MS/FID, and a comparison of different classes of compounds can be seen in Fig. 1 and 2.

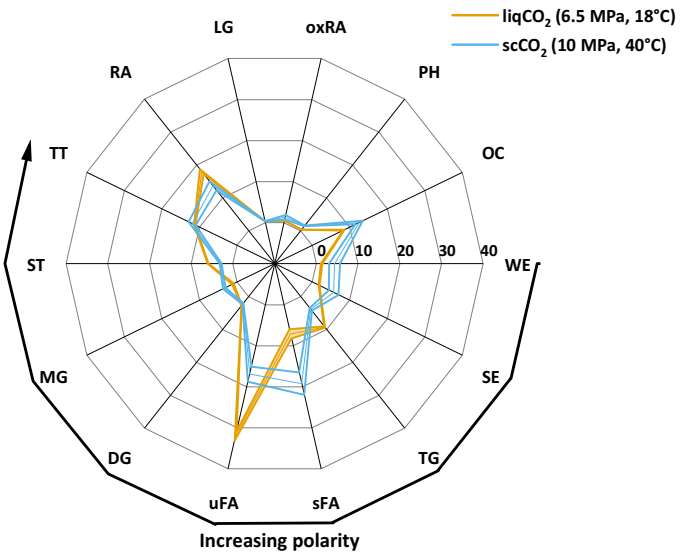

Fig. 1. Liquid CO_2 and the first $scCO_2$ (10.0 MPa, 40°C) extractions are compared. All axes are expressed with the same scale (% composition). From the least polar to the most polar compounds are shown in clockwise direction: WE: wax esters; SE: sterol esters; TG: triglycerides; sFA: saturated free fatty acids; uFA: unsaturated free fatty acids; DG: diglycerides; MG: monoglycerides; ST: free sterols; TT: triterpenoids; RA: resin acids; LG : lignans; oxRA: oxidized resin acids; PH: phenolics; OC: other compounds.

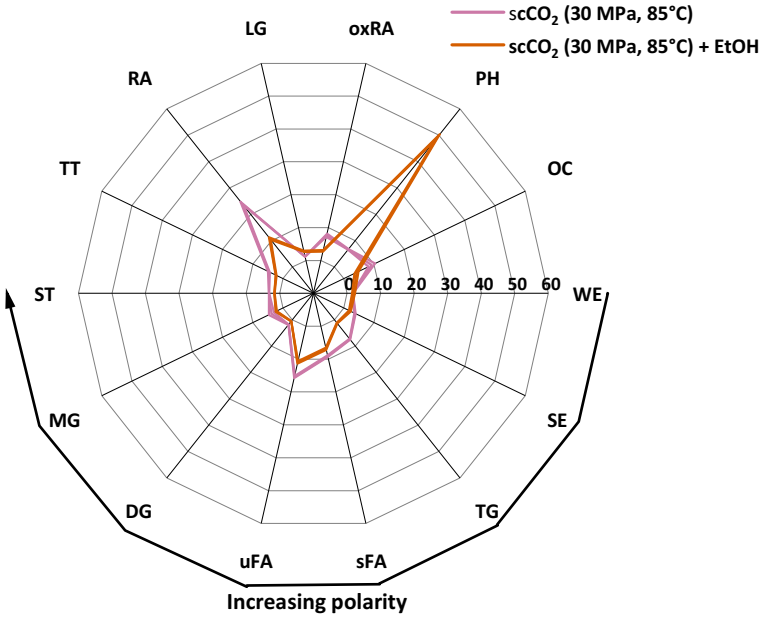

Fig. 2. Two experiments carried out at the same conditions (p and T) except for the use of ethanol as co-solvent (6.5% wt).

Heavy classes of molecules, such as triglycerides and sterol esters, were poorly ionized by electron impact using GC-MS, therefore, no qualitative data about the composition of these classes were obtained (Fig. 3).

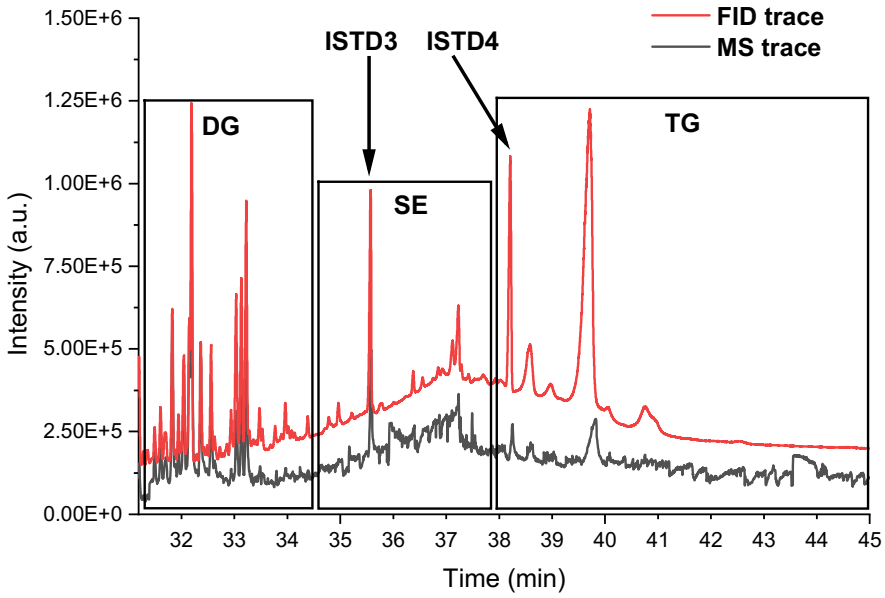

Figure 3. MS and FID traces in comparison for pine bark extract. DG: diglycerides interval; SE: sterol esters interval; TG: triglycerides interval; ISTD3: cholesteryl palmitate; ISTD4: glyceryl triheptadecanoate.

However, when UPC^2-QTof-ESI-MS was used as an analytical method, very detailed information was achieved using a homemade library counting 175 sterol esters and 2925 triglycerides. This was made possible by the ability to fragment each parent peak (precursor ion) into daughter peaks (product ions) by MS/MS technique included as an additional option in the QTof mass spectrometer (Fig. 4).

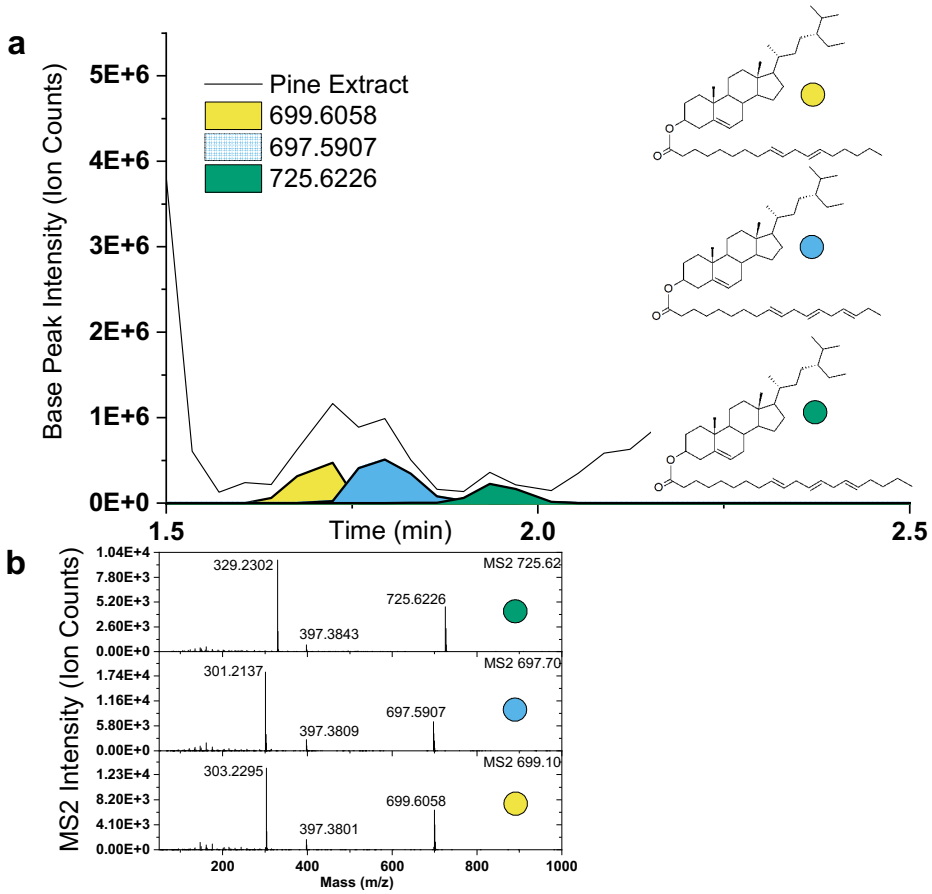

Figure 4. a) Base Peak Ion chromatogram of the three most intense sterol esters according to peak height in pine bark extract analysed in positive mode by UPC^2-QTof-ESI-MS. The double bonds associated with each esterified fatty acid were not studied in detail, no information about clear position and cis/trans geometry was obtained. b) Intensity Ion count of each parent peak (725.6226; 697.5907; 699.6058) fragmented by MS/MS experiment. The common ion 397 indicates the β-sitosteryl unit as $[M\text{-}H_2O+H]^+$ adduct while 329.2302, 301.2137, and 303.2295 ions indicate C20:3, C18:3 and C18:2 fatty acids as $[M+Na]^+$ adducts respectively. The coloured circles indicate each sterol ester.

Summary

A new method of investigation was developed based on supercritical carbon dioxide for extraction and analysis of the bark extracts. A new understanding of the solubility of classes of compounds was achieved using different conditions of extraction. In liquid carbon dioxide, unsaturated fatty acids are more soluble than saturated ones, while using $scCO_2$ at 100 bar and 40°C, almost an equal percentage was extracted for both classes (Fig. 1).

When ethanol was added as co-solvent, a considerable part of the extract was constituted of phenolics such as dihydroconiferyl alcohol, 1-guaiacyl-3-hydroxy-propanone, and 4-hydroxybenzoic acid. A high percentage of glycerol was also obtained in the last extract, where ethanol was used as co-solvent, indicating that hydrolysis of acyl glycerides or depolymerization of cork suberin may have happened during extraction.

Acknowledgment

The authors gratefully acknowledge Svenska Cellulosa Aktiebolaget SCA (Sundsvall, Sweden) for providing the bark as matrix material and WoodKplus (linz, Austria) for access to milling and screening equipment. The County of Lower Austria supported this work within the Austrian Biorefinery Center Tulln (ABCT), BOKU University, and Svenska Cellulosa Aktiebolaget SCA (Sundsvall, Sweden) as participating industry partner and the BOKU doctoral school ABCM.

References

(1) Barbini, S.; Jaxel, J.; Karlström, K.; Rosenau, T.; Potthast, A. Multistage Fractionation of Pine Bark by Liquid and Supercritical Carbon Dioxide. *Bioresour. Technol.* **2021**, *341*, 125862. https://doi.org/10.1016/j.biortech.2021.125862.

(2) Barbini, S.; Sriranganadane, D.; España Orozco, S.; Kabrelian, A.; Karlström, K.; Rosenau, T.; Potthast, A. Tools for Bark Biorefineries: Studies toward Improved Characterization of Lipophilic Lignocellulosic Extractives by Combining Supercritical Fluid and Gas Chromatography. *ACS Sustain. Chem. Eng.* **2021**, *9* (3), 1323–1332. https://doi.org/10.1021/acssuschemeng.0c07914.

Lecturers ERASMUS+ BIP ESS HPT 2023

	University/ Company	Name	Email
AT	Graz	Prof. Thomas Gamse	thomas.gamse@tugraz.at
AT	NATEX	DI Martin Sova	m.sova@natex.at
AT	NATEX	Dr. Eduard Lack	e.lack@natex.at
AT	INNOWELD	Maximilian Schrittwieser	m.schrittwieser@innoweld.at
CZ	Prag	Dr. Helena Sovova	helsov@seznam.cz
DE	Bochum	Prof. Marcus Petermann	petermann@fvt.ruhr-uni-bochum.de
DE	Bochum	Prof. Thomas Müller	mueller@ls-csc.rub.de
DE	Darmstadt	Prof. Markus Busch	markus.busch@pre.tu-darmstadt.de
DE	Freising	Prof. Sabine Grüner-Lempart	sabine.gruener-lempart@hswt.de
DE	Hamburg	Dr. Carsten Zetzl	zetzl@tu-harburg.de
DE	Hamburg	Prof. Pavel Gurikov	pavel.gurikov@tuhh.de
DE	Erlangen	Prof. Eberhard Schlücker	eberhard.schluecker@fau.de
ES	Valladolid	Prof. Maria Cocero	mjcocero@iq.uva.es
ES	Valladolid	Prof. Angel Martin	angel.martin.martinez@uva.es
FR	Albi	Prof. Martial Sauceau	martial.sauceau@mines-albi.fr
HU	Budapest	Prof. Edit Szekely	edit.szekely@edu.bme.hu
HU	Budapest	Dr. Erika Vagi	vagi.erika.maria@vbk.bme.hu
PL	Wroclaw	Prof. Irena Zizovic	irena.zizovic@pwr.edu.pl
PT	Lisbon	Dr. Ana V.M. Nunes	avn07929@fct.unl.pt
SI	Maribor	Prof. Zeljko Knez	zeljko.knez@um.si
SI	Maribor	Dr. Maša Knez-Marevci	masa.knez@um.si
SI	Maribor	Prof. Urban Bren	urban.bren@um.si
SI	Maribor	Dr. Amra Perva	amra.perva@um.si
UK	Glasgow	Prof. Carl Schaschke	carl.schaschke@gcu.ac.uk

Participants ESS HPT 2023

	University / Company	First Name	Family Name	Sex	Nationality
AT	Graz	Roland	Gall	m	Austria
AT	NATEX	Stefano	Barbini	m	Italy
CZ	Ostrava	Adela	Slachtova	f	Czech
DE	Bochum	Stephan	Heuser	m	Germany
DE	Bochum	Laura	Göhlich	f	Germany
DE	Bochum	Abhinav Chandrasekar	Nagarajan	m	India
DE	Darmstadt	Svenja Nicole	Albus	f	Germany
DE	Darmstadt	Sandra	Pietrasch	f	Germany
DE	Darmstadt	Joshua	Stahl	m	Germany
DE	Darmstadt	Emil	Schwarz	m	Germany
DE	Darmstadt	Anne	Rott	f	Germany
DE	Darmstadt	Laura Maria	Ständecke	f	Germany
DE	Darmstadt	Julian	Kirsch	m	Germany
DE	Hamburg	Dennis	Arigbe	m	German
ES	Valladolid	Maurício	De Souza Ribeiro	m	Brazil
ES	Valladolid	Alberto	Goicoechea Torres	m	Spain
ES	Valladolid	Maria Constanza	Maciel	f	Argentina
ES	Valladolid	Nataly	Castro Ferro	f	Colombia
ES	Valladolid	Aránzazu	Redondo Hernangómez	f	Spain
HR	Zagreb	Martina	Miloloža	f	Croatia
HU	Budapest	Dora	Arany	f	Hungary
HU	Budapest	Petra	Kantor	f	Hungary
HU	Budapest	Ghazwan	Saleh Ahmed	m	Iraq
IT	Padova	Gunay	Ismiyeva	f	Aserbaidschan
IT	Padova	Mahdi	Miravandi	m	Iran
PL	Warsaw	Przemysław	Rakowski	m	Poland
PL	Wroclaw	Mateusz	Jackowski	m	Poland
PL	Wroclaw	Aleksandra	Modzelewska	f	Poland
RS	Belgrade	Ivana	Nikolic	f	Serbia
SI	Maribor	Gal	Slacek	m	Slovenia
SI	Maribor	Franjo	Frešer	m	Slovenia
SI	Maribor	Marcell	Gyurkac	m	Slovenia
SI	Tastepoint	Luka	Romanic	m	Slovenia